CAPITAL UNIVERSITY OF SCIENCE AND
TECHNOLOGY, ISLAMABAD

Effect of the Weissenberg Number on Upper Convective Maxwell Flow within a Square Cavity

by

Madiha Khan

A thesis submitted in partial fulfillment for the
degree of Master of Philosophy

in the

Faculty of Computing
Department of Mathematics

2025

I dedicate my thesis to

My Mother,

Whose unconditional love, sacrifices, and prayers have been my greatest strength and inspiration.

CERTIFICATE OF APPROVAL

Effect of the Weissenberg Number on Upper Convective Maxwell Flow within a Square Cavity

by

Madiha Khan

(Registration No: MMT233002)

THESIS EXAMINING COMMITTEE

S. No.	Examiner	Name	Organization
(a)	External Examiner	Dr. Muhammad Ashraf	UOS,Sargodha
(b)	Internal Examiner	Dr. Abid Kamran	CUST, Islamabad

Dr. Muhammad Sabeel Khan
Thesis Supervisor
October, 2025

Dr. Muhammad Sagheer
Head
Dept. of Mathematics
October, 2025

Dr. M. Abdul Qadir
Dean
Faculty of Computing
October, 2025

Author's Declaration

I, **Madiha Khan**, hereby state that my MPhil thesis titled "**Effect of the Weissenberg Number on Upper Convective Maxwell Flow within a Square Cavity**" is my work and has not been submitted previously by me for taking any degree from Capital University of Science and Technology, Islamabad or anywhere else in the country/abroad.

At any time if my statement is found to be incorrect even after my graduation, the University has the right to withdraw my MPhil Degree.

(Madiha Khan)

Registration No: MMT233002

Plagiarism Undertaking

I solemnly declare that the research work presented in this thesis titled **"Effect of the Weissenberg Number on Upper Convective Maxwell Flow within a Square Cavity"** is solely my research work with no significant contribution from any other person. Small contribution/help wherever taken has been duly acknowledged, and that complete thesis has been written by me.

I understand the zero-tolerance policy of the HEC and Capital University of Science and Technology towards plagiarism. Therefore, I, as an author of the above titled thesis declare that no portion of my thesis has been plagiarized and any material used as reference is properly referred/cited.

I undertake that if I am found guilty of any formal plagiarism in the above titled thesis even after awarding of MPhil Degree, the University reserves the right to withdraw/revoke my MPhil degree and that HEC and the University have the right to publish my name on the HEC/University website on which names of students are placed who submitted plagiarized work.

(Madiha Khan)

Registration No: MMT233002

Acknowledgement

In the name of Allah, the Most Gracious and Compassionate, the source of all knowledge and wisdom.

I wish to express my sincere appreciation to my supervisor, Dr. Muhammad Sabeel Khan, for his valuable guidance, constructive feedback, and consistent support throughout the preparation of this thesis. His supervision has been integral to the completion of this work.

I am also grateful to my teachers for their encouragement and for instilling in me the pursuit of academic excellence, particularly in mathematics. My thanks are further extended to Capital University of Science and Technology (CUST) for providing a supportive environment that facilitated this research.

Finally, I acknowledge with gratitude the support of my husband and family, whose patience, encouragement, and prayers have been a source of strength during this journey.

Abstract

This thesis presents a comprehensive numerical investigation of viscoelastic fluid flow in a square lid-driven cavity using the Upper Convected Maxwell model. The governing equations, representing the coupled momentum and constitutive relations, are first derived in their complete component form and subsequently transformed into a non-dimensional formulation incorporating two key dimensionless parameters: the Reynolds number and the Weissenberg number. To solve the problem, a weak formulation of the governing equations is developed and implemented using the finite element method within the FreeFEM++ framework.

The primary objective of this work is to analyze the influence of Weissenberg number on the flow dynamics, drag force, and drag coefficient at the top lid of the cavity for a range of Reynolds numbers. Simulations are performed for small values of Weissenberg number, and the results demonstrate that viscoelastic effects significantly alter the flow structure compared to Newtonian behavior. At low Reynolds numbers, elastic stresses dominate the flow, leading to anisotropy in the velocity and stress fields, deformation of primary vortices, and the generation of secondary flows. At higher Reynolds number, inertial effects become more pronounced; however, elasticity continues to strongly influence the flow, particularly near boundary layers and regions of high strain rates. The study further examines the extreme values of horizontal and vertical velocities for different Reynolds and Wissenberg numbers, revealing nonlinear and occasionally non-monotonic trends that highlight the complex interplay between elasticity and inertia. Additionally, the drag force and drag coefficient on the top lid are evaluated, showing that increasing Wissenberg number consistently reduces both drag force and drag coefficient, with the effect becoming more pronounced at higher Reynolds number.

Contents

List of Figures

List of Tables

Abbreviations

FEM	Finite Element Method
GFEM	Galerkin Finite Element Method
NSE	Navier Stokes Equations
PDEs	Partial Differential Equations
UCM	Upper Convected Maxwell

Symbols

τ	Cauchy stress tensor
∇	Gradient operator
W_i	Weissenberg number
ϕ_i	Velocity shape function
ψ_i	Pressure shape function
u	x-component of velocity
v	y-component of velocity
m	Mass
V	Volume
F	Force applied
A	Area
$\delta_{i,j}$	Kronecker delta
R_e	Reynolds number
ρ	Density
ν	Kinematic viscosity
$\boldsymbol{u}$	Velocity vector
λ	Relaxation time
F_D	Drag Force
C_D	Drag Coefficient
p	Pressure
v_{max}	Maximum velocity
$\boldsymbol{K}$	Block stiffness matrix
$\boldsymbol{X}$	Block solution vector
$\boldsymbol{Q}$	Block boundary vector

Chapter 1

Introduction and Literature Survey

1.1 Introduction

Viscoelastic fluids, such as polymer melts, biological fluids, and various industrial suspensions, exhibit both viscous and elastic characteristics during deformation. Understanding their flow dynamics is crucial due to their widespread applications in fields including microfluidics, biomedical engineering, and industrial processing. Among the constitutive models used to describe such fluids, the Upper Convected Maxwell (UCM) model is widely adopted as it effectively captures the combined influence of fluid viscosity and relaxation time, representing the material's elastic memory.

The Weissenberg number (W_i), a key dimensionless parameter described as the result of multiplying the shear rate by the typical relaxation time., quantifies the relative significance of elastic effects compared to viscous effects in viscoelastic flows. In confined geometries such as square cavities, variations in W_i significantly influence flow behavior by altering vortex formation, velocity gradients, and stress distributions. These effects are particularly important for optimizing processes like mixing, extrusion, and fluid transport, where precise control of flow patterns is required.

This study's principal goal is to numerically investigate the influence of the Weissenberg number on UCM fluid flow within a square lid-driven cavity. The finite element method (FEM) is employed to analyze the resulting changes in flow structure as W_i increases. This work is motivated by and builds upon the model discussed

in the work [1] by Khan et al., where the effects of relaxation time on viscoelastic flow characteristics were studied in baffled cavities using FreeFEM++.

1.2 Literature Review

Viscoelastic fluid flows are encountered in a wide range of natural and industrial systems, including polymer processing, biomedical applications, and microfluidics. Unlike Newtonian fluids, viscoelastic fluids exhibit complex behaviors such as normal stress differences, stress relaxation, shear thinning, and elastic recoil. Understanding these phenomena is crucial for accurately predicting flow behavior in practical applications.

The mathematical framework for modeling viscoelastic fluids was established in the foundational works of Bird [2] and Oldroyd [3], introducing models such as the UCM formulation. These models are widely employed due to their ability to capture the elastic memory effects inherent in polymeric fluids. Over the years, the UCM model and its variants have been applied to investigate diverse flow configurations, including lid-driven cavities, channel flows, and flows around obstacles.

One of the central challenges in simulating viscoelastic flows arises from the so-called high Weissenberg number problem. The Weissenberg number, is a dimensionless quantity that characterizes the relative strength of elastic to viscous forces. At high W_i, numerical instabilities often emerge, leading to convergence issues. To address this, Fattal and Kupferman [4] developed the log-conformation formulation, later refined by Hulsen [5], significantly improving stability for high-W_i simulations.

A wide body of literature has explored the influence of W_i on viscoelastic flow characteristics. Zhu et al. [6] demonstrated its critical role in microswimmer propulsion, while Sebastian and Dittrich [7] highlighted its relevance in mimicking physiological flows in biomedical microfluidic systems. Alves [8] provided a comprehensive review of numerical techniques for simulating viscoelastic flows, identifying persistent challenges in high-W_i regimes due to the stiffness of governing equations. Lopez et al.

[9] further investigated symmetry-breaking transitions in microcavity flows, shedding light on elastic instabilities relevant to mixing and transport processes.

Khan et al. [1] conducted an extensive finite element study using the UCM model to analyze the effects of relaxation time (and consequently W_i) on baffled cavity flows. Their results highlighted strong elastic-memory effects, showing significant variations in vortex strength, drag forces, and stream function behavior with increasing W_i. Similarly, several researchers have investigated viscoelastic effects in lid-driven cavities. For example, Renardy [10] reported numerical convergence issues at high W_i for UCM flows, while Pakdel and McKinley [11] introduced a criterion to predict elastic instabilities in corner-dominated flows. Sureshkumar and Beris [12] further analyzed stress boundary layers and instability mechanisms using spectral element simulations.

Souvaliotis and Beris [13] demonstrated the emergence of complex stress distributions and corner vortices in UCM cavity flows using spectral element techniques. Gezae [14] studied viscoelastic lid-driven cavity flows via finite volume simulations, analyzing variations in drag, vorticity, and velocity with different W_i. Aboubacar and Webster [15] compared UCM and Oldroyd-B models in cavity flows, revealing significant changes in streamline patterns due to elasticity. Extending this line of research, Xue et al. [16] investigated three-dimensional cavity flows and reported secondary flow formations and stress concentration zones.

Experimental studies have further enriched this field. Grillet et al. [17] and Poole et al. [18] validated theoretical predictions of flow asymmetries and vortex dynamics in viscoelastic cavities. Li and Fang [19] explored the influence of elasticity on thermal boundary layers by coupling heat transfer with viscoelastic cavity flows. Cheddadi et al. [20] developed a matrix-free finite element formulation to improve numerical stability in high-W_i simulations. Oliveira and Pinho [21] demonstrated that elasticity significantly alters secondary vortex structures and wall shear stress in square cavities using the Oldroyd-B model, which reduces to UCM in the zero-solvent-viscosity limit. Comparative studies, such as those by Fan et al. [22], have highlighted the distinct features of UCM fluids relative to other viscoelastic models, including Phan-Thien and Tanner's shear-thinning formulation [23]. Moreover, Arratia et al. [24] observed

symmetry-breaking transitions in microfluidic experiments, consistent with vortex dynamics predicted in cavity geometries. Similar behaviors were reported by Zydney and Colton [25] in porous media flows under viscoelastic effects.

Despite these significant advancements, most studies focus on regularized models such as Oldroyd-B, Giesekus, or FENE-P, as well as baffled cavity configurations. Direct investigations of viscoelastic flow in unbaffled square cavities using the standard UCM model remain comparatively limited due to the numerical stiffness of the governing equations at high W_i. Furthermore, a comprehensive analysis of energy-related metrics—such as drag forces, velocity extremum and drag coefficients—has received little attention.

This thesis addresses these gaps by performing a systematic numerical investigation of viscoelastic UCM fluid flow in a square lid-driven cavity. A finite element method is developed and implemented in FreeFEM++, and the effect of varying W_i on vortex structures, streamline topology, flow symmetry, and energetics is analyzed while keeping the Reynolds number constant. By advancing the understanding of elastic effects in confined flows, this work contributes to improved modeling of applications in polymer processing, microfluidics, and biological transport systems.

1.3 Thesis Contribution

This thesis presents a comprehensive numerical investigation of the impact that the (W_i) has on the flow properties of an UCM fluid in a square lid-driven cavity. The primary contribution lies in systematically examining how viscoelastic elasticity, quantified by W_i, affects the internal flow structure, vortex formation, streamline topology, and velocity distribution within the cavity.

Unlike most prior studies, which primarily focused on baffled cavities or explored relaxation time indirectly, this work directly investigates the role of W_i in a non-baffled square cavity. A robust finite element framework is developed based on the weak formulation of the governing equations, enabling accurate and stable simulations over a wide range of W_i.

Key flow attributes, including vortex strength and position, extrema of the stream function, velocity variations, and drag forces, are computed and analyzed in detail. The findings reveal significant modifications in flow symmetry, vortex dynamics, and energy distribution as elasticity increases. Furthermore, the results are compared against recent work by Khan [1], which studied baffled viscoelastic flows, thereby highlighting the novel contributions of this study in a simpler geometric configuration.

Overall, this thesis advances the understanding of viscoelastic fluid behavior in confined cavity flows and provides a scalable computational framework. The methodology and findings can be extended to more complex geometries, three-dimensional simulations, and industrial applications, thereby contributing to the broader field of non-Newtonian fluid dynamics.

1.4 Objectives

The main goal of this thesis is to enhance the understanding of viscoelastic fluid flow behavior through finite element modeling and numerical simulation. Specifically, the goals of this research are as follows

- To numerically investigate the flow characteristics of viscoelastic fluids in a square lid-driven cavity using the UCM model.
- To develop a robust mathematical model describing the governing physics of the problem, formulate its component form, and systematically derive the non-dimensional form of the equations to reduce the number of governing parameters and highlight dominant physical effects.
- To derive the weak formulation of the governing equations and implement the FEM using FreeFEM++ for accurate and efficient numerical simulations.
- To examine the influence of the (W_i), which represents the fluid's relaxation time effects, on velocity distributions, streamline patterns, and overall flow structure within the cavity.

- To compute and analyze the drag force on the moving lid and investigate how variations in W_i affect the drag force and drag coefficient.

1.5 Thesis Layout

This thesis is organized into six chapters, focusing on the mathematical modeling, numerical analysis, and simulation of viscoelastic fluid flows using the Upper Convected Maxwell (UCM) model. Each chapter is structured to build upon the concepts introduced in the previous ones, with a particular emphasis on the Finite Element Method (FEM) for solving two-dimensional UCM flow problems.

- Chapter 2 introduces the fundamental concepts necessary to understand viscoelastic fluid dynamics and the UCM model. Key terminologies such as stress tensors, convected derivatives, and constitutive relations are explained. In addition, the essential mathematical foundations of the Finite Element Method, including function spaces, boundary conditions, and weak formulations, are presented.

- Chapter 3 focuses on the numerical techniques used to discretize the governing equations. The spatial and temporal discretization strategies are discussed in detail, along with the FEM implementation required to solve the partial differential equations efficiently.

- Chapter 4 is dedicated to the complete process of mathematical modeling. The governing equations for two-dimensional viscoelastic fluid flow based on the UCM model are first derived and then systematically non-dimensionalized to highlight key dimensionless parameters, such as the Reynolds number (R_e) and the Weissenberg number (W_i). The weak formulation of the equations is then obtained step by step, introducing auxiliary variables where necessary. Finally, the finite element formulation is developed, leading to a discrete algebraic system suitable for implementation in FreeFEM++.

- Chapter 5 presents the numerical results and their detailed discussion. The impact of varying the (W_i) on flow characteristics is analyzed while keeping

the (R_e) fixed. Velocity profiles, streamline patterns, vortex formations, and stress fields are examined comprehensively. Key flow parameters, including drag forces on the moving lid and velocity extrema, are computed and compared to demonstrate the influence of fluid elasticity.

- Chapter 6 summarizes the key findings and contributions of the thesis. It highlights how elasticity, governed by the Weissenberg number, significantly affects the cavity's flow characteristics. The chapter also emphasizes the effectiveness of the FEM-based FreeFEM++ framework and provides insights into potential future research directions.

Chapter 2

Numerical Notions and Theoretical Background

This chapter presents the mathematical notions and theoretical background used in this thesis.

2.1 Mathematical Notions

This section include the mathematical notions and the concepts utilized in this study.

2.1.1 Divergence of a Vector

"The divergence of a vector-valued function $\mathbf{F} = (f_1, f_2, ..., f_n)$ is expressed as

$$\nabla.\mathbf{F} = \frac{\partial f_1}{\partial x_1} + \frac{\partial f_2}{\partial x_2} + ... + \frac{\partial f_n}{\partial x_n},$$

where f_2, f_2 and all the way up to f_n are components of the vector field along the $x_1, x_2, ..., x_n$ directions. Divergence measures the rate at which fluid expands or compresses at a given point. For example, a positive divergence indicates a source of fluid, whereas a negative divergence indicates a sink". [26]

2.1.2 Gradient of a Scaler-Valued Function

"The gradient of a scalar-valued function $f = f(x_1, x_2, ..., x_n)$ is expressed mathematically as

$$\nabla f = \left(\frac{\partial f}{\partial x_1}, \frac{\partial f}{\partial x_2}, ..., \frac{\partial f}{\partial x_n} \right).$$

The gradient of a scalar-valued function provides valuable information about how the function changes in space. It is a vector that shows both the direction of the steepest increase and the rate of change in that direction". [26]

2.1.3 The Laplace Operator

"The Laplace operator, or the Laplacian, is a second-order differential operator that measures how the value of a scalar-valued function $f(x_1, x_2, \ldots, x_n)$ defined in an n-dimensional space diverges from its average value in a given neighborhood. The Laplace operator is defined as

$$\nabla^2 f = \frac{\partial^2 f}{\partial x_1^2} + \frac{\partial^2 f}{\partial x_2^2} + ... + \frac{\partial^2 f}{\partial x_n^2}." \quad [26]$$

2.1.4 Product of a Second-Order Tensor with a Vector

"A second-order tensor **A** may be thought of as a linear operator that acts on a vector u,generating a new vector v. Thus, we may write:

$$v = Au." \quad [27]$$

2.1.5 Tensor/ Dyadic Product

"The tensor (or direct or matrix) product or the dyad of vectors u and v is denoted by

$$u \otimes v.$$

It is a second-order tensor that linearly transforms a vector w into another vector in the direction of u, according to the rule,

$$(u \otimes v)w = u(v \cdot w) = (v \cdot w)u.\text{"} \quad [27]$$

2.2 Fluid

"A fluid will continuously deform when subjected to shear (tangential) stress, regardless of how small the stress may be." [28]

2.2.1 Types of Fluid

2.2.2 Ideal Fluid

"A fluid that is incompressible and has no viscosity is called an *ideal fluid*. An ideal fluid is a theoretical concept, as all real fluids have some viscosity." [29]

2.2.3 Real Fluid

"A *real fluid* is a fluid that has viscosity. In practice, all fluids are real fluids." [29]

2.2.4 Newtonian Fluid

"A *Newtonian fluid* is a real fluid in which the shear stress is directly proportional to the rate of shear strain (or velocity gradient), and is mathematically expressed as

$$\tau = \mu \frac{du}{dy},$$

where τ is the shear stress, μ is the dynamic viscosity, and $\frac{du}{dy}$ is the velocity gradient perpendicular to the direction of flow." [29]

2.2.5 Non-Newtonian Fluid

"A real fluid in which the shear stress is not directly proportional to the rate of shear strain (or velocity gradient) is called a *non-Newtonian fluid*. The relationship between shear stress and velocity gradient for such fluids can be expressed as,

$$\tau_{xy} \propto \left(\frac{du}{dy}\right)^m, \quad m \neq 1, \tag{2.1}$$

or equivalently,

$$\tau_{xy} = \mu \left(\frac{du}{dy}\right)^m, \tag{2.2}$$

where τ_{xy} is the shear stress, $\frac{du}{dy}$ is the rate of shear strain, μ is the viscosity, and m is a constant that is not equal to 1." [29]

2.3 Types of Flow

2.3.1 Rotational Flow

"*Rotational flow* refers to a type of fluid flow in which fluid particles, while moving along streamlines, also rotate about their own axis." [29]

2.3.2 Irrotational Flow

"*Irrotational flow* refers to a type of fluid flow in which fluid particles, while moving along streamlines, do not rotate about their own axis." [29]

2.3.3 Compressible Flow

"*Compressible flow* is characterized by changes in fluid density at different points. In other words, the density (ρ) of the fluid is not constant. Mathematically,

$$\rho \neq c, \tag{2.3}$$

where c is a constant." [29]

2.3.4 Incompressible Flow

"*Incompressible flow* refers to a type of flow where the fluid's density remains constant. Liquids are typically incompressible, whereas gases are generally compressible. Mathematically,

$$\rho = c, \tag{2.4}$$

where c is a constant." [29]

2.3.5 Internal Flow

"*Internal flow* describes fluid flow that is entirely confined within solid boundaries, such as in pipes or ducts." [28]

2.3.6 External Flow

"*External flow* occurs when a fluid flows around a body that is immersed in an unbounded fluid domain, such as the flow over an aircraft wing or a cylinder." [28]

2.4 States of Flow

The following are the two states of flow:

2.4.1 Steady Flow

"*Steady flow* occurs when the flow characteristics, such as velocity, depth, or rate of flow, remain constant over time at any given point in an open channel. Mathematically,

$$\frac{\partial Q}{\partial t} = 0, \tag{2.5}$$

where Q represents any fluid property." [29]

2.4.2 Unsteady Flow

"*Unsteady flow* refers to a flow condition where the velocity, depth, or rate of flow varies with time at any given point in an open channel. Mathematically,

$$\frac{\partial Q}{\partial t} \neq 0, \tag{2.6}$$

where Q represents any fluid property." [29]

2.5 Theoretical Background

2.5.1 The Upper Convected Maxwell Model

"The upper convected Maxwell (UCM) model is a nonlinear viscoelastic constitutive relation that extends the classical Maxwell model to continuum mechanics by including convected derivatives. It is written as:

$$\boldsymbol{\tau} + \lambda \overset{\triangledown}{\boldsymbol{\tau}} = 2\eta \, \mathbf{D},$$

where $\boldsymbol{\tau}$ is the extra stress tensor, λ is the relaxation time, and η is the viscosity. The rate-of-deformation tensor D is given by

$$\mathbf{D} = \frac{1}{2}(\nabla \mathbf{v} + \nabla \mathbf{v}^T).$$

The upper convected derivative of the stress tensor is

$$\overset{\triangledown}{\boldsymbol{\tau}} = \frac{D\boldsymbol{\tau}}{Dt} - \boldsymbol{\tau} \cdot \nabla \mathbf{v} - (\nabla \mathbf{v})^T \cdot \boldsymbol{\tau}.$$

This model captures the elastic memory of polymeric fluids while ensuring frame invariance under arbitrary motions." [2]

2.5.2 Relaxation Time

"The relaxation time is the characteristic time required for the stress in a viscoelastic fluid to relax after the cessation of a constant deformation. In the Maxwell model it

is given by

$$\lambda = \frac{\eta}{G}, \tag{2.7}$$

where η is the viscosity and G is the elastic modulus." [2]

2.5.3 Stress Tensor $\boldsymbol{\tau}$

"The symbol $\boldsymbol{\tau}$ denotes the extra (or deviatoric) stress tensor in the continuum mechanics of fluids. This tensor represents the stress arising from deformation (viscous or elastic) excluding hydrostatic pressure.

The total Cauchy stress tensor is decomposed as

$$\boldsymbol{\sigma} = -p\,\mathbf{I} + \boldsymbol{\tau},$$

where $\boldsymbol{\tau}$ encapsulates the shear and memory effects. In Newtonian fluids, for instance,

$$\boldsymbol{\tau} = 2\mu\,\mathbf{D},$$

where μ is the viscosity and D is the rate-of-deformation tensor. For viscoelastic fluids, $\boldsymbol{\tau}$ evolves according to specific constitutive equations, such as the upper-convected Maxwell model." [2]

2.6 Constitutive Equations

2.6.1 Momentum Equation

"The general form of the unsteady incompressible momentum equation (Cauchy equation) is given by

$$\rho\left(\frac{\partial \mathbf{v}}{\partial t} + \mathbf{v}\cdot\nabla\mathbf{v}\right) = -\nabla p + \nabla\cdot\boldsymbol{\tau} + \rho\mathbf{g}, \tag{2.8}$$

where:

- ρ is the density of the fluid $\left[\mathrm{kg/m^3}\right]$,
- $\mathbf{v} = (u, v)$ is the velocity vector [m/s],
- p is the isotropic pressure [Pa],
- $\boldsymbol{\tau}$ is the extra (deviatoric) stress tensor [Pa],
- $\mathbf{g}$ is the body force per unit mass (e.g., gravity) $\left[\mathrm{m/s^2}\right]$.

The left-hand side represents the **rate of change of momentum**, including local acceleration $\left(\frac{\partial \mathbf{v}}{\partial t}\right)$ and convective acceleration $(\mathbf{v} \cdot \nabla \mathbf{v})$, while the right-hand side expresses the sum of the forces acting on the fluid element, including the pressure gradient, the divergence of the extra stress tensor, and any body forces." [2]

2.6.2 Mass Conservation (Continuity Equation)

"For an incompressible fluid, the conservation of mass requires that the volume of any fluid element remains constant, which leads to the continuity equation:

$$\nabla \cdot \mathbf{v} = 0. \tag{2.9}$$

Equation (2.9) states that the velocity field must be divergence-free, indicating that there is no net volumetric expansion or compression within the fluid domain." [2]

2.7 Dimensionless Parameter

2.7.1 Reynolds Number

"It is a dimensionless quantity represented by R_e that characterizes the ratio of inertial forces to viscous forces in a fluid flow. It determines the flow regime, distinguishing between laminar flow ($R_e < 2000$) and turbulent flow ($R_e > 4000$). Re is expressed as

$$R_e = \frac{\rho u L}{\mu},$$

where L denotes the characteristic length and u denotes the fluid's velocity." [30]

2.7.2 Weissenberg Number

"The Weissenberg number (W_i) is a dimensionless parameter that quantifies the relative importance of elastic effects to viscous effects in viscoelastic fluid flows. It is defined as the product of the characteristic relaxation time of the fluid (λ) and a characteristic shear rate ($\dot{\gamma}$)

$$Wi = \lambda\dot{\gamma}. \tag{2.10}$$

where:

λ = relaxation time of the fluid, and $\dot{\gamma}$ = characteristic shear rate (or strain rate).

In essence, the Weissenberg number measures the degree to which a viscoelastic fluid retains memory of its deformation. When $Wi \ll 1$, viscous behavior dominates, and the fluid behaves similarly to a Newtonian fluid. Conversely, when $Wi \gg 1$, elastic effects become significant, often leading to complex flow phenomena such as elastic instabilities or flow-induced anisotropy." [2]

2.7.3 Viscosity

"*Viscosity* refers to the property of a fluid that resists the movement of one layer of fluid over another adjacent layer. Mathematically,

$$\mu = \frac{\tau}{\frac{\partial u}{\partial y}}, \tag{2.11}$$

where μ is the viscosity coefficient, τ is the shear stress, and $\dfrac{\partial u}{\partial y}$ represents the velocity gradient." [29]

2.7.4 Kinematic Viscosity

"*Kinematic viscosity* is the ratio of the dynamic viscosity to the density of a fluid. It is denoted by the symbol ν, called *nu*. Mathematically,

$$\nu = \frac{\mu}{\rho}, \tag{2.12}$$

where ν is the kinematic viscosity, μ is the dynamic viscosity, and ρ is the density of the fluid." [29]

2.7.5 Mass Density or Density

"Mass density, denoted by ρ, is a fundamental property of a substance that represents its mass per unit volume. It quantifies how much mass is contained within a given volume and is mathematically expressed as

$$\rho = \frac{m}{V}, \tag{2.13}$$

The SI unit of density is kilogram per cubic meter ($\mathrm{kg/m^3}$). Density plays a crucial role in fluid dynamics, determining buoyancy, pressure distribution, and flow characteristics. Incompressible fluids maintain a constant density, whereas compressible fluids exhibit density variations under changing pressure and temperature conditions". [31]

2.7.6 Pressure

"The pressure, denoted by P, is defined as the force exerted per unit area on a surface. It describes the intensity of a force acting normally to a given area and is mathematically expressed as

$$P = \frac{F}{A}, \tag{2.14}$$

The SI unit of pressure is Pascal ($\mathrm{Pa} = \mathrm{N/m^2}$). Pressure plays a fundamental role in fluid mechanics, influencing fluid motion, buoyancy, and the behavior of gases and liquids under different conditions. In a static fluid, pressure increases with depth due to the weight of the overlying fluid column, following the hydrostatic pressure equation". [31]

Chapter 3

Introduction to Finite Element Method

3.1 Finite Element Method

FEM is an essential computational tool for the approximate solution of boundary value problems governed by partial differential equations (PDEs). FEM is a general-purpose technique that can be used in a variety of fields, such as solid mechanics, fluid dynamics, heat transfer, electromagnetics, biomechanics, and more. It was first developed in the 1960s for structural analysis in civil and aerospace engineering.

Fundamentally, FEM tackles the problem that most methods do not, especially those defined over complicated geometries or incorporating heterogeneous material properties. Conventional analytical techniques are frequently restricted to idealized situations with straightforward boundary conditions and domains. By dividing the spatial domain into smaller, more manageable areas (finite elements) and employing a collection of basis (shape) functions to approximate the unknown solution inside each element, FEM gets over these restrictions. Over the whole domain, the set of these local approximations are used to create a global solution.

It is based on a variational approach. Its foundation is based on the weighted residual Galerkin technique, which selects the test functions from the same space as the trial

(approximation) functions. The PDE's solution is sought in a weaker (integrated) form rather than the classical meaning, allowing for less smooth and better suited numerical approximation solutions.

FEM can handle complex geometries through unstructured meshes. It accommodates a wide variety of boundary conditions. It supports varying material properties, nonlinearities, and coupled multi-physics problems.

A standard FEM process involves discretizing the continuous domain, converting the governing equations into their weak (variational) form, computing local element matrices and vectors, and assembling and solving a global system of algebraic equations. Additional quantities of interest can be derived from the final numerical solution, which gives approximate values of the field variable (such as temperature, and velocity) at the mesh's nodal points.

3.2 The Workflow and Detailed Description of Finite Element Method

In this section a detailed description of FEM is given.

3.2.1 Domain Discretization

The computational domain Ω is discretized into a finite number of smaller, non-overlapping subdomains known as elements. These components could be tetrahedra or hexahedra (3D), triangles or quadrilaterals (2D), or line segments (1D). Elements' corners are referred to as nodes. The mesh is the collection of all elements and nodes.

3.2.2 Selection of Shape Functions

Interpolation or shape functions defined over the element are used to approximate the unknown field variable (such as temperature, displacement, or velocity) within

each finite element. In a triangular element, for instance

$$u(x,y) \approx \sum_{i=1}^{3} u_i \, \phi_i(x,y)$$

where u_i are the nodal values and $\phi_i(x,y)$ are the shape functions associated with each node of the triangle, satisfying the Kronecker delta property

$$\phi_i(x_j) = \delta_{ij}$$

where, the Kronecker delta $\delta_{i,j}$ is defined as

$$\delta_{i,j} = \begin{cases} 1, & \text{if } i = j, \\ 0, & \text{if } i \neq j. \end{cases}$$

3.2.3 Derivation of the Weak Form

We transform the governing PDE into its *weak form* in order to develop the finite element equations. This is accomplished by integrating over the domain after multiplying the strong form by a test function v. For the PDE $\nabla u = f$,the weak form of the problem reads

$$\text{Find } u \in V \text{ such that } \int_\Omega \nabla u \cdot \nabla v \, d\Omega = \int_\Omega f v \, d\Omega, \quad \forall v \in V$$

This method makes it simpler to numerically approximate the answer by lowering the order of derivatives.

3.2.4 Element-Level Equation Formation

We calculate the local contributions to the load vector and stiffness matrix for every element by

$$[K^e]_{ij} = \int_{\Omega^e} \nabla \phi_i \cdot \nabla \phi_j \, d\Omega$$

and

$$[F^e]_i = \int_{\Omega^e} f\,\phi_i\,d\Omega.$$

Typically, numerical quadrature techniques like Gaussian quadrature are used to compute these integrals.

3.2.5 Assembly and the Global System

By integrating the contributions from each element, the local element matrices and vectors are put together into a global linear system while accounting for node connectivity. The globel system is expressed as

$$\mathbf{Ku} = \mathbf{F},$$

where $\mathbf{K}$ is the global stiffness matrix, $\mathbf{u}$ is the vector of unknowns at all nodes, and $\mathbf{F}$ is the global load vector.

3.2.6 Application of Boundary Conditions

Boundary conditions are incorporated into the system, which are of the following types

a) Dirichlet (essential) boundary conditions apply by adjusting the system of equations to describe the value of the solution on the boundary.

b) Neumann (natural) boundary conditions are added to the weak form as extra integrals and define the derivative (flux) on the boundary.

3.2.7 Solution of Algebraic System

The assembled linear system:

$$\mathbf{Ku} = \mathbf{F},$$

is solved by applying linear algebraic numerical methods.

3.2.8 Summary of the FEM Workflow

The steps involved in the FEM workflow are summarized as follows.

1. The domain is discretized into finite elements.
2. Choose shape functions for every piece.
3. Derive the weak form of the governing equations
4. Calculate local element matrices and vectors
5. Put together the global system of equations
6. Apply boundary conditions
7. Solve the algebraic system

3.3 The Galerkin Finite Element Method

One kind of weighted residual approach for approximating the solution of differential equations is the Galerkin technique. This approach is detailed on a working example in the next section.

3.4 Galerkin Finite Element Method: A Worked Example

Consider the boundary value problem as given below.

$$-\frac{d^2v}{dx^2} = 1, \quad x \in [0,1], \quad v(0) = v(1) = 0.$$

The exact solution of this problem is given as

$$v(x) = \frac{1}{2}x(1-x).$$

Next, we demostrate stepwise the GFEM for above boundary value problem.

3.4.1 Step 1: Weak Formulation

Multiply both sides by a test function $y(x)$ and integrate:

$$\int_0^1 -\frac{d^2v}{dx^2}y(x)\,dx = \int_0^1 y(x)\cdot 1\,dx.$$

Using integration by parts and $v(0) = v(1) = 0$

$$\int_0^1 \frac{dv}{dx}\frac{dy}{dx}\,dx = \int_0^1 y(x)\,dx.$$

The weak form is: find $v \in V$ such that

$$a(v, y) = l(y), \quad \forall y \in V,$$

where

$$a(v, y) = \int_0^1 v'(x)y'(x)\,dx, \quad l(y) = \int_0^1 y(x)\,dx.$$

3.4.2 Step 2: Finite Element Discretization

We divide the domain $[0, 1]$ into two finite elements as follows. The nodes are selected at $x_0 = 0$, $x_1 = 0.5$, and $x_2 = 1$.

Chose the basis function $\phi_1(x)$ as defined below

$$\phi_1(x) = \begin{cases} 2x, & 0 \le x \le 0.5 \\ 2(1-x), & 0.5 < x \le 1 \end{cases}$$

The basis function $\phi_1(x)$ satisfies the boundary conditions, i.e, $\phi_1(0) = \phi_1(1) = 0$, and $\phi_1(0.5) = 1$.

The solution is approximated as

$$v_h(x) = V_1 \cdot \phi_1(x),$$

where, V_1 is the undetermined coefficient.

3.4.3 Step 3: Stiffness Matrix

Compute the single entry of the stiffness matrix as

$$K_{11} = \int_0^1 (\phi_1'(x))^2 \, dx,$$

where,

$$\phi_1'(x) = \begin{cases} 2, & 0 \le x \le 0.5 \\ -2, & 0.5 < x \le 1 \end{cases}$$

$$\Rightarrow (\phi_1')^2 = 4$$

Thus,

$$K_{11} = \int_0^{0.5} 4 \, dx + \int_{0.5}^1 4 \, dx = 4(0.5) + 4(0.5) = 2 + 2 = 4.$$

3.4.4 Step 4: Load Vector

The load vector is computed as

$$F_1 = \int_0^1 f(x) \cdot \phi_1(x) \, dx = \int_0^{0.5} 2x \, dx + \int_{0.5}^1 2(1-x) \, dx. \tag{3.1}$$

In Eq. (3.1) the first integral is evaluated as

$$\int_0^{0.5} 2x \, dx = \left[x^2\right]_0^{0.5} = 0.25, \tag{3.2}$$

and the second integral is evaluated as

$$\int_{0.5}^1 2(1-x) \, dx = \left[2x - x^2\right]_{0.5}^1 = (2-1) - (1-0.25) = 1 - 0.75 = 0.25. \tag{3.3}$$

Adding Eq. (3.2) and Eq. (3.3) gives

$$F_1 = 0.25 + 0.25 = 0.5.$$

3.4.5 Step 5: Solve the System

The system is solved as

$$K_{11}V_1 = F_1 \Rightarrow 4V_1 = 0.5 \Rightarrow V_1 = \frac{1}{8} = 0.125.$$

3.4.6 Step 6: Final Approximate Solution

The final approximate solution is computed as

$$v_h(x) = 0.125 \cdot \phi_1(x) = \begin{cases} 0.125 \cdot 2x = \frac{x}{4}, & 0 \leq x \leq 0.5 \\ 0.125 \cdot 2(1-x) = \frac{1-x}{4}, & 0.5 < x \leq 1. \end{cases}$$

Step 7: Comparison with Exact Solution

The exact solution at $x = 0.5$ is given by

$$v(0.5) = \frac{1}{2} \cdot 0.5 \cdot 0.5 = 0.125.$$

The FEM solution also gives

$$u_h(0.5) = 0.125,$$

which matches exactly.

Thus, a good approximation is given by the Galerkin FEM with a single basis function, which matches the exact solution.

3.5 Two-dimensional Heat Equation Solved using the Galerkin Finite Element Method

3.5.1 Problem Statement

We solve the two-dimension steady-state heat equation given below

$$-\nabla^2 u = 1 \quad \text{in } \Omega = [0,1] \times [0,1], \tag{3.4}$$

with homogeneous Dirichlet boundary conditions as

$$u = 0 \quad \text{on } \partial\Omega.$$

The weak formulation of this problem is discussed below.

3.5.2 Weak Formulation

To develop the weak formulation we multiply the Eq (3.4) by a test function $v \in H_0^1(\Omega)$ and integrate over the domain Ω as follows

$$\int_\Omega -\nabla^2 u \cdot v \, d\Omega = \int_\Omega v \cdot 1 \, d\Omega. \tag{3.5}$$

Applying integration by parts implies

$$\int_\Omega \nabla u \cdot \nabla v \, d\Omega = \int_\Omega v \, d\Omega. \tag{3.6}$$

Thus, the weak formulation reads, find $u \in H_0^1(\Omega)$ such that:

$$\int_\Omega \nabla u \cdot \nabla v \, d\Omega = \int_\Omega v \, d\Omega \quad \forall v \in H_0^1(\Omega).$$

3.5.3 Mesh and Domain Discretization

We divide the unit square $[0,1] \times [0,1]$ into two right triangles where in triangle 1 the nodes are positioned at $(0,0), (1,0)$, and $(0,1)$, and in triangle 2 the nodes are positioned at $(1,1), (1,0)$, and $(0,1)$.

3.5.4 Shape Functions on Triangle 1

Since, the triangle 1 have vertices at

$$(x_1, y_1) = (0,0), \quad (x_2, y_2) = (1,0), \quad (x_3, y_3) = (0,1).$$

The linear shape functions are defined by

$$\phi_1 = 1 - x - y, \quad \phi_2 = x, \quad \phi_3 = y.$$

Their gradients are given as

$$\nabla\phi_1 = \begin{bmatrix} -1 \\ -1 \end{bmatrix}, \quad \nabla\phi_2 = \begin{bmatrix} 1 \\ 0 \end{bmatrix}, \quad \nabla\phi_3 = \begin{bmatrix} 0 \\ 1 \end{bmatrix}.$$

3.5.5 Element Stiffness Matrix

The local element stiffness matrix entries are calculate by

$$K_{ij}^{(e)} = \int_T \nabla\phi_i \cdot \nabla\phi_j \, d\Omega. \tag{3.7}$$

The area of the triangle T is given as

$$A = \frac{1}{2}.$$

Computing the dot products between $\nabla\phi_i$ and $\nabla\phi_j$ and integratig over thetriangular domain T we get

$$K^{(e)} = \frac{1}{2} \begin{bmatrix} 2 & -1 & -1 \\ -1 & 1 & 0 \\ -1 & 0 & 1 \end{bmatrix}. \tag{3.8}$$

3.5.6 Element Load Vector

The element load vector is computed as follows.

In our case $f = 1$, the local load vector is thus given as.

$$F_i^{(e)} = \int_T \phi_i \, d\Omega = \frac{A}{3} \quad \Rightarrow \quad F^{(e)} = \frac{1}{6} \begin{bmatrix} 1 \\ 1 \\ 1 \end{bmatrix}. \tag{3.9}$$

3.5.7 Global Assembly

For the assembly of finite elements the golbal nodes are numbered as below.

The node 1 is positioned at $(0, 0)$. Node number 2 is positioned as $(1, 0)$. Node number 3 is positioned as $(0, 1)$. And node number 4 is positioned at $(1, 1)$.

Global stiffness matrix $K \in \mathbb{R}^{4\times4}$ and load vector $F \in \mathbb{R}^4$ are assembled by adding the element matrices and vectors at the corresponding positions.

3.5.8 Boundary Conditions

Since all nodes lie on the boundary, we apply the boundary condition

$$u_i = 0 \quad \text{for } i = 1, 2, 3, 4$$

The system equations

$$KU = F$$

are solved to get the solution

$$u = \begin{bmatrix} 0 \\ 0 \\ 0 \\ 0 \end{bmatrix}.$$

This simple example illustrates the Galerkin FEM procedure in two-dimensional framework.

Chapter 4

Upper Convected Maxwell Flow in a Unit Square Domain

In this chapter, we investigate the unsteady flow of an incompressible UCM fluid inside a unit square domain, commonly referred to as the lid-driven cavity problem. This configuration serves as an ideal benchmark for understanding the dynamics of viscoelastic fluids under confined geometries, as it combines shear-dominated regions near the moving lid with recirculating vortical structures in the cavity interior. The UCM constitutive model is employed to describe the stress–strain relationship,in contrast, the constitutive equation for the extra-stress tensor and the continuity and momentum equations make up the governing equations.

4.1 Upper Convected Maxwell Constitutive Equation

The Upper Convected Maxwell (UCM) model is one of the most used models for describing the behavior of viscoelastic fluids. This model combines the effects of viscosity and relaxation time to characterize the fluid's response under deformation. The constitutive equation for the UCM model is expressed as:

$$\boldsymbol{\tau} + \lambda \boldsymbol{\tau}^{\nabla} = \frac{1}{2}\nu \left(\nabla \mathbf{u} + \nabla \mathbf{u}^{\intercal}\right), \tag{4.1}$$

which can be rearranged as:

$$\boldsymbol{\tau} = \frac{1}{2}\nu\left(\nabla\mathbf{u} + \nabla\mathbf{u}^{\intercal}\right) - \lambda\boldsymbol{\tau}^{\nabla}, \tag{4.2}$$

where λ denotes the characteristic relaxation time of the fluid and ν represents its viscosity.

The term $\boldsymbol{\tau}^{\nabla}$ in Eq. (4.2) is the upper-convected derivative of the extra-stress tensor $\boldsymbol{\tau}$, defined as:

$$\boldsymbol{\tau}^{\nabla} = \frac{\partial\boldsymbol{\tau}}{\partial t} + \mathbf{u}\cdot\nabla\boldsymbol{\tau} - \left(\nabla\mathbf{u}^{\intercal}\cdot\boldsymbol{\tau} + \boldsymbol{\tau}\cdot\nabla\mathbf{u}\right). \tag{4.3}$$

In this formulation, both λ and ν are assumed constant; however, in practice, they may vary with temperature, pressure, and local shear rate.

Substituting Eq. (4.3) into Eq. (4.2), we obtain the final form of the constitutive equation:

$$\boldsymbol{\tau} = \frac{1}{2}\nu\left(\nabla\mathbf{u} + \nabla\mathbf{u}^{\intercal}\right) - \lambda\left(\frac{\partial\boldsymbol{\tau}}{\partial t} + \mathbf{u}\cdot\nabla\boldsymbol{\tau} - \left(\nabla\mathbf{u}^{\intercal}\cdot\boldsymbol{\tau} + \boldsymbol{\tau}\cdot\nabla\mathbf{u}\right)\right). \tag{4.4}$$

For the present study, the flow inside a square lid-driven cavity is considered. The governing equations are based on the continuity and momentum equations for an incompressible viscoelastic fluid. The unsteady incompressible momentum equation is given by:

$$\rho\left(\frac{\partial\mathbf{u}}{\partial t} + \mathbf{u}\cdot\nabla\mathbf{u}\right) = -\nabla p + \nabla\cdot\boldsymbol{\tau}, \tag{4.5}$$

subject to the mass conservation constraint:

$$\nabla\cdot\mathbf{u} = 0, \tag{4.6}$$

where $\mathbf{u} = (u, v)$ represents the velocity vector, p is the pressure, ρ is the fluid density, and $\boldsymbol{\tau}$ denotes the extra-stress tensor arising from the viscoelastic nature of the fluid.

4.2 Calculation of Model Equations in Component Form

In order to derive the explicit component-wise form of the governing equations, each term of the Upper Convected Maxwell (UCM) constitutive relation is expanded systematically. The divergence of the extra-stress tensor, $\nabla \cdot \boldsymbol{\tau}$, is calculated by evaluating the derivatives of its individual components. These expressions are then substituted into the momentum equation to obtain the complete flow-governing set of coupled nonlinear partial differential equations inside the cavity. Detailed step-by-step derivations are presented below.

From Eq. (4.4), we take the divergence on both sides:

$$\nabla \cdot \tau = \nabla \cdot \left(\frac{1}{2}\nu(\nabla u + \nabla u^{\intercal}) - \lambda \left(\frac{\partial \tau}{\partial t} + u \cdot \nabla \tau - (\nabla u^{\intercal} \cdot \tau + \tau \cdot \nabla u) \right) \right). \tag{4.7}$$

We now compute each term in Eq. (4.7) step by step. Step 1: Gradient of the Velocity Tensor

The gradient of the velocity field is given by:

$$(\nabla u)_{ij} = \nabla_j \mathbf{e}_j \times u_i \mathbf{e}_i = u_{i,j}\, \mathbf{e}_i \times \mathbf{e}_j.$$

Thus,
$$\frac{1}{2}\nu(\nabla u + \nabla u^{\intercal}) = \frac{1}{2}\nu(u_{i,j} + u_{j,i})\, \mathbf{e}_i \times \mathbf{e}_j.$$

Taking the divergence of both sides

$$\nabla \cdot \frac{1}{2}\nu(\nabla u + \nabla u^{\intercal}) = \frac{1}{2}\nabla_j \mathbf{e}_j \cdot [\nu(u_{i,j} + u_{j,i})\mathbf{e}_i \times \mathbf{e}_j],$$

$$= \frac{1}{2}\nu(u_{j,jj} + u_{j,jj})\mathbf{e}_j,$$

$$= \nu\, \Delta u.$$

Step 2: Time Derivative of the Stress Tensor

For steady-state flow, the time derivative vanishes

$$\frac{\partial \tau}{\partial t} = 0.$$

Step 3: Convective Term

The convective term is computed as

$$(u\cdot\nabla)\left(\frac{1}{2}\nu(\nabla u+\nabla u^{\intercal})\right)=\frac{1}{2}\nu\left(u_i\nabla_i(u_{i,j}+u_{j,i})\mathbf{e}_i\times\mathbf{e}_j\right),$$

$$=\frac{1}{2}\nu\left(u_i(u_{i,ji}+u_{j,ii})\mathbf{e}_i\times\mathbf{e}_j\right).$$

Taking divergence on both sides yields

$$\nabla\cdot(u\cdot\nabla\tau)=\nabla_j\mathbf{e}_j\cdot\frac{1}{2}\nu\left(u_i(u_{i,ji}+u_{j,ii})\mathbf{e}_i\times\mathbf{e}_j\right),$$

$$=\frac{1}{2}\nu\nabla_k\left(u_k(u_{i,ki}+u_{k,ii})\mathbf{e}_k\right),$$

$$=\frac{1}{2}\nu\mathbf{e}_k\left(u_{k,k}(u_{i,ki}+u_{k,ii})+u_k(u_{i,kik}+u_{k,iik})\right).$$

Step 4: Other Tensor Contractions

The remaining terms involving $\nabla u^{\intercal}\cdot\tau$ and $\tau\cdot\nabla u$ are expanded similarly using index notation. After carrying out the expansions and collecting terms, we substitute the results back into Eq. (4.7), leading to

$$\nabla\cdot\tau_k=\frac{1}{2}\nu\mathbf{e}_k\Bigg(u_{k,kk}-\lambda\Big(u_{k,k}(u_{i,ki}+u_{k,ii})+u_k(u_{i,kik}+u_{k,iik})$$
$$-2u_{k,ik}u_{i,k}-2u_{k,i}u_{i,kk}-2u_{k,ik}u_{k,i}-2u_{i,kk}u_{i,k}\Big)\Bigg).\quad(4.8)$$

Step 5: Substitution into the Momentum Equation

Finally, substituting Eq. (4.8) into the momentum equation (4.5) gives the full component-wise form of the governing equation:

$$\rho\left(\frac{\partial u}{\partial t}+u\cdot\nabla u\right)=-\nabla p+\nu\Delta u-\frac{1}{2}\nu\lambda\Bigg(u\left(\frac{\partial^3 v}{\partial x^2\partial y}+\frac{\partial^3 u}{\partial x\partial y^2}+2\frac{\partial^3 u}{\partial x^3}\right)$$
$$+v\left(\frac{\partial^3 u}{\partial x\partial y^2}+\frac{\partial^3 v}{\partial x^2\partial y}+2\frac{\partial^3 v}{\partial y^3}\right)-6\left(\frac{\partial^2 u}{\partial x^2}\frac{\partial u}{\partial x}+\frac{\partial^2 v}{\partial y^2}\frac{\partial v}{\partial y}\right)$$
$$+\frac{\partial u}{\partial x}\left(\frac{\partial^2 v}{\partial x\partial y}+\frac{\partial^2 u}{\partial y^2}\right)+\frac{\partial v}{\partial y}\left(\frac{\partial^2 u}{\partial x\partial y}+\frac{\partial^2 v}{\partial x^2}\right)-2\left(\frac{\partial v}{\partial x}\frac{\partial^2 u}{\partial x\partial y}+\frac{\partial u}{\partial y}\frac{\partial^2 v}{\partial x^2}\right)$$
$$-2\left(\frac{\partial u}{\partial y}\frac{\partial^2 u}{\partial x\partial y}+\frac{\partial v}{\partial x}\frac{\partial^2 v}{\partial x^2}\right)-2\left(\frac{\partial u}{\partial y}\frac{\partial^2 v}{\partial x\partial y}+\frac{\partial v}{\partial x}\frac{\partial^2 u}{\partial y^2}\right)\Bigg).\quad(4.9)$$

4.3 Dimensional Form of the Governing Equations

The governing equations for the incompressible viscoelastic fluid flow based on the Upper Convected Maxwell (UCM) model are presented in this section in their dimensional form. The velocity vector is defined as $\mathbf{u} = (u, v)$, where u and v represent the velocity components in the x- and y-directions, respectively. The fluid pressure is denoted by p, and ρ represents the fluid density.

The governing equations consist of the continuity equation and the momentum equations, which are derived by combining the conservation of mass and momentum with the UCM constitutive relation.

Continuity Equation

The continuity equation for an incompressible fluid is expressed as:

$$\frac{\partial u}{\partial x} + \frac{\partial v}{\partial y} = 0. \tag{4.10}$$

Momentum Equations

The momentum equations for the two velocity components are derived from the Navier– Stokes equations(NSE) coupled with the UCM constitutive model. Momentum Equation for u-Velocity

$$\begin{aligned}\frac{\partial u}{\partial t} + u\frac{\partial u}{\partial x} + v\frac{\partial u}{\partial y} + \frac{1}{2}\nu\lambda\Bigg(u\left(\frac{\partial^3 v}{\partial x^2\partial y} + \frac{\partial^3 u}{\partial x\partial y^2} + 2\frac{\partial^3 u}{\partial x^3}\right) - 6\left(\frac{\partial^2 u}{\partial x^2}\right)\frac{\partial u}{\partial x} \\ + \frac{\partial u}{\partial x}\left(\frac{\partial^2 v}{\partial x\partial y} + \frac{\partial^2 u}{\partial y^2}\right) - 2\left(\frac{\partial v}{\partial x}\right)\left(\frac{\partial^2 u}{\partial x\partial y}\right) - 2\left(\frac{\partial u}{\partial y}\right)\left(\frac{\partial^2 v}{\partial x^2}\right) \\ - 2\left(\frac{\partial u}{\partial y}\right)\left(\frac{\partial^2 u}{\partial x\partial y}\right) - 2\left(\frac{\partial v}{\partial x}\right)\left(\frac{\partial^2 v}{\partial x^2}\right)\Bigg) = -\frac{1}{\rho}\frac{\partial p}{\partial x} + \nu\left(\frac{\partial^2 u}{\partial x^2} + \frac{\partial^2 u}{\partial y^2}\right).\end{aligned} \tag{4.11}$$

Momentum Equation for v-Velocity

$$\frac{\partial v}{\partial t} + u\frac{\partial v}{\partial x} + v\frac{\partial v}{\partial y} + \frac{1}{2}\nu\lambda\Bigg(v\left(\frac{\partial^3 u}{\partial x\partial y^2} + \frac{\partial^3 v}{\partial x^2\partial y} + 2\frac{\partial^3 v}{\partial y^3}\right) - 6\left(\frac{\partial^2 v}{\partial y^2}\right)\frac{\partial v}{\partial y} + \frac{\partial v}{\partial y}\left(\frac{\partial^2 u}{\partial x\partial y} + \frac{\partial^2 v}{\partial x^2}\right) - 2\left(\frac{\partial u}{\partial y}\right)\left(\frac{\partial^2 v}{\partial x\partial y}\right) - 2\left(\frac{\partial v}{\partial x}\right)\left(\frac{\partial^2 u}{\partial y^2}\right) - 2\left(\frac{\partial v}{\partial x}\right)\left(\frac{\partial^2 v}{\partial x\partial y}\right) - 2\left(\frac{\partial u}{\partial y}\right)\left(\frac{\partial^2 u}{\partial y^2}\right)\Bigg) = -\frac{1}{\rho}\frac{\partial p}{\partial y} + \nu\left(\frac{\partial^2 v}{\partial x^2} + \frac{\partial^2 v}{\partial y^2}\right). \quad (4.12)$$

4.4 Geometry of the Problem

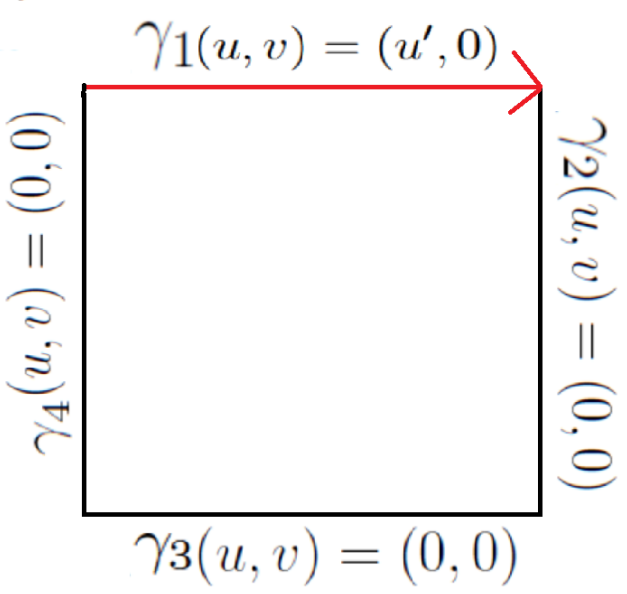

FIGURE 4.1: Schematic diagram of the square lid-driven cavity domain.

The computational domain, illustrated in Figure 4.1, is defined as a unit square region $\Omega = [0,1]\times[0,1]$. The domain is bounded by four sides, denoted as γ_1 (top), γ_2 (right), γ_3 (bottom), and γ_4 (left). The boundary conditions are imposed to represent the classical lid-driven cavity flow configuration, Where the top boundary travels at a steady speed, while the remaining three boundaries remain stationary.

The velocity boundary conditions are specified as follows:

- Top boundary (γ_1): The upper lid moves with a constant velocity u' along the x-direction, while there is no flow in the y-direction:

$$\mathbf{u} = (u,v) = (u',0), \quad \text{on } \gamma_1.$$

- Right boundary (γ_2): Stationary vertical wall with no-slip condition:

$$\mathbf{u} = (u, v) = (0, 0), \quad \text{on } \gamma_2.$$

- Bottom boundary (γ_3): Stationary horizontal wall with no-slip condition:

$$\mathbf{u} = (u, v) = (0, 0), \quad \text{on } \gamma_3.$$

- Left boundary (γ_4): Stationary vertical wall with no-slip condition:

$$\mathbf{u} = (u, v) = (0, 0), \quad \text{on } \gamma_4.$$

This configuration induces a primary circulation within the cavity, along with secondary vortices near the corners at higher Reynolds numbers, which will be analyzed in subsequent sections.

4.5 Dimensionless Form of the Governing Equations

In this section, the governing equations are transformed into their dimensionless form by introducing suitable characteristic scales for velocity, length, time, and pressure. This non-dimensionalization process simplifies the equations and highlights the influence of the key controlling parameters of the flow.

4.5.1 Dimensionless Parameters

The system of equations is normalized by adding the following non-dimensional variables given in Eqs. (4.10)–(4.12):

$$U = \frac{u}{u'}, \qquad V = \frac{v}{u'}, \qquad T = \frac{u't}{L}, \qquad X = \frac{x}{L}, \qquad Y = \frac{y}{L}, \qquad P = \frac{p}{\rho u'^2},$$

where:

- u and v are the velocity components along the x- and y-directions, respectively,
- u' is the characteristic lid velocity,
- L represents the characteristic length scale (taken as the cavity side length),
- t denotes time,
- p is the pressure, and
- ρ is the fluid density.

By substituting these dimensionless variables into the governing equations, the system is reformulated in a compact form where the dependence on the characteristic scales is eliminated. The resulting equations will be presented in the subsequent subsection.

4.6 Conversion from Dimensional to Dimensionless Form

To transform the governing equations (Eqs. (4.10)–(4.12)) into their dimensionless form, we introduce the following normalized variables:

$$X = \frac{x}{L}, \qquad Y = \frac{y}{L}, \qquad U = \frac{u}{u'}, \qquad V = \frac{v}{u'}, \qquad T = \frac{u't}{L}.$$

Here, L is the characteristic length scale, and u' is the reference velocity of the moving lid. By substituting these relations, the derivatives of the dimensional variables can be expressed in terms of their dimensionless counterparts.

4.6.1 First-Order Derivatives

Using the chain rule, the first-order derivatives become:

$$\frac{\partial u}{\partial t} = \frac{\partial (u'U)}{\partial T} \cdot \frac{\partial T}{\partial t} = \frac{u'^2}{L} \frac{\partial U}{\partial T},$$

$$\frac{\partial u}{\partial x} = \frac{\partial (u'U)}{\partial X} \cdot \frac{\partial X}{\partial x} = \frac{u'}{L} \frac{\partial U}{\partial X},$$

$$\frac{\partial u}{\partial y} = \frac{\partial (u'U)}{\partial Y} \cdot \frac{\partial Y}{\partial y} = \frac{u'}{L}\frac{\partial U}{\partial Y},$$
$$\frac{\partial v}{\partial x} = \frac{\partial (u'V)}{\partial X} \cdot \frac{\partial X}{\partial x} = \frac{u'}{L}\frac{\partial V}{\partial X},$$
$$\frac{\partial v}{\partial y} = \frac{\partial (u'V)}{\partial Y} \cdot \frac{\partial Y}{\partial y} = \frac{u'}{L}\frac{\partial V}{\partial Y}.$$

4.6.2 Second-Order Derivatives

Similarly, the second-order spatial derivatives are obtained as:

$$\frac{\partial^2 u}{\partial x^2} = \frac{u'}{L^2}\frac{\partial^2 U}{\partial X^2}, \qquad \frac{\partial^2 u}{\partial y^2} = \frac{u'}{L^2}\frac{\partial^2 U}{\partial Y^2},$$

$$\frac{\partial^2 v}{\partial x^2} = \frac{u'}{L^2}\frac{\partial^2 V}{\partial X^2}, \qquad \frac{\partial^2 v}{\partial y^2} = \frac{u'}{L^2}\frac{\partial^2 V}{\partial Y^2}.$$

4.6.3 Third-Order Derivatives

For third-order derivatives appearing in the UCM model, we obtain:

$$\frac{\partial^3 u}{\partial x^3} = \frac{u'}{L^3}\frac{\partial^3 U}{\partial X^3}, \qquad \frac{\partial^3 v}{\partial y^3} = \frac{u'}{L^3}\frac{\partial^3 V}{\partial Y^3},$$

$$\frac{\partial^3 u}{\partial x \partial y^2} = \frac{u'}{L^3}\frac{\partial^3 U}{\partial X \partial Y^2}, \qquad \frac{\partial^3 v}{\partial x^2 \partial y} = \frac{u'}{L^3}\frac{\partial^3 V}{\partial X^2 \partial Y}.$$

4.6.4 Nonlinear Derivative Combinations

For nonlinear terms involving products of first- and second-order derivatives, the dimensionless forms are:

$$\left(\frac{\partial^2 u}{\partial x^2}\right)\frac{\partial u}{\partial x} = \frac{u'^2}{L^3}\frac{\partial^2 U}{\partial X^2}\frac{\partial U}{\partial X},$$

$$\left(\frac{\partial^2 u}{\partial y^2}\right)\frac{\partial u}{\partial x} = \frac{u'^2}{L^3}\frac{\partial^2 U}{\partial Y^2}\frac{\partial U}{\partial X},$$
$$\left(\frac{\partial^2 v}{\partial x^2}\right)\frac{\partial u}{\partial y} = \frac{u'^2}{L^3}\frac{\partial^2 V}{\partial X^2}\frac{\partial U}{\partial Y},$$

$$\left(\frac{\partial^2 u}{\partial y^2}\right)\frac{\partial v}{\partial x} = \frac{u'^2}{L^3}\frac{\partial^2 U}{\partial Y^2}\frac{\partial V}{\partial X}.$$

All remaining mixed-product derivatives follow the same approach and scale similarly by a factor of $\frac{u'^2}{L^3}$.

By substituting these derivative transformations into the dimensional governing equations, we systematically obtain their dimensionless form.

This process eliminates explicit dependence on u', L, and ρ while introducing key dimensionless groups such as the Reynolds number and Weissenberg number, which govern the flow behavior.

4.7 Derivation of Dimensionless Governing Equations

In this section, we derive the dimensionless form of the governing equations from their dimensional counterparts by substituting the normalized variables:

$$X = \frac{x}{L}, \qquad Y = \frac{y}{L}, \qquad U = \frac{u}{u'}, \qquad V = \frac{v}{u'}, \qquad T = \frac{u't}{L}, \qquad P = \frac{p}{\rho u'^2}.$$

Here, L denotes the characteristic length, u' is the characteristic lid velocity, and ρ is the fluid density.

4.7.1 Continuity Equation

Starting from the dimensional continuity equation:

$$\frac{\partial u}{\partial x} + \frac{\partial v}{\partial y} = 0,$$

we substitute $u = u'U$, $v = u'V$, $x = LX$, and $y = LY$.

$$\frac{u'}{L}\frac{\partial U}{\partial X} + \frac{u'}{L}\frac{\partial V}{\partial Y} = 0.$$

Dividing through by $\frac{u'}{L} \neq 0$, the dimensionless form becomes:

$$\frac{\partial U}{\partial X} + \frac{\partial V}{\partial Y} = 0. \tag{4.13}$$

4.7.2 U-Momentum Equation

The dimensional u-momentum equation is

$$\begin{aligned}\frac{\partial u}{\partial t} + u\frac{\partial u}{\partial x} + v\frac{\partial u}{\partial y} + \frac{1}{2}\nu\lambda\Bigg[u\left(\frac{\partial^3 v}{\partial x^2\partial y} + \frac{\partial^3 u}{\partial x\partial y^2} + 2\frac{\partial^3 u}{\partial x^3}\right) \\ - 6\left(\frac{\partial^2 u}{\partial x^2}\right)\frac{\partial u}{\partial x} + \frac{\partial u}{\partial x}\left(\frac{\partial^2 v}{\partial x\partial y} + \frac{\partial^2 u}{\partial y^2}\right) - 2\frac{\partial v}{\partial x}\frac{\partial^2 u}{\partial x\partial y} - 2\frac{\partial u}{\partial y}\frac{\partial^2 v}{\partial x^2} - 2\frac{\partial u}{\partial y}\frac{\partial^2 u}{\partial x\partial y} \\ - 2\frac{\partial v}{\partial x}\frac{\partial^2 v}{\partial x^2}\Bigg] = -\frac{1}{\rho}\frac{\partial p}{\partial x} + \nu\left(\frac{\partial^2 u}{\partial x^2} + \frac{\partial^2 u}{\partial y^2}\right).\end{aligned} \tag{4.14}$$

Substitution of Dimensionless Variables

Using the relations:

$$\frac{\partial u}{\partial t} = \frac{u'^2}{L}\frac{\partial U}{\partial T}, \qquad \frac{\partial u}{\partial x} = \frac{u'}{L}\frac{\partial U}{\partial X}, \qquad \frac{\partial^2 u}{\partial x^2} = \frac{u'}{L^2}\frac{\partial^2 U}{\partial X^2}, \qquad \frac{\partial^3 u}{\partial x^3} = \frac{u'}{L^3}\frac{\partial^3 U}{\partial X^3},$$

Dividing through by $\frac{u'^2}{L}$ and substituting $P = \frac{p}{\rho u'^2}$ yields the compact dimensionless U-momentum equation:

$$\begin{aligned}\frac{\partial U}{\partial T} + U\frac{\partial U}{\partial X} + V\frac{\partial U}{\partial Y} + \frac{1}{2}\frac{W_i}{R_e}\Bigg[U\left(\frac{\partial^3 V}{\partial X^2\partial Y} + \frac{\partial^3 U}{\partial X\partial Y^2} + 2\frac{\partial^3 U}{\partial X^3}\right) \\ - 6\frac{\partial^2 U}{\partial X^2}\frac{\partial U}{\partial X} + \frac{\partial U}{\partial X}\left(\frac{\partial^2 V}{\partial X\partial Y} + \frac{\partial^2 U}{\partial Y^2}\right) - 2\frac{\partial V}{\partial X}\frac{\partial^2 U}{\partial X\partial Y} - 2\frac{\partial U}{\partial Y}\frac{\partial^2 V}{\partial X^2} \\ - 2\frac{\partial U}{\partial Y}\frac{\partial^2 U}{\partial X\partial Y} - 2\frac{\partial V}{\partial X}\frac{\partial^2 V}{\partial X^2}\Bigg] = -\frac{\partial P}{\partial X} + \frac{1}{R_e}\left(\frac{\partial^2 U}{\partial X^2} + \frac{\partial^2 U}{\partial Y^2}\right).\end{aligned} \tag{4.15}$$

4.7.3 V-Momentum Equation

Following the same procedure for the v-momentum equation, we obtain its dimensionless form:

$$\frac{\partial V}{\partial T} + U\frac{\partial V}{\partial X} + V\frac{\partial V}{\partial Y} + \frac{1}{2}\frac{W_i}{R_e}\Bigg[V\left(\frac{\partial^3 U}{\partial X \partial Y^2} + \frac{\partial^3 V}{\partial X^2 \partial Y} + 2\frac{\partial^3 V}{\partial Y^3}\right) - 6\frac{\partial^2 V}{\partial Y^2}\frac{\partial V}{\partial Y} + \frac{\partial V}{\partial Y}\left(\frac{\partial^2 U}{\partial X \partial Y} + \frac{\partial^2 V}{\partial X^2}\right) - 2\frac{\partial U}{\partial Y}\frac{\partial^2 V}{\partial X \partial Y} - 2\frac{\partial V}{\partial X}\frac{\partial^2 U}{\partial Y^2} - 2\frac{\partial V}{\partial X}\frac{\partial^2 V}{\partial X \partial Y} - 2\frac{\partial U}{\partial Y}\frac{\partial^2 U}{\partial Y^2}\Bigg] = -\frac{\partial P}{\partial Y} + \frac{1}{R_e}\left(\frac{\partial^2 V}{\partial X^2} + \frac{\partial^2 V}{\partial Y^2}\right). \quad (4.16)$$

4.7.4 Final Set of Dimensionless Equations

The complete non-dimensional governing equations are:

Continuity Equation:

$$\frac{\partial U}{\partial X} + \frac{\partial V}{\partial Y} = 0.$$

U-Momentum Equation: Eq. (4.15). V-Momentum Equation: Eq. (4.16).

Here, the two key non-dimensional numbers are:

$$R_e = \frac{Lu'}{\nu}, \qquad W_i = \frac{\lambda u'}{L}.$$

4.7.5 Dimensionless Boundary Conditions

The dimensionless boundary conditions for the square lid-driven cavity are defined as follows:

- **Top boundary** γ_1: Moving lid with a constant unit velocity in the x-direction

$$\mathbf{U} = (U, V) = (1, 0), \quad \text{on } \gamma_1.$$

- **Right boundary** γ_2: Stationary vertical wall

$$\mathbf{U} = (U, V) = (0, 0), \quad \text{on } \gamma_2.$$

- **Bottom boundary** γ_3: Stationary horizontal wall

$$\mathbf{U} = (U, V) = (0, 0), \quad \text{on } \gamma_3.$$

- **Left boundary** γ_4: Stationary vertical wall

$$\mathbf{U} = (U, V) = (0, 0), \quad \text{on } \gamma_4.$$

4.8 Weak Formulation of the Problem

In this section, we present the weak formulation corresponding to the governing equations defined in Eq. (4.13)–Eq. (4.16). To derive the weak form, we first revisit the strong form of the governing equations.

4.8.1 Strong Form of the Governing Equations

The non-dimensional form of the incompressible Upper Convected Maxwell (UCM) equations in a unit square domain $\Omega = [0, 1] \times [0, 1]$ with boundary Γ is given as follows:

4.8.1.1 Continuity Equation

$$\frac{\partial U}{\partial X} + \frac{\partial V}{\partial Y} = 0, \tag{4.17}$$

which ensures the incompressibility condition.

4.8.1.2 Momentum Equation in the X-Direction

$$\frac{\partial U}{\partial T} + U\frac{\partial U}{\partial X} + V\frac{\partial U}{\partial Y} + \frac{1}{2}\frac{W_i}{R_e}\Bigg[U\left(\frac{\partial^3 V}{\partial X^2 \partial Y} + \frac{\partial^3 U}{\partial X \partial Y^2} + 2\frac{\partial^3 U}{\partial X^3}\right) - 6\left(\frac{\partial^2 U}{\partial X^2}\right)\frac{\partial U}{\partial X}$$
$$+ \frac{\partial U}{\partial X}\left(\frac{\partial^2 V}{\partial X \partial Y} + \frac{\partial^2 U}{\partial Y^2}\right) - 2\frac{\partial V}{\partial X}\frac{\partial^2 U}{\partial X \partial Y} - 2\frac{\partial U}{\partial Y}\frac{\partial^2 V}{\partial X^2} - 2\frac{\partial U}{\partial Y}\frac{\partial^2 U}{\partial X \partial Y} - 2\frac{\partial V}{\partial X}\frac{\partial^2 V}{\partial X^2}\Bigg]$$
$$= -\frac{\partial P}{\partial X} + \frac{1}{R_e}\left(\frac{\partial^2 U}{\partial X^2} + \frac{\partial^2 U}{\partial Y^2}\right). \tag{4.18}$$

4.8.1.3 Momentum Equation in the Y-Direction

$$\frac{\partial V}{\partial T}+U\frac{\partial V}{\partial X}+V\frac{\partial V}{\partial Y}+\frac{1}{2}\frac{W_i}{R_e}\Bigg[V\left(\frac{\partial^3 U}{\partial X\partial Y^2}+\frac{\partial^3 V}{\partial X^2\partial Y}+2\frac{\partial^3 V}{\partial Y^3}\right)-6\left(\frac{\partial^2 V}{\partial Y^2}\right)\frac{\partial V}{\partial Y}$$
$$+\frac{\partial V}{\partial Y}\left(\frac{\partial^2 U}{\partial X\partial Y}+\frac{\partial^2 V}{\partial X^2}\right)-2\frac{\partial U}{\partial Y}\frac{\partial^2 V}{\partial X\partial Y}-2\frac{\partial V}{\partial X}\frac{\partial^2 U}{\partial Y^2}-2\frac{\partial V}{\partial X}\frac{\partial^2 V}{\partial X\partial Y}-2\frac{\partial U}{\partial Y}\frac{\partial^2 U}{\partial Y^2}\Bigg]$$
$$=-\frac{\partial P}{\partial Y}+\frac{1}{R_e}\left(\frac{\partial^2 V}{\partial X^2}+\frac{\partial^2 V}{\partial Y^2}\right). \quad (4.19)$$

4.8.2 Weak Formulation of the u-Momentum Equation

The weak form of the u-component of the momentum Eq. (4.18) is derived in this section. Starting from the strong form:

$$\frac{\partial U}{\partial T}+U\frac{\partial U}{\partial X}+V\frac{\partial U}{\partial Y}+\frac{1}{2}\frac{W_i}{R_e}\Bigg[U\left(\frac{\partial^3 V}{\partial X^2\partial Y}+\frac{\partial^3 U}{\partial X\partial Y^2}+2\frac{\partial^3 U}{\partial X^3}\right)-6\left(\frac{\partial^2 U}{\partial X^2}\right)\frac{\partial U}{\partial X}$$
$$+\frac{\partial U}{\partial X}\left(\frac{\partial^2 V}{\partial X\partial Y}+\frac{\partial^2 U}{\partial Y^2}\right)-2\frac{\partial V}{\partial X}\frac{\partial^2 U}{\partial X\partial Y}-2\frac{\partial U}{\partial Y}\frac{\partial^2 V}{\partial X^2}-2\frac{\partial U}{\partial Y}\frac{\partial^2 U}{\partial X\partial Y}-2\frac{\partial V}{\partial X}\frac{\partial^2 V}{\partial X^2}\Bigg]$$
$$=-\frac{\partial P}{\partial X}+\frac{1}{R_e}\left(\frac{\partial^2 U}{\partial X^2}+\frac{\partial^2 U}{\partial Y^2}\right).$$

4.8.2.1 Step 1: Multiplying by Test Function and Integrating

We integrate throughout the computational domain Ω after multiplying the equation by a test function $\tilde{U}$:

$$\int_\Omega\left(\frac{\partial U}{\partial T}+U\frac{\partial U}{\partial X}+V\frac{\partial U}{\partial Y}\right)\tilde{U}\,d\Omega+\frac{1}{2}\frac{W_i}{R_e}\int_\Omega\Bigg[U\left(\frac{\partial^3 V}{\partial X^2\partial Y}+\frac{\partial^3 U}{\partial X\partial Y^2}+2\frac{\partial^3 U}{\partial X^3}\right)\tilde{U}$$
$$-6\frac{\partial^2 U}{\partial X^2}\frac{\partial U}{\partial X}\tilde{U}+\frac{\partial U}{\partial X}\left(\frac{\partial^2 V}{\partial X\partial Y}+\frac{\partial^2 U}{\partial Y^2}\right)\tilde{U}-2\frac{\partial V}{\partial X}\frac{\partial^2 U}{\partial X\partial Y}\tilde{U}-2\frac{\partial U}{\partial Y}\frac{\partial^2 V}{\partial X^2}\tilde{U}$$
$$-2\frac{\partial U}{\partial Y}\frac{\partial^2 U}{\partial X\partial Y}\tilde{U}-2\frac{\partial V}{\partial X}\frac{\partial^2 V}{\partial X^2}\tilde{U}\Bigg]\,d\Omega=-\int_\Omega\frac{\partial P}{\partial X}\tilde{U}\,d\Omega+\frac{1}{R_e}\int_\Omega\left(\frac{\partial^2 U}{\partial X^2}+\frac{\partial^2 U}{\partial Y^2}\right)\tilde{U}\,d\Omega. \quad (4.20)$$

4.8.2.2 Step 2: Integration by Parts for Third-Order Derivatives

To reduce third-order derivatives, we repeatedly apply integration by parts. For example, consider:

$$\frac{\partial}{\partial Y}\left(U\frac{\partial^2 V}{\partial X^2}\tilde{U}\right) = \frac{\partial U}{\partial Y}\frac{\partial^2 V}{\partial X^2}\tilde{U} + U\frac{\partial^3 V}{\partial X^2 \partial Y}\tilde{U} + U\frac{\partial^2 V}{\partial X^2}\frac{\partial \tilde{U}}{\partial Y}.$$

Rearranging gives:

$$U\frac{\partial^3 V}{\partial X^2 \partial Y}\tilde{U} = \frac{\partial}{\partial Y}\left(U\frac{\partial^2 V}{\partial X^2}\tilde{U}\right) - \frac{\partial U}{\partial Y}\frac{\partial^2 V}{\partial X^2}\tilde{U} - U\frac{\partial^2 V}{\partial X^2}\frac{\partial \tilde{U}}{\partial Y}.$$

Similar manipulations are applied to all other third-order derivative terms in Eq. (4.20).

4.8.2.3 Step 3: Final Weak Form

After simplification and applying the divergence theorem, the weak form of the u-momentum equation becomes

$$\int_\Omega \frac{\partial U}{\partial T}\tilde{U}\,d\Omega + \int_\Omega \left(U\frac{\partial U}{\partial X} + V\frac{\partial U}{\partial Y}\right)\tilde{U}\,d\Omega + \frac{W_i}{2R_e}\int_\Omega \mathcal{N}_U(U,V,\tilde{U})\,d\Omega = \int_\Omega P\frac{\partial \tilde{U}}{\partial X}\,d\Omega + \frac{1}{R_e}\int_\Omega \left(\frac{\partial^2 U}{\partial X^2} + \frac{\partial^2 U}{\partial Y^2}\right)\tilde{U}\,d\Omega, \quad (4.21)$$

where $\mathcal{N}_U(U,V,\tilde{U})$ collects all the nonlinear higher-order derivative terms involving U, V, and $\tilde{U}$.

4.8.3 Weak Formulation of the v-Momentum Equation

Similarly, we derive the weak form of the v-component of the momentum equation (4.19). The strong form is

$$\frac{\partial V}{\partial T} + U\frac{\partial V}{\partial X} + V\frac{\partial V}{\partial Y} + \frac{1}{2}\frac{W_i}{R_e}\left[V\left(\frac{\partial^3 U}{\partial X \partial Y^2} + \frac{\partial^3 V}{\partial X^2 \partial Y} + 2\frac{\partial^3 V}{\partial Y^3}\right) - 6\left(\frac{\partial^2 V}{\partial Y^2}\right)\frac{\partial V}{\partial Y} + \frac{\partial V}{\partial Y}\left(\frac{\partial^2 U}{\partial X \partial Y} + \frac{\partial^2 V}{\partial X^2}\right) - 2\frac{\partial U}{\partial Y}\frac{\partial^2 V}{\partial X \partial Y} - 2\frac{\partial V}{\partial X}\frac{\partial^2 U}{\partial Y^2} - 2\frac{\partial V}{\partial X}\frac{\partial^2 V}{\partial X \partial Y} - 2\frac{\partial U}{\partial Y}\frac{\partial^2 U}{\partial Y^2}\right] = -\frac{\partial P}{\partial Y} + \frac{1}{R_e}\left(\frac{\partial^2 V}{\partial X^2} + \frac{\partial^2 V}{\partial Y^2}\right).$$

4.8.3.1 Step 1: Multiplying by Test Function

We integrate throughout the computational domain Ω after multiplying the equation by a test function $\tilde{v}$.

$$\int_\Omega \left(\frac{\partial V}{\partial T} + U\frac{\partial V}{\partial X} + V\frac{\partial V}{\partial Y}\right)\tilde{V}\,d\Omega + \frac{1}{2}\frac{W_i}{R_e}\int_\Omega \Bigg[V\left(\frac{\partial^3 U}{\partial X\partial Y^2} + \frac{\partial^3 V}{\partial X^2\partial Y} + 2\frac{\partial^3 V}{\partial Y^3}\right)\tilde{V}$$
$$-6\frac{\partial^2 V}{\partial Y^2}\frac{\partial V}{\partial Y}\tilde{V} + \frac{\partial V}{\partial Y}\left(\frac{\partial^2 U}{\partial X\partial Y} + \frac{\partial^2 V}{\partial X^2}\right)\tilde{V} - 2\frac{\partial U}{\partial Y}\frac{\partial^2 V}{\partial X\partial Y}\tilde{V} - 2\frac{\partial V}{\partial X}\frac{\partial^2 U}{\partial Y^2}\tilde{V} - 2\frac{\partial V}{\partial X}\frac{\partial^2 V}{\partial X\partial Y}\tilde{V}$$
$$- 2\frac{\partial U}{\partial Y}\frac{\partial^2 U}{\partial Y^2}\tilde{V}\Bigg]\,d\Omega = -\int_\Omega \frac{\partial P}{\partial Y}\tilde{V}\,d\Omega + \frac{1}{R_e}\int_\Omega \left(\frac{\partial^2 V}{\partial X^2} + \frac{\partial^2 V}{\partial Y^2}\right)\tilde{V}\,d\Omega. \quad (4.22)$$

4.8.3.2 Step 2: Integration by Parts for Higher-Order Terms

To handle the third-order derivatives, we repeatedly apply integration by parts.

For example, consider:

$$\frac{\partial}{\partial X}\left(V\frac{\partial^2 U}{\partial Y^2}\tilde{V}\right) = \frac{\partial V}{\partial X}\frac{\partial^2 U}{\partial Y^2}\tilde{V} + V\frac{\partial^3 U}{\partial X\partial Y^2}\tilde{V} + V\frac{\partial^2 U}{\partial Y^2}\frac{\partial \tilde{V}}{\partial X},$$

which leads to

$$V\frac{\partial^3 U}{\partial X\partial Y^2}\tilde{V} = \frac{\partial}{\partial X}\left(V\frac{\partial^2 U}{\partial Y^2}\tilde{V}\right) - \frac{\partial V}{\partial X}\frac{\partial^2 U}{\partial Y^2}\tilde{V} - V\frac{\partial^2 U}{\partial Y^2}\frac{\partial \tilde{V}}{\partial X}.$$

Similar manipulations are applied to other terms involving $\partial^3 V/\partial X^2\partial Y$ and $\partial^3 V/\partial Y^3$.

4.8.3.3 Step 3: Final Weak Form

After simplifying and using the divergence theorem, we obtain the weak form of the v-momentum equation

$$\int_\Omega \frac{\partial V}{\partial T}\tilde{V}\,d\Omega + \int_\Omega \left(U\frac{\partial V}{\partial X} + V\frac{\partial V}{\partial Y}\right)\tilde{V}\,d\Omega + \frac{W_i}{2R_e}\int_\Omega \mathcal{N}_V(U,V,\tilde{V})\,d\Omega$$
$$= \int_\Omega P\frac{\partial \tilde{V}}{\partial Y}\,d\Omega + \frac{1}{R_e}\int_\Omega \left(\frac{\partial^2 V}{\partial X^2} + \frac{\partial^2 V}{\partial Y^2}\right)\tilde{V}\,d\Omega, \quad (4.23)$$

where $\mathcal{N}_V(U, V, \tilde{V})$ collects all nonlinear viscoelastic and higher-order derivative terms.

4.9 Finite Element Modeling

For the Galerkin discretization and finite element modeling, we define the following approximation space:

$$\bar{W}_h := \{\mathbf{V} \in [H^2(\Omega)]^2\},$$

where the trial and test functions are approximated as:

$$U \approx U_h, \quad V \approx V_h, \quad \tilde{U} \approx \tilde{U}_h, \quad \tilde{V} \approx \tilde{V}_h, \quad P \approx P_h.$$

1. Discretized Weak Form for the U-Momentum Equation

The discrete formulation for the x-momentum equation reads

$$\begin{aligned}
&\frac{1}{\delta t}\int_{\Omega^{n+1}} U_h^{n+1}\tilde{U}_h\,d\Omega - \frac{1}{\delta t}\int_{\Omega^{n+1}} (U_h^n \circ X^n)\,\tilde{U}_h\,d\Omega \\
&\quad + \frac{1}{2}\frac{W_i}{R_e}\Bigg(\int_{\Omega^{n+1}} \frac{\partial^2 U_h^n}{\partial X \partial Y}\frac{\partial V_h^{n+1}}{\partial X}\tilde{U}_h\,d\Omega + \int_{\Omega^{n+1}} \frac{\partial U_h^{n+1}}{\partial Y}\frac{\partial V_h^n}{\partial X}\frac{\partial \tilde{U}_h}{\partial X}\,d\Omega \\
&\qquad - \int_{\Omega^{n+1}} U_h^n \frac{\partial^2 V_h^{n+1}}{\partial X^2}\frac{\partial \tilde{U}_h}{\partial Y}\,d\Omega + \int_{\Omega^{n+1}} \frac{\partial^2 U_h^{n+1}}{\partial X \partial Y}\frac{\partial U_h^n}{\partial Y}\tilde{U}_h\,d\Omega \\
&\qquad + \int_{\Omega^{n+1}} \frac{\partial U_h^n}{\partial X}\frac{\partial U_h^{n+1}}{\partial Y}\frac{\partial \tilde{U}_h}{\partial Y}\,d\Omega - \int_{\Omega^{n+1}} U_h^{n+1}\frac{\partial^2 U_h^n}{\partial Y^2}\frac{\partial \tilde{U}_h}{\partial X}\,d\Omega \\
&\qquad + \int_{\Omega^{n+1}} \frac{\partial U_h^n}{\partial X}\frac{\partial U_h^{n+1}}{\partial X}\frac{\partial \tilde{U}_h}{\partial X}\,d\Omega - 2\int_{\Omega^{n+1}} U_h^n \frac{\partial^2 U_h^{n+1}}{\partial X^2}\frac{\partial \tilde{U}_h}{\partial X}\,d\Omega \\
&\qquad - 3\int_{\Omega^{n+1}} \frac{\partial U_h^{n+1}}{\partial X}\frac{\partial U_h^n}{\partial X}\frac{\partial \tilde{U}_h}{\partial X}\,d\Omega - \int_{\Omega^{n+1}} \frac{\partial^2 U_h^n}{\partial X^2}\frac{\partial V_h^{n+1}}{\partial Y}\tilde{U}_h\,d\Omega \\
&\qquad - \int_{\Omega^{n+1}} \frac{\partial U_h^{n+1}}{\partial X}\frac{\partial V_h^n}{\partial Y}\frac{\partial \tilde{U}_h}{\partial X}\,d\Omega - \int_{\Omega^{n+1}} \frac{\partial^2 U_h^{n+1}}{\partial X \partial Y}\frac{\partial U_h^n}{\partial Y}\tilde{U}_h\,d\Omega \\
&\qquad - \int_{\Omega^{n+1}} \frac{\partial U_h^n}{\partial X}\frac{\partial U_h^{n+1}}{\partial Y}\frac{\partial \tilde{U}_h}{\partial Y}\,d\Omega - 2\int_{\Omega^{n+1}} \frac{\partial^2 V_h^n}{\partial X^2}\frac{\partial U_h^{n+1}}{\partial Y}\tilde{U}_h\,d\Omega \\
&\qquad - 2\int_{\Omega^{n+1}} \frac{\partial V_h^{n+1}}{\partial X}\frac{\partial U_h^n}{\partial Y}\frac{\partial \tilde{U}_h}{\partial X}\,d\Omega - 2\int_{\Omega^{n+1}} \frac{\partial^2 U_h^{n+1}}{\partial X \partial Y}\frac{\partial V_h^n}{\partial X}\tilde{U}_h\,d\Omega \\
&\qquad - 2\int_{\Omega^{n+1}} \frac{\partial U_h^n}{\partial Y}\frac{\partial V_h^{n+1}}{\partial X}\frac{\partial \tilde{U}_h}{\partial X}\,d\Omega - 2\int_{\Omega^{n+1}} \frac{\partial^2 U_h^n}{\partial Y^2}\frac{\partial U_h^{n+1}}{\partial X}\tilde{U}_h\,d\Omega
\end{aligned}$$

$$
\begin{aligned}
&- 2\int_{\Omega^{n+1}} \frac{\partial U_h^{n+1}}{\partial Y}\frac{\partial U_h^{n}}{\partial X}\frac{\partial \tilde{U}_h}{\partial Y}\,d\Omega - \int_{\Omega^{n+1}} \frac{\partial V_h^{n+1}}{\partial X}\frac{\partial V_h^{n}}{\partial X}\frac{\partial \tilde{U}_h}{\partial X}\,d\Omega\Bigg) \\
&\quad = P_h^{n+1}\int_{\Omega^n}\frac{\partial \tilde{U}_h}{\partial X}\,d\Omega + \frac{1}{R_e}\Bigg[-\int_{\Omega^{n+1}}\frac{\partial U_h^{n+1}}{\partial X}\frac{\partial \tilde{U}_h}{\partial X}\,d\Omega + \int_\Gamma \tilde{U}_h\, n_x \frac{\partial U_h^{n+1}}{\partial X}\,d\Gamma \\
&\qquad\qquad - \int_{\Omega^{n+1}}\frac{\partial U_h^{n+1}}{\partial Y}\frac{\partial \tilde{U}_h}{\partial Y}\,d\Omega + \int_\Gamma \tilde{U}_h\, n_y \frac{\partial U_h^{n+1}}{\partial Y}\,d\Gamma\Bigg]. \quad (4.24)
\end{aligned}
$$

2. Discretized Weak Form for the V-Momentum Equation

Similarly, the discrete formulation for the y-momentum equation reads

$$
\begin{aligned}
&\frac{1}{\delta t}\int_{\Omega^{n+1}} V_h^{n+1}\tilde{V}_h\,d\Omega - \frac{1}{\delta t}\int_{\Omega^{n+1}}(V_h^n\circ Y^n)\,\tilde{V}_h\,d\Omega \\
&\qquad + \frac{1}{2}\frac{W_i}{R_e}\Bigg(\int_{\Omega^{n+1}}\frac{\partial^2 V_h^n}{\partial X\partial Y}\frac{\partial U_h^{n+1}}{\partial Y}\tilde{V}_h\,d\Omega + \int_{\Omega^{n+1}}\frac{\partial V_h^{n+1}}{\partial X}\frac{\partial U_h^{n}}{\partial Y}\frac{\partial \tilde{V}_h}{\partial Y}\,d\Omega \\
&- \int_{\Omega^{n+1}} V_h^{n+1}\frac{\partial^2 U_h^n}{\partial Y^2}\frac{\partial \tilde{V}_h}{\partial X}\,d\Omega + \int_{\Omega^{n+1}}\frac{\partial^2 V_h^n}{\partial X\partial Y}\frac{\partial V_h^{n+1}}{\partial X}\tilde{V}_h d\Omega + \int_{\Omega^{n+1}}\frac{\partial V_h^n}{\partial Y}\frac{\partial V_h^{n+1}}{\partial X}\frac{\partial \tilde{V}_h}{\partial X}d\Omega \\
&- \int_{\Omega^{n+1}} V_h^{n+1}\frac{\partial^2 V_h^n}{\partial X^2}\frac{\partial \tilde{V}_h}{\partial Y}d\Omega + \int_{\Omega^{n+1}}\frac{\partial V_h^{n+1}}{\partial Y}\frac{\partial V_h^n}{\partial Y}\frac{\partial \tilde{V}_h}{\partial Y}d\Omega - 2\int_{\Omega^{n+1}} V_h^n\frac{\partial^2 V_h^{n+1}}{\partial Y^2}\frac{\partial \tilde{V}_h}{\partial Y}d\Omega \\
&- 3\int_{\Omega^{n+1}}\frac{\partial V_h^n}{\partial Y}\frac{\partial V_h^{n+1}}{\partial Y}\frac{\partial \tilde{V}_h}{\partial Y}d\Omega - \int_{\Omega^{n+1}}\frac{\partial^2 V_h^{n+1}}{\partial Y^2}\frac{\partial U_h^n}{\partial X}\tilde{V}_h d\Omega - \int_{\Omega^{n+1}}\frac{\partial V_h^{n+1}}{\partial Y}\frac{\partial U_h^n}{\partial X}\cdot\frac{\partial \tilde{V}_h}{\partial Y}d\Omega \\
&\quad - \int_{\Omega^{n+1}}\frac{\partial^2 V_h^n}{\partial X\partial Y}\frac{\partial V_h^{n+1}}{\partial X}\cdot\tilde{V}_h d\Omega - \int_{\Omega^{n+1}}\frac{\partial V_h^n}{\partial Y}\frac{\partial V_h^{n+1}}{\partial X}\frac{\partial \tilde{V}_h}{\partial X}d\Omega - 2\int_{\Omega^{n+1}}\frac{\partial^2 U_h^{n+1}}{\partial Y^2} \\
&\quad \frac{\partial V_h^n}{\partial X}\tilde{V}_h d\Omega - 2\int_{\Omega^{n+1}}\frac{\partial U_h^{n+1}}{\partial Y}\frac{\partial V_h^n}{\partial X}\cdot\frac{\partial \tilde{V}_h}{\partial Y}d\Omega - 2\int_{\Omega^{n+1}}\frac{\partial^2 V_h^n}{\partial X\partial Y}\frac{\partial U_h^{n+1}}{\partial Y}\tilde{V}_h d\Omega \\
&\quad - 2\int_{\Omega^{n+1}}\frac{\partial V_h^n}{\partial X}\cdot\frac{\partial U_h^{n+1}}{\partial Y}\frac{\partial \tilde{V}_h}{\partial Y}d\Omega - 2\int_{\Omega^{n+1}}\frac{\partial^2 V_h^{n+1}}{\partial X^2}\frac{\partial V_h^n}{\partial Y}\tilde{V}_h d\Omega - 2\int_{\Omega^{n+1}}\frac{\partial V_h^{n+1}}{\partial X} \\
&\qquad \frac{\partial V_h^n}{\partial Y}\frac{\partial \tilde{V}_h}{\partial X}d\Omega - \int_{\Omega^{n+1}}\frac{\partial U_h^n}{\partial Y}\frac{\partial U_h^{n+1}}{\partial Y}\frac{\partial \tilde{V}_h}{\partial Y}d\Omega\Bigg) = P_h^{n+1}\int_{\Omega^n}\frac{\partial \tilde{V}_h}{\partial Y}\,d\Omega \\
&\quad + \frac{1}{R_e}\Bigg[-\int_{\Omega^{n+1}}\frac{\partial V_h^{n+1}}{\partial X}\frac{\partial \tilde{V}_h}{\partial X}\,d\Omega + \int_\Gamma \tilde{V}_h\, n_x\frac{\partial V_h^{n+1}}{\partial X}\,d\Gamma - \int_{\Omega^{n+1}}\frac{\partial V_h^{n+1}}{\partial Y}\frac{\partial \tilde{V}_h}{\partial Y}\,d\Omega \\
&\qquad\qquad + \int_\Gamma \tilde{V}_h\, n_y\frac{\partial V_h^{n+1}}{\partial Y}\,d\Gamma\Bigg]. \quad (4.25)
\end{aligned}
$$

For all $\tilde{U}_h, \tilde{V}_h \in W_h$ and $P_h \in Q_h$.

4.10 Finite Element Approximation

The finite element approximation is carried out by representing the unknown field variables using approximate trial solution functions, which are expressed as linear combinations of nodal unknowns and shape functions. These shape functions are chosen to be linearly independent and satisfy the required interpolation properties.

The approximate trial solutions for velocity components and pressure are defined as:

$$U_h = \sum_{i=1}^{m} U_i \, \phi_i, \qquad V_h = \sum_{i=1}^{m} V_i \, \phi_i, \qquad P_h = \sum_{i=1}^{l} P_i \, \psi_i,$$

where U_i, V_i, and P_i represent the nodal values of the respective variables, while ϕ_i and ψ_i are the velocity and pressure shape functions, respectively.

Similarly, the test (weighting) functions for the velocity components are approximated as:

$$\tilde{U}_h = \sum_{j=1}^{m} \tilde{U}_j \, \phi_j, \qquad \tilde{V}_h = \sum_{j=1}^{m} \tilde{V}_j \, \phi_j.$$

By substituting these approximations into the variational formulation given by Eqs. (4.24) and (4.25), the weak form of the problem is obtained.

4.10.1 Weak Formulation for the U-Momentum Equation

Using the trial and test functions, the weak formulation of the U-momentum equation is expressed as

$$\begin{aligned}
&\frac{1}{\delta t} \int_{\Omega^{n+1}} \left(\sum_{i=1}^{m} U_i \, \phi_i \right)^{n+1} \sum_{j=1}^{m} \tilde{U}_j \phi_j \, d\Omega - \frac{1}{\delta t} \int_{\Omega^{n+1}} \left(\left(\sum_{i=1}^{m} U_i \, \phi_i \right)^{n} \circ X^n \right) \sum_{j=1}^{m} \tilde{U}_j \phi_j \, d\Omega \\
&\qquad + \frac{1}{2} \frac{W_i}{R_e} \left(\int_{\Omega^{n+1}} \frac{\partial^2 \left(\sum_{i=1}^{m} U_i \phi_i \right)}{\partial X \partial Y} \frac{\partial \left(\sum_{i=1}^{m} V_i \phi_i \right)}{\partial X} \sum_{j=1}^{m} \tilde{U}_j \phi_j \, d\Omega \right. \\
&\left. + \int_{\Omega^{n+1}} \frac{\partial \left(\sum_{i=1}^{m} U_i \phi_i \right)}{\partial Y} \frac{\partial \left(\sum_{i=1}^{m} V_i \phi_i \right)}{\partial X} \frac{\partial \left(\sum_{j=1}^{m} \tilde{U}_j \phi_j \right)}{\partial X} \, d\Omega - \int_{\Omega^{n+1}} \sum_{i=1}^{m} U_i \phi_i \right.
\end{aligned}$$

$$\frac{\partial^2\left(\sum_{i=1}^{m} V_i\phi_i\right)}{\partial X^2}\frac{\partial\left(\sum_{j=1}^{m}\tilde{U}_j\phi_j\right)}{\partial Y}d\Omega+\int_{\Omega^{n+1}}\frac{\partial^2\left(\sum_{i=1}^{m} U_i\phi_i\right)}{\partial X\partial Y}\frac{\partial\sum_{i=1}^{m} U_i\phi_i}{\partial Y}$$

$$\sum_{j=1}^{m}\tilde{U}_j\phi_j d\Omega+\int_{\Omega^{n+1}}\frac{\partial\left(\sum_{i=1}^{m} U_i\phi_i\right)}{\partial X}\frac{\partial\left(\sum_{i=1}^{m} U_i\phi_i\right)}{\partial Y}\frac{\partial\left(\sum_{j=1}^{m}\tilde{U}_j\phi_j\right)}{\partial Y}d\Omega$$

$$-\int_{\Omega^{n+1}}\sum_{i=1}^{m} U_i\phi_i\frac{\partial^2\left(\sum_{i=1}^{m} U_i\phi_i\right)}{\partial Y^2}\frac{\partial\left(\sum_{j=1}^{m}\tilde{U}_j\phi_j\right)}{\partial X}d\Omega+\int_{\Omega^{n+1}}\frac{\partial\left(\sum_{i=1}^{m} U_i\phi_i\right)}{\partial X}$$

$$\frac{\partial\left(\sum_{i=1}^{m} U_i\phi_i\right)}{\partial X}\frac{\partial\left(\sum_{j=1}^{m}\tilde{U}_j\phi_j\right)}{\partial X}d\Omega-2\int_{\Omega^{n+1}}\sum_{i=1}^{m} U_i\phi_i\frac{\partial^2\left(\sum_{i=1}^{m} U_i\phi_i\right)}{\partial X^2}\frac{\partial\left(\sum_{j=1}^{m}\tilde{U}_j\phi_j\right)}{\partial X}d\Omega$$

$$-3\int_{\Omega^{n+1}}\frac{\partial\left(\sum_{i=1}^{m} U_i\,\phi_i\right)}{\partial X}\frac{\partial\left(\sum_{i=1}^{m} U_i\,\phi_i\right)}{\partial X}\frac{\partial\left(\sum_{j=1}^{m}\tilde{U}_j\,\phi_j\right)}{\partial X}d\Omega-\int_{\Omega^{n+1}}\frac{\partial^2\left(\sum_{i=1}^{m} U_i\,\phi_i\right)}{\partial X^2}$$

$$\frac{\partial\left(\sum_{i=1}^{m} V_i\,\phi_i\right)}{\partial Y}\sum_{j=1}^{m}\tilde{U}_j\,\phi_j d\Omega-\int_{\Omega^{n+1}}\frac{\partial\left(\sum_{i=1}^{m} U_i\,\phi_i\right)}{\partial X}\frac{\partial\left(\sum_{i=1}^{m} V_i\,\phi_i\right)}{\partial Y}\frac{\partial\left(\sum_{j=1}^{m}\tilde{U}_j\,\phi_j\right)}{\partial X}d\Omega$$

$$-\int_{\Omega^{n+1}}\frac{\partial^2\left(\sum_{i=1}^{m} U_i\,\phi_i\right)}{\partial X\partial Y}\frac{\partial\left(\sum_{i=1}^{m} U_i\,\phi_i\right)}{\partial Y}\sum_{j=1}^{m}\tilde{U}_j\,\phi_j d\Omega-\int_{\Omega^{n+1}}\frac{\partial\left(\sum_{i=1}^{m} U_i\,\phi_i\right)}{\partial X}\frac{\partial\sum_{i=1}^{m} U_i\,\phi_i}{\partial Y}$$

$$\frac{\partial\left(\sum_{j=1}^{m}\tilde{U}_j\,\phi_j\right)}{\partial Y}d\Omega-2\int_{\Omega^{n+1}}\frac{\partial^2\left(\sum_{i=1}^{m} V_i\,\phi_i\right)}{\partial X^2}\frac{\partial\left(\sum_{i=1}^{m} U_i\,\phi_i\right)}{\partial Y}\sum_{j=1}^{m}\tilde{U}_j\,\phi_j d\Omega$$

$$-2\int_{\Omega^{n+1}}\frac{\partial\left(\sum_{i=1}^{m} V_i\,\phi_i\right)}{\partial X}\frac{\partial\left(\sum_{i=1}^{m} U_i\,\phi_i\right)}{\partial Y}\frac{\partial\left(\sum_{j=1}^{m}\tilde{U}_j\,\phi_j\right)}{\partial X}d\Omega-2\int_{\Omega^{n+1}}\frac{\partial^2\left(\sum_{i=1}^{m} U_i\,\phi_i\right)}{\partial X\partial Y}$$

$$\frac{\partial\left(\sum_{i=1}^{m} U_i\,\phi_i\right)}{\partial X}\sum_{j=1}^{m}\tilde{U}_j\,\phi_j d\Omega-2\int_{\Omega^{n+1}}\frac{\partial\left(\sum_{i=1}^{m} U_i\,\phi_i\right)}{\partial Y}\frac{\partial\left(\sum_{i=1}^{m} V_i\,\phi_i\right)}{\partial X}\frac{\partial\left(\sum_{j=1}^{m}\tilde{U}_j\,\phi_j\right)}{\partial X}d\Omega$$

$$-2\int_{\Omega^{n+1}}\frac{\partial^2\left(\sum_{i=1}^{m} U_i\,\phi_i\right)}{\partial Y^2}\frac{\partial\left(\sum_{i=1}^{m} U_i\,\phi_i\right)}{\partial X}\sum_{j=1}^{m}\tilde{U}_j\,\phi_j d\Omega-2\int_{\Omega^{n+1}}\frac{\partial\left(\sum_{i=1}^{m} U_i\,\phi_i\right)}{\partial Y}$$

$$\frac{\partial\left(\sum_{i=1}^{m} U_i\,\phi_i\right)}{\partial X}\frac{\partial\left(\sum_{j=1}^{m}\tilde{U}_j\,\phi_j\right)}{\partial Y}d\Omega-\int_{\Omega^{n+1}}\frac{\partial\left(\sum_{i=1}^{m} V_i\,\phi_i\right)}{\partial X}\frac{\partial\left(\sum_{i=1}^{m} V_i\,\phi_i\right)}{\partial X}$$

$$\frac{\partial\left(\sum_{j=1}^{m}\tilde{U}_j\,\phi_j\right)}{\partial X}d\Omega\Bigg)-\sum_{i=1}^{l} P_i\,\psi_i\int_{\Omega^n}\frac{\partial\left(\sum_{j=1}^{m}\tilde{U}_j\phi_j\right)}{\partial X}d\Omega-\frac{1}{R_e}\Bigg[\int_{\Omega^{n+1}}\frac{\partial\left(\sum_{i=1}^{m} U_i\phi_i\right)}{\partial X}$$

$$\frac{\partial\left(\sum_{j=1}^{m}\tilde{U}_j\phi_j\right)}{\partial X}d\Omega-\int_{\Omega^{n+1}}\frac{\partial\left(\sum_{i=1}^{m} U_i\phi_i\right)}{\partial Y}\frac{\partial\left(\sum_{j=1}^{m}\tilde{U}_j\phi_j\right)}{\partial Y}d\Omega\Bigg]=0.$$

By Galerkins,

$$\tilde{U}_h=\sum_{j=1}^{m}\phi_J$$

$$\frac{1}{\delta t}\int_{\Omega^{n+1}}\left(\sum_{i=1}^{m}U_i\,\phi_i\right)^{n+1}\sum_{j=1}^{m}\phi_j\,d\Omega-\frac{1}{\delta t}\int_{\Omega^{n+1}}\left(\left(\sum_{i=1}^{m}U_i\,\phi_i\right)^{n}\circ X^n\right)\sum_{j=1}^{m}\phi_j\,d\Omega$$
$$+\frac{1}{2}\frac{W_i}{R_e}\left(\int_{\Omega^{n+1}}\frac{\partial^2\left(\sum_{i=1}^{m}U_i\phi_i\right)}{\partial X\partial Y}\frac{\partial\left(\sum_{i=1}^{m}V_i\phi_i\right)}{\partial X}\sum_{j=1}^{m}\phi_j d\Omega+\int_{\Omega^{n+1}}\frac{\partial\left(\sum_{i=1}^{m}U_i\phi_i\right)}{\partial Y}\right.$$
$$\left.\frac{\partial\left(\sum_{i=1}^{m}V_i\phi_i\right)}{\partial X}\frac{\partial\left(\sum_{j=1}^{m}\phi_j\right)}{\partial X},d\Omega-\int_{\Omega^{n+1}}\sum_{i=1}^{m}U_i\phi_i\frac{\partial^2\left(\sum_{i=1}^{m}V_i\phi_i\right)}{\partial X^2}\frac{\partial\left(\sum_{j=1}^{m}\phi_j\right)}{\partial Y}d\Omega\right.$$
$$+\int_{\Omega^{n+1}}\frac{\partial^2\left(\sum_{i=1}^{m}U_i\phi_i\right)}{\partial X\partial Y}\frac{\partial\left(\sum_{i=1}^{m}U_i\phi_i\right)}{\partial Y}\sum_{j=1}^{m}\phi_j d\Omega+\int_{\Omega^{n+1}}\frac{\partial\left(\sum_{i=1}^{m}U_i\phi_i\right)}{\partial X}\frac{\partial\left(\sum_{i=1}^{m}U_i\phi_i\right)}{\partial Y}$$
$$\frac{\partial\left(\sum_{j=1}^{m}\phi_j\right)}{\partial Y}d\Omega-\int_{\Omega^{n+1}}\sum_{i=1}^{m}U_i\phi_i\frac{\partial^2\left(\sum_{i=1}^{m}U_i\phi_i\right)}{\partial Y^2}\frac{\partial\left(\sum_{j=1}^{m}\phi_j\right)}{\partial X}d\Omega+\int_{\Omega^{n+1}}\frac{\partial\left(\sum_{i=1}^{m}U_i\phi_i\right)}{\partial X}$$
$$\frac{\partial\left(\sum_{i=1}^{m}U_i\phi_i\right)}{\partial X}\frac{\partial\left(\sum_{j=1}^{m}\phi_j\right)}{\partial X}d\Omega-2\int_{\Omega^{n+1}}\sum_{i=1}^{m}U_i\phi_i\frac{\partial^2\left(\sum_{i=1}^{m}U_i\phi_i\right)}{\partial X^2}\frac{\partial\left(\sum_{j=1}^{m}\phi_j\right)}{\partial X}d\Omega$$
$$-3\int_{\Omega^{n+1}}\frac{\partial\left(\sum_{i=1}^{m}U_i\,\phi_i\right)}{\partial X}\frac{\partial\left(\sum_{i=1}^{m}U_i\,\phi_i\right)}{\partial X}\frac{\partial\left(\sum_{j=1}^{m}\phi_j\right)}{\partial X}d\Omega-\int_{\Omega^{n+1}}\frac{\partial^2\left(\sum_{i=1}^{m}U_i\,\phi_i\right)}{\partial X^2}$$
$$\frac{\partial\left(\sum_{i=1}^{m}V_i\,\phi_i\right)}{\partial Y}\sum_{j=1}^{m}\phi_j d\Omega-\int_{\Omega^{n+1}}\frac{\partial\left(\sum_{i=1}^{m}U_i\,\phi_i\right)}{\partial X}\frac{\partial\left(\sum_{i=1}^{m}V_i\,\phi_i\right)}{\partial Y}\frac{\partial\left(\sum_{j=1}^{m}\phi_j\right)}{\partial X}d\Omega$$
$$-\int_{\Omega^{n+1}}\frac{\partial^2\left(\sum_{i=1}^{m}U_i\,\phi_i\right)}{\partial X\partial Y}\frac{\partial\left(\sum_{i=1}^{m}U_i\,\phi_i\right)}{\partial Y}\sum_{j=1}^{m}\phi_j d\Omega-\int_{\Omega^{n+1}}\frac{\partial\left(\sum_{i=1}^{m}U_i\,\phi_i\right)}{\partial X}\frac{\partial\left(\sum_{i=1}^{m}U_i\,\phi_i\right)}{\partial Y}$$
$$\frac{\partial\left(\sum_{j=1}^{m}\phi_j\right)}{\partial Y}\,d\Omega-2\int_{\Omega^{n+1}}\frac{\partial^2\left(\sum_{i=1}^{m}V_i\,\phi_i\right)}{\partial X^2}\frac{\partial\left(\sum_{i=1}^{m}U_i\,\phi_i\right)}{\partial Y}\left(\sum_{j=1}^{m}\phi_j\right)d\Omega$$
$$-2\int_{\Omega^{n+1}}\frac{\partial\left(\sum_{i=1}^{m}V_i\,\phi_i\right)}{\partial X}\cdot\frac{\partial\left(\sum_{i=1}^{m}U_i\,\phi_i\right)}{\partial Y}\frac{\partial\left(\sum_{j=1}^{m}\phi_j\right)}{\partial X}\,d\Omega-2\int_{\Omega^{n+1}}\frac{\partial^2\left(\sum_{i=1}^{m}U_i\,\phi_i\right)}{\partial X\partial Y}$$
$$\frac{\partial\left(\sum_{i=1}^{m}U_i\,\phi_i\right)}{\partial X}\sum_{j=1}^{m}\phi_j d\Omega-2\int_{\Omega^{n+1}}\frac{\partial\left(\sum_{i=1}^{m}U_i\,\phi_i\right)}{\partial Y}\,\frac{\partial\left(\sum_{i=1}^{m}V_i\,\phi_i\right)}{\partial X}\frac{\partial\left(\sum_{j=1}^{m}\phi_j\right)}{\partial X}\,d\Omega$$
$$-2\int_{\Omega^{n+1}}\frac{\partial^2\left(\sum_{i=1}^{m}U_i\,\phi_i\right)}{\partial Y^2}\frac{\partial\left(\sum_{i=1}^{m}U_i\,\phi_i\right)}{\partial X}\sum_{j=1}^{m}\phi_j d\Omega-2\int_{\Omega^{n+1}}\frac{\partial\left(\sum_{i=1}^{m}U_i\,\phi_i\right)}{\partial Y}$$
$$\frac{\partial\left(\sum_{i=1}^{m}U_i\,\phi_i\right)}{\partial X}\cdot\frac{\partial\left(\sum_{j=1}^{m}\phi_j\right)}{\partial Y}\,d\Omega-\int_{\Omega^{n+1}}\frac{\partial\left(\sum_{i=1}^{m}V_i\,\phi_i\right)}{\partial X}\cdot\frac{\partial\left(\sum_{i=1}^{m}V_i\,\phi_i\right)}{\partial X}$$
$$\left.\frac{\partial\left(\sum_{j=1}^{m}\phi_j\right)}{\partial X}\,d\Omega\right)-\sum_{i=1}^{L}P_i\,\psi_i\int_{\Omega^n}\frac{\partial\left(\sum_{j=1}^{m}\phi_j\right)}{\partial X}\,d\Omega-\frac{1}{R_e}\left[-\int_{\Omega^{n+1}}\frac{\partial\left(\sum_{i=1}^{m}U_i\,\phi_i\right)}{\partial X}\right.$$

$$\frac{\partial\left(\sum_{j=1}^{m}\phi_j\right)}{\partial X}\,d\Omega+\int_{\Gamma}\left(\sum_{j=1}^{m}\phi_j\right)n_x\frac{\partial\left(\sum_{i=1}^{m}U_i\,\phi_i\right)}{\partial X}\,d\Gamma-\int_{\Omega^{n+1}}\frac{\partial\left(\sum_{i=1}^{m}U_i\,\phi_i\right)}{\partial Y}$$
$$\frac{\partial\left(\sum_{j=1}^{m}\phi_j\right)}{\partial Y}\,d\Omega+\int_{\Gamma}\left(\sum_{j=1}^{m}\phi_j\right)n_y\frac{\partial\left(\sum_{i=1}^{m}U_i\,\phi_i\right)}{\partial Y}\,d\Gamma\Bigg]=0$$

$$\frac{1}{\delta t}\int_{\Omega^{n+1}}\left(\sum_{i=1}^{m}U_i\,\phi_i\right)^{n+1}\sum_{j=1}^{m}\phi_j\,d\Omega-\frac{1}{\delta t}\int_{\Omega^{n+1}}\left(\left(\sum_{i=1}^{m}U_i\,\phi_i\right)^{n}\circ X^n\right)\sum_{j=1}^{m}\phi_j\,d\Omega$$
$$+\frac{1}{2}\frac{W_i}{R_e}\Bigg(\int_{\Omega^{n+1}}\sum_{i=1}^{m}\frac{\partial^2\phi_i}{\partial X\partial Y}U_i\sum_{i=1}^{m}\frac{\partial\phi_i}{\partial X}V_i\sum_{j=1}^{m}\phi_j d\Omega+\int_{\Omega^{n+1}}\sum_{i=1}^{m}\frac{\partial\phi_i}{\partial Y}U_i\sum_{i=1}^{m}\frac{\partial\phi_i}{\partial X}V_i\sum_{j=1}^{m}\frac{\partial\phi_j}{\partial X}$$
$$d\Omega-\int_{\Omega^{n+1}}\sum_{i=1}^{m}U_i\phi_i\sum_{i=1}^{m}\frac{\partial^2\phi_i}{\partial X^2}V_i\sum_{j=1}^{m}\frac{\partial\phi_j}{\partial Y}d\Omega+\int_{\Omega^{n+1}}\sum_{i=1}^{m}\frac{\partial^2\phi_i}{\partial X\partial Y}U_i\sum_{i=1}^{m}\frac{\partial\phi_i}{\partial Y}U_i\sum_{j=1}^{m}\phi_j d\Omega$$
$$+\int_{\Omega^{n+1}}\left(\sum_{i=1}^{m}\frac{\partial\phi_i}{\partial X}U_i\right)\left(\sum_{i=1}^{m}\frac{\partial\phi_i}{\partial Y}U_i\right)\left(\sum_{j=1}^{m}\frac{\partial\phi_j}{\partial Y}\right)d\Omega-\int_{\Omega^{n+1}}\sum_{i=1}^{m}U_i\phi_i\sum_{i=1}^{m}\frac{\partial^2\phi_i}{\partial Y^2}U_i$$
$$\sum_{j=1}^{m}\frac{\partial\phi_j}{\partial X}d\Omega+\int_{\Omega^{n+1}}\sum_{i=1}^{m}\frac{\partial\phi_i}{\partial X}U_i\sum_{i=1}^{m}\frac{\partial\phi_i}{\partial X}U_i\sum_{j=1}^{m}\frac{\partial\phi_j}{\partial X}d\Omega-2\int_{\Omega^{n+1}}\sum_{i=1}^{m}U_i\phi_i\sum_{i=1}^{m}\frac{\partial^2\phi_i}{\partial X^2}U_i$$
$$\sum_{j=1}^{m}\frac{\partial\phi_j}{\partial X}d\Omega-3\int_{\Omega^{n+1}}\sum_{i=1}^{m}\frac{\partial\phi_i}{\partial X}U_i\sum_{i=1}^{m}\frac{\partial\phi_i}{\partial X}U_i\sum_{j=1}^{m}\frac{\partial\phi_j}{\partial X}d\Omega-\int_{\Omega^{n+1}}\sum_{i=1}^{m}\frac{\partial^2\phi_i}{\partial X^2}U_i\sum_{i=1}^{m}\frac{\partial\phi_i}{\partial Y}V_i$$
$$\sum_{j=1}^{m}\phi_j d\Omega-\int_{\Omega^{n+1}}\sum_{i=1}^{m}\frac{\partial\phi_i}{\partial X}U_i\sum_{i=1}^{m}\frac{\partial\phi_i}{\partial Y}V_i\sum_{j=1}^{m}\frac{\partial\phi_j}{\partial X}d\Omega-\int_{\Omega^{n+1}}\sum_{i=1}^{m}\frac{\partial^2\phi_i}{\partial X\partial Y}U_i\sum_{i=1}^{m}\frac{\partial\phi_i}{\partial Y}U_i$$
$$\left(\sum_{j=1}^{m}\phi_j\right)d\Omega-\int_{\Omega^{n+1}}\sum_{i=1}^{m}\frac{\partial\phi_i}{\partial X}U_i\sum_{i=1}^{m}\frac{\partial\phi_i}{\partial Y}U_i\sum_{j=1}^{m}\frac{\partial\phi_j}{\partial Y}\,d\Omega-2\int_{\Omega^{n+1}}\sum_{i=1}^{m}\frac{\partial^2\phi_i}{\partial X^2}V_i\sum_{i=1}^{m}\frac{\partial\phi_i}{\partial Y}U_i$$
$$\sum_{j=1}^{m}\phi_j d\Omega-2\int_{\Omega^{n+1}}\sum_{i=1}^{m}\frac{\partial\phi_i}{\partial X}V_i\sum_{i=1}^{m}\frac{\partial\phi_i}{\partial Y}U_i\sum_{j=1}^{m}\frac{\partial\phi_j}{\partial X}\,d\Omega-2\int_{\Omega^{n+1}}\sum_{i=1}^{m}\frac{\partial^2\phi_i}{\partial X\partial Y}U_i\sum_{i=1}^{m}\frac{\partial\phi_i}{\partial X}U_i$$
$$\sum_{j=1}^{m}\phi_j d\Omega-2\int_{\Omega^{n+1}}\sum_{i=1}^{m}\frac{\partial\phi_i}{\partial Y}U_i\sum_{i=1}^{m}\frac{\partial\phi_i}{\partial X}V_i\sum_{j=1}^{m}\frac{\partial\phi_j}{\partial X}\,d\Omega-2\int_{\Omega^{n+1}}\sum_{i=1}^{m}\frac{\partial^2\phi_i}{\partial Y^2}U_i\sum_{i=1}^{m}\frac{\partial\phi_i}{\partial X}U_i$$
$$\sum_{j=1}^{m}\phi_j d\Omega-2\int_{\Omega^{n+1}}\sum_{i=1}^{m}\frac{\partial\phi_i}{\partial Y}U_i\sum_{i=1}^{m}\frac{\partial\phi_i}{\partial X}U_i\sum_{j=1}^{m}\frac{\partial\phi_j}{\partial Y}\,d\Omega-\int_{\Omega^{n+1}}\sum_{i=1}^{m}\frac{\partial\phi_i}{\partial X}V_i\sum_{i=1}^{m}\frac{\partial\phi_i}{\partial X}V_i$$
$$\sum_{j=1}^{m}\frac{\partial\phi_j}{\partial X}\,d\Omega-\left(\sum_{i=1}^{L}P_i\,\psi_i\right)\int_{\Omega^n}\sum_{j=1}^{m}\frac{\partial\phi_j}{\partial X}\,d\Omega-\frac{1}{R_e}\Bigg[-\int_{\Omega^{n+1}}\sum_{i=1}^{m}\frac{\partial\phi_i}{\partial X}U_i\sum_{j=1}^{m}\frac{\partial\phi_j}{\partial X}\,d\Omega$$
$$+\int_{\Gamma}\left(\sum_{j=1}^{m}\phi_j\right)n_x\sum_{i=1}^{m}\frac{\partial\phi_i}{\partial X}U_i\,d\Gamma-\int_{\Omega^{n+1}}\sum_{i=1}^{m}\frac{\partial\phi_i}{\partial Y}U_i\sum_{j=1}^{m}\frac{\partial\phi_j}{\partial Y}\,d\Omega+\int_{\Gamma}\left(\sum_{j=1}^{m}\phi_j\right)n_y$$
$$\sum_{i=1}^{m}\frac{\partial\phi_i}{\partial Y}U_i\,d\Gamma\Bigg]=0$$

$$\frac{1}{\delta t}\int_{\Omega^{n+1}}(U_i\phi_i)^{n+1}\,\phi_j\,d\Omega-\frac{1}{\delta t}\int_{\Omega^{n+1}}((U_i\phi_i)^n\circ X^n)\,\phi_j\,d\Omega+\frac{1}{2}\frac{W_i}{R_e}$$
$$\left(\int_{\Omega^{n+1}}\left(\frac{\partial^2\phi_i}{\partial X\partial Y}\right)\left(\frac{\partial\phi_i}{\partial X}\right)(\phi_j)\;d\Omega+\int_{\Omega^{n+1}}\left(\frac{\partial\phi_i}{\partial Y}\right)\left(\frac{\partial\phi_i}{\partial X}\right)\left(\frac{\partial\phi_j}{\partial X}\right)\;d\Omega\right.$$
$$-\int_{\Omega^{n+1}}(U_i\phi_i)\left(\frac{\partial^2\phi_i}{\partial X^2}\right)\left(\frac{\partial\phi_j}{\partial Y}\right)\;d\Omega+\int_{\Omega^{n+1}}\left(\frac{\partial^2\phi_i}{\partial X\partial Y}\right)\left(\frac{\partial\phi_i}{\partial Y}\right)(\phi_j)\;d\Omega$$
$$+\int_{\Omega^{n+1}}\left(\frac{\partial\phi_i}{\partial X}\right)\left(\frac{\partial\phi_i}{\partial Y}\right)\left(\frac{\partial\phi_j}{\partial Y}\right)\;d\Omega-\int_{\Omega^{n+1}}(U_i\phi_i)\left(\frac{\partial^2\phi_i}{\partial Y^2}\right)\left(\frac{\partial\phi_j}{\partial X}\right)d\Omega$$
$$+\int_{\Omega^{n+1}}\left(\frac{\partial\phi_i}{\partial X}\right)\left(\frac{\partial\phi_i}{\partial X}\right)\left(\frac{\partial\phi_j}{\partial X}\right)\;d\Omega-2\int_{\Omega^{n+1}}(U_i\phi_i)\left(\frac{\partial^2\phi_i}{\partial X^2}\right)\left(\frac{\partial\phi_j}{\partial X}\right)\;d\Omega$$
$$-3\int_{\Omega^{n+1}}\left(\frac{\partial\phi_i}{\partial X}\right)\left(\frac{\partial\phi_i}{\partial X}\right)\left(\frac{\partial\phi_j}{\partial X}\right)\;d\Omega-\int_{\Omega^{n+1}}\left(\frac{\partial^2\phi_i}{\partial X^2}\right)\left(\frac{\partial\phi_i}{\partial Y}\right)(\phi_j)\;d\Omega$$
$$-\int_{\Omega^{n+1}}\left(\frac{\partial\phi_i}{\partial X}\right)\left(\frac{\partial\phi_i}{\partial Y}\right)\left(\frac{\partial\phi_j}{\partial X}\right)\;d\Omega-\int_{\Omega^{n+1}}\frac{\partial^2\phi_i}{\partial X\partial Y}\frac{\partial\phi_i}{\partial Y}(\phi_j)\,d\Omega$$
$$-\int_{\Omega^{n+1}}\frac{\partial\phi_i}{\partial X}\frac{\partial\phi_i}{\partial Y}\frac{\partial\phi_j}{\partial Y}\,d\Omega-2\int_{\Omega^{n+1}}\frac{\partial^2\phi_i}{\partial X^2}\frac{\partial\phi_i}{\partial Y}U_i\,(\phi_j)\,d\Omega-2\int_{\Omega^{n+1}}\frac{\partial\phi_i}{\partial X}\frac{\partial\phi_i}{\partial Y}\frac{\partial\phi_j}{\partial X}\,d\Omega$$
$$-2\int_{\Omega^{n+1}}\frac{\partial^2\phi_i}{\partial X\partial Y}\frac{\partial\phi_i}{\partial X}\phi_j d\Omega-2\int_{\Omega^{n+1}}\frac{\partial\phi_i}{\partial Y}\frac{\partial\phi_i}{\partial X}\frac{\partial\phi_j}{\partial X}\,d\Omega-2\int_{\Omega^{n+1}}\frac{\partial^2\phi_i}{\partial Y^2}\frac{\partial\phi_i}{\partial X}\phi_j d\Omega$$
$$\left.-2\int_{\Omega^{n+1}}\frac{\partial\phi_i}{\partial Y}\frac{\partial\phi_i}{\partial X}\frac{\partial\phi_j}{\partial Y}\,d\Omega-\int_{\Omega^{n+1}}\frac{\partial\phi_i}{\partial X}\frac{\partial\phi_i}{\partial X}\frac{\partial\phi_j}{\partial X}\,d\Omega\right)-\phi_i\int_{\Omega^n}\frac{\partial\phi_j}{\partial X}\,d\Omega-\frac{1}{R_e}$$
$$\left[-\int_{\Omega^{n+1}}\frac{\partial\phi_i)}{\partial X}\frac{\partial\phi_j}{\partial X}\,d\Omega+\int_\Gamma(\phi_j)\,n_x\frac{\partial\phi_i}{\partial X}d\Gamma-\int_{\Omega^{n+1}}\frac{\partial\phi_i}{\partial Y}\frac{\partial\phi_j}{\partial Y}\,d\Omega+\int_\Gamma(\phi_j)\,n_y\frac{\partial\phi_i}{\partial Y}d\Gamma\right]=0$$

$$\frac{1}{\delta t}\int_{\Omega^{n+1}}U_i^{n+1}\phi_i^{n+1}\phi_j^{n+1}\,d\Omega-\frac{1}{\delta t}\int_{\Omega^{n+1}}(U_i^n\,\phi_i^n\circ X^n)\,\phi_j^{n+1}\,d\Omega+\frac{1}{2}\frac{W_i}{R_e}\left(\int_{\Omega^{n+1}}\frac{\partial^2\phi_i^n}{\partial X\partial Y}\right.$$
$$\frac{\partial\phi_i^{n+1}}{\partial X}\phi_j^{n+1}\,d\Omega+\int_{\Omega^{n+1}}\frac{\partial\phi_i^{n+1}}{\partial Y}\frac{\partial\phi_i^n}{\partial X}\frac{\partial\phi_j^{n+1}}{\partial X}\,d\Omega-\int_{\Omega^{n+1}}U_i^{n+1}\phi_i^{n+1}\frac{\partial^2\phi_i^n}{\partial X^2}\frac{\partial\phi_j^{n+1}}{\partial Y}\,d\Omega$$
$$+\int_{\Omega^{n+1}}\frac{\partial^2\phi_i^n}{\partial X\partial Y}\frac{\partial\phi_i^{n+1}}{\partial Y}\phi_j^{n+1}\,d\Omega+\int_{\Omega^{n+1}}\frac{\partial\phi_i^n}{\partial X}\frac{\partial\phi_i^{n+1}}{\partial Y}\frac{\partial\phi_j^{n+1}}{\partial Y}\,d\Omega-\int_{\Omega^{n+1}}U_i^{n+1}\phi_i^{n+1}\frac{\partial^2\phi_i^n}{\partial Y^2}$$
$$\frac{\partial\phi_j^{n+1}}{\partial X}\,d\Omega+\int_{\Omega^{n+1}}\left(\frac{\partial\phi_i^{n+1}}{\partial X}\right)\frac{\partial\phi_i^n}{\partial X}\frac{\partial\phi_j^{n+1}}{\partial X}\,d\Omega-2\int_{\Omega^{n+1}}U_i^n\phi_i^n\frac{\partial^2\phi_i^{n+1}}{\partial X^2}\frac{\partial\phi_j^{n+1}}{\partial X}\,d\Omega$$
$$-3\int_{\Omega^{n+1}}\left(\frac{\partial\phi_i^n}{\partial X}\right)\frac{\partial\phi_i^{n+1}}{\partial X}\frac{\partial\phi_j^{n+1}}{\partial X}\,d\Omega-\int_{\Omega^{n+1}}\frac{\partial^2\phi_i^{n+1}}{\partial X^2}\frac{\partial\phi_i^n}{\partial Y}\phi_j^{n+1}\,d\Omega-\int_{\Omega^{n+1}}\frac{\partial\phi_i^{n+1}}{\partial X}$$
$$\frac{\partial\phi_i^n}{\partial Y}\frac{\partial\phi_j^{n+1}}{\partial X}\,d\Omega-\int_{\Omega^{n+1}}\frac{\partial^2\phi_i^n}{\partial X\partial Y}\frac{\partial\phi_i^{n+1}}{\partial Y}\phi_j^{n+1}\,d\Omega-\int_{\Omega^{n+1}}\frac{\partial\phi_i^n}{\partial X}\frac{\partial\phi_i^{n+1}}{\partial Y}\frac{\partial\phi_j^{n+1}}{\partial Y}\,d\Omega$$
$$-2\int_{\Omega^{n+1}}\frac{\partial^2\phi_i^{n+1}}{\partial X^2}\frac{\partial\phi_i^n}{\partial Y}\phi_j^{n+1}\,d\Omega-2\int_{\Omega^{n+1}}\frac{\partial\phi_i^{n+1}}{\partial X}\frac{\partial\phi_i^n}{\partial Y}\frac{\partial\phi_j^{n+1}}{\partial X}\,d\Omega-2\int_{\Omega^{n+1}}\frac{\partial^2\phi_i^n}{\partial X\partial Y}$$

$$\frac{\partial\phi_i^{n+1}}{\partial X}\phi_j^{n+1}\,d\Omega - 2\int_{\Omega^{n+1}}\frac{\partial\phi_i^n}{\partial Y}\frac{\partial\phi_i^{n+1}}{\partial X}\frac{\partial\phi_j^{n+1}}{\partial X}\,d\Omega - 2\int_{\Omega^{n+1}}\frac{\partial^2\phi_i^{n+1}}{\partial Y^2}\frac{\partial\phi_i^n}{\partial X}\phi_j^{n+1}\,d\Omega$$
$$- 2\int_{\Omega^{n+1}}\frac{\partial\phi_i^{n+1}}{\partial Y}\frac{\partial\phi_i^n}{\partial X}\frac{\partial\phi_j^{n+1}}{\partial Y}\,d\Omega - \int_{\Omega^{n+1}}\left(\frac{\partial\phi_i^n}{\partial X}\right)^2\frac{\partial\phi_j^{n+1}}{\partial X}\,d\Omega\Big) - \psi_i^{n+1}\int_{\Omega^n}\frac{\partial\phi_j^{n+1}}{\partial X}\,d\Omega$$
$$- \frac{1}{R_e}\Big(\int_{\Omega^{n+1}}\frac{\partial\phi_i^{n+1}}{\partial X}\frac{\partial\phi_j^{n+1}}{\partial X}\,d\Omega + \int_{\Omega^{n+1}}\frac{\partial\phi_i^{n+1}}{\partial Y}\frac{\partial\phi_j^{n+1}}{\partial Y}\,d\Omega\Big) = \int_\Gamma\phi_j^{n+1}n_x\frac{\partial\phi_i^{n+1}}{\partial X}\,d\Gamma$$
$$+ \int_\Gamma\phi_j^{n+1}n_y\frac{\partial\phi_i^{n+1}}{\partial Y}\,d\Gamma \quad (4.26)$$

Eq. (4.25) $\Rightarrow$

$$\frac{1}{\delta t}\int_{\Omega^{n+1}}\left(\sum_{i=1}^m V_i\phi_i\right)^{n+1}\sum_{j=1}^m\tilde{V}_j\phi_j\,d\Omega - \frac{1}{\delta t}\int_{\Omega^{n+1}}\left(\left(\sum_{i=1}^m V_i\phi_i\right)^n\circ Y^n\right)\sum_{j=1}^m\tilde{V}_j\phi_j\,d\Omega$$
$$+\frac{1}{2}\frac{W_i}{R_e}\Bigg(\int_{\Omega^{n+1}}\frac{\partial^2\left(\sum_{i=1}^m V_i\phi_i\right)}{\partial X\partial Y}\frac{\partial\left(\sum_{i=1}^m U_i\phi_i\right)}{\partial Y}\sum_{j=1}^m\tilde{V}_j\phi_j\,d\Omega + \int_{\Omega^{n+1}}\frac{\partial\left(\sum_{i=1}^m V_i\phi_i\right)}{\partial X}$$
$$\frac{\partial\left(\sum_{i=1}^m U_i\phi_i\right)}{\partial Y}\frac{\partial\left(\sum_{j=1}^m\tilde{V}_j\phi_j\right)}{\partial Y}\,d\Omega - \int_{\Omega^{n+1}}\sum_{i=1}^m V_i\phi_i\frac{\partial^2\left(\sum_{i=1}^m U_i\phi_i\right)}{\partial Y^2}\frac{\partial\left(\sum_{j=1}^m\tilde{V}_j\phi_j\right)}{\partial X}\,d\Omega$$
$$+\int_{\Omega^{n+1}}\frac{\partial^2\left(\sum_{i=1}^m V_i\phi_i\right)}{\partial X\partial Y}\frac{\partial\left(\sum_{i=1}^m V_i\phi_i\right)}{\partial X}\sum_{j=1}^m\tilde{V}_j\phi_j\,d\Omega + \int_{\Omega^{n+1}}\frac{\partial\left(\sum_{i=1}^m V_i\phi_i\right)}{\partial Y}$$
$$\frac{\partial\left(\sum_{i=1}^m V_i\phi_i\right)}{\partial X}\frac{\partial\left(\sum_{j=1}^m\tilde{V}_j\phi_j\right)}{\partial X}\,d\Omega - \int_{\Omega^{n+1}}\sum_{i=1}^m V_i\phi_i\frac{\partial^2\left(\sum_{i=1}^m V_i\phi_i\right)}{\partial X^2}\frac{\partial\left(\sum_{j=1}^m\tilde{V}_j\phi_j\right)}{\partial Y}\,d\Omega$$
$$+\int_{\Omega^{n+1}}\frac{\partial\left(\sum_{i=1}^m V_i\phi_i\right)}{\partial Y}\frac{\partial\left(\sum_{i=1}^m V_i\phi_i\right)}{\partial Y}\frac{\partial\left(\sum_{j=1}^m\tilde{V}_j\phi_j\right)}{\partial Y}\,d\Omega - 2\int_{\Omega^{n+1}}\sum_{i=1}^m V_i\phi_i\frac{\partial^2\left(\sum_{i=1}^m V_i\phi_i\right)}{\partial Y^2}$$
$$\frac{\partial\left(\sum_{j=1}^m\tilde{V}_j\phi_j\right)}{\partial Y}\,d\Omega - 3\int_{\Omega^{n+1}}\frac{\partial\left(\sum_{i=1}^m V_i\phi_i\right)}{\partial Y}\frac{\partial\left(\sum_{i=1}^m V_i\phi_i\right)}{\partial Y}\frac{\partial\left(\sum_{j=1}^m\tilde{V}_j\phi_j\right)}{\partial Y}\,d\Omega$$
$$-\int_{\Omega^{n+1}}\frac{\partial^2\left(\sum_{i=1}^m V_i\phi_i\right)}{\partial Y^2}\frac{\partial\left(\sum_{i=1}^m U_i\phi_i\right)}{\partial X}\sum_{j=1}^m\tilde{V}_j\phi_j\,d\Omega - \int_{\Omega^{n+1}}\frac{\partial\left(\sum_{i=1}^m V_i\phi_i\right)}{\partial Y}\frac{\partial\left(\sum_{i=1}^m U_i\phi_i\right)}{\partial X}$$
$$\frac{\partial\left(\sum_{j=1}^m\tilde{V}_j\phi_j\right)}{\partial Y}\,d\Omega - \int_{\Omega^{n+1}}\frac{\partial^2\left(\sum_{i=1}^m U_i\phi_i\right)}{\partial X\partial Y}\frac{\partial\left(\sum_{i=1}^m V_i\phi_i\right)}{\partial X}\sum_{j=1}^m\tilde{V}_j\phi_j\,d\Omega$$
$$-\int_{\Omega^{n+1}}\frac{\partial\left(\sum_{i=1}^m V_i\phi_i\right)}{\partial Y}\frac{\partial\left(\sum_{i=1}^m V_i\phi_i\right)}{\partial X}\frac{\partial\left(\sum_{j=1}^m\tilde{V}_j\phi_j\right)}{\partial X}\,d\Omega - 2\int_{\Omega^{n+1}}\frac{\partial^2\left(\sum_{i=1}^m U_i\phi_i\right)}{\partial Y^2}$$
$$\frac{\partial\left(\sum_{i=1}^m V_i\phi_i\right)}{\partial X}\sum_{j=1}^m\tilde{V}_j\phi_j\,d\Omega - 2\int_{\Omega^{n+1}}\frac{\partial\left(\sum_{i=1}^m U_i\phi_i\right)}{\partial Y}\frac{\partial\left(\sum_{i=1}^m V_i\phi_i\right)}{\partial X}$$

$$\frac{\partial\left(\sum_{j=1}^{m}\tilde{V}_j\phi_j\right)}{\partial Y}\,d\Omega - 2\int_{\Omega^{n+1}}\frac{\partial^2\left(\sum_{i=1}^{m}V_i\phi_i\right)}{\partial X\partial Y}\frac{\partial\left(\sum_{i=1}^{m}U_i\phi_i\right)}{\partial Y}\sum_{j=1}^{m}\tilde{V}_j\phi_j\,d\Omega$$

$$-2\int_{\Omega^{n+1}}\frac{\partial\left(\sum_{i=1}^{m}V_i\phi_i\right)}{\partial X}\frac{\partial\left(\sum_{i=1}^{m}U_i\phi_i\right)}{\partial Y}\frac{\partial\left(\sum_{j=1}^{m}\tilde{V}_j\phi_j\right)}{\partial Y}\,d\Omega - 2\int_{\Omega^{n+1}}\frac{\partial^2\left(\sum_{i=1}^{m}V_i\phi_i\right)}{\partial X^2}$$

$$\frac{\partial\left(\sum_{i=1}^{m}V_i\phi_i\right)}{\partial Y}\sum_{j=1}^{m}\tilde{V}_j\phi_j\,d\Omega - 2\int_{\Omega^{n+1}}\frac{\partial\left(\sum_{i=1}^{m}V_i\phi_i\right)}{\partial X}\frac{\partial\left(\sum_{i=1}^{m}V_i\phi_i\right)}{\partial Y}\frac{\partial\left(\sum_{j=1}^{m}\tilde{V}_j\phi_j\right)}{\partial X}\,d\Omega$$

$$-\int_{\Omega^{n+1}}\frac{\partial\left(\sum_{i=1}^{m}U_i\phi_i\right)}{\partial Y}\frac{\partial\left(\sum_{i=1}^{m}U_i\phi_i\right)}{\partial Y}\frac{\partial\left(\sum_{j=1}^{m}\tilde{V}_j\phi_j\right)}{\partial Y}\,d\Omega - \sum_{i=1}^{l}P_i\psi_i\int_{\Omega^n}\frac{\partial\tilde{V}}{\partial Y}\,d\Omega$$

$$-\frac{1}{R_e}\left[-\int_{\Omega^{n+1}}\frac{\partial\left(\sum_{i=1}^{m}V_i\phi_i\right)}{\partial X}\frac{\partial\left(\sum_{j=1}^{m}\tilde{V}_j\phi_j\right)}{\partial X}\,d\Omega + \int_{\Gamma}\sum_{j=1}^{m}\tilde{V}_j\phi_j\,n_x\frac{\partial\left(\sum_{i=1}^{m}V_i\phi_i\right)}{\partial X}\,d\Gamma\right.$$

$$\left.-\int_{\Omega^{n+1}}\frac{\partial\left(\sum_{i=1}^{m}V_i\phi_i\right)}{\partial Y}\frac{\partial\left(\sum_{j=1}^{m}\tilde{V}_j\phi_j\right)}{\partial Y}\,d\Omega + \int_{\Gamma}\left(\sum_{j=1}^{m}\tilde{V}_j\phi_j\right)n_y\frac{\partial\left(\sum_{i=1}^{m}V_i\phi_i\right)}{\partial Y}\,d\Gamma\right] = 0$$

By Galerkin's method, we have:

$$\tilde{V}_h = \sum_{j=1}^{m}\phi_j$$

$$\frac{1}{\delta t}\int_{\Omega^{n+1}}\left(\sum_{i=1}^{m}V_i\phi_i\right)^{n+1}\sum_{j=1}^{m}\phi_j\,d\Omega \;-\; \frac{1}{\delta t}\int_{\Omega^{n+1}}\left(\left(\sum_{i=1}^{m}V_i\phi_i\right)^{n}\circ Y^n\right)\sum_{j=1}^{m}\phi_j\,d\Omega$$

$$+\frac{1}{2}\frac{W_i}{R_e}\left(\int_{\Omega^{n+1}}\frac{\partial^2\left(\sum_{i=1}^{m}V_i\phi_i\right)}{\partial X\,\partial Y}\frac{\partial\left(\sum_{i=1}^{m}U_i\phi_i\right)}{\partial Y}\sum_{j=1}^{m}\phi_j\,d\Omega + \int_{\Omega^{n+1}}\frac{\partial\left(\sum_{i=1}^{m}V_i\phi_i\right)}{\partial X}\right.$$

$$\frac{\partial\left(\sum_{i=1}^{m}U_i\phi_i\right)}{\partial Y}\frac{\partial\left(\sum_{j=1}^{m}\phi_j\right)}{\partial Y}\,d\Omega - \int_{\Omega^{n+1}}\sum_{i=1}^{m}V_i\phi_i\frac{\partial^2\left(\sum_{i=1}^{m}U_i\phi_i\right)}{\partial Y^2}\frac{\partial\left(\sum_{j=1}^{m}\phi_j\right)}{\partial X}\,d\Omega$$

$$+\int_{\Omega^{n+1}}\frac{\partial^2\left(\sum_{i=1}^{m}V_i\phi_i\right)}{\partial X\,\partial Y}\frac{\partial\left(\sum_{i=1}^{m}V_i\phi_i\right)}{\partial X}\sum_{j=1}^{m}\phi_j\,d\Omega + \int_{\Omega^{n+1}}\frac{\partial\left(\sum_{i=1}^{m}V_i\phi_i\right)}{\partial Y}$$

$$\frac{\partial\left(\sum_{i=1}^{m}V_i\phi_i\right)}{\partial X}\frac{\partial\left(\sum_{j=1}^{m}\phi_j\right)}{\partial X}\,d\Omega - \int_{\Omega^{n+1}}\sum_{i=1}^{m}V_i\phi_i\frac{\partial^2\left(\sum_{i=1}^{m}V_i\phi_i\right)}{\partial X^2}\frac{\partial\left(\sum_{j=1}^{m}\phi_j\right)}{\partial Y}\,d\Omega$$

$$+\int_{\Omega^{n+1}}\frac{\partial\left(\sum_{i=1}^{m}V_i\phi_i\right)}{\partial Y}\frac{\partial\left(\sum_{i=1}^{m}V_i\phi_i\right)}{\partial Y}\frac{\partial\left(\sum_{j=1}^{m}\phi_j\right)}{\partial Y}\,d\Omega - 2\int_{\Omega^{n+1}}\sum_{i=1}^{m}V_i\phi_i\frac{\partial^2\left(\sum_{i=1}^{m}V_i\phi_i\right)}{\partial Y^2}$$

$$\frac{\partial\left(\sum_{j=1}^{m}\phi_j\right)}{\partial Y}\,d\Omega - 3\int_{\Omega^{n+1}}\frac{\partial\left(\sum_{i=1}^{m}V_i\phi_i\right)}{\partial Y}\frac{\partial\left(\sum_{i=1}^{m}V_i\phi_i\right)}{\partial Y}\frac{\partial\left(\sum_{j=1}^{m}\phi_j\right)}{\partial Y}\,d\Omega$$
$$-\int_{\Omega^{n+1}}\frac{\partial^2\left(\sum_{i=1}^{m}V_i\phi_i\right)}{\partial Y^2}\frac{\partial\left(\sum_{i=1}^{m}U_i\phi_i\right)}{\partial X}\sum_{j=1}^{m}\phi_j\,d\Omega - \int_{\Omega^{n+1}}\frac{\partial\left(\sum_{i=1}^{m}V_i\phi_i\right)}{\partial Y}$$
$$\frac{\partial\left(\sum_{i=1}^{m}U_i\phi_i\right)}{\partial X}\frac{\partial\left(\sum_{j=1}^{m}\phi_j\right)}{\partial Y}\,d\Omega - \int_{\Omega^{n+1}}\frac{\partial^2\left(\sum_{i=1}^{m}U_i\phi_i\right)}{\partial X\,\partial Y}\frac{\partial\left(\sum_{i=1}^{m}V_i\phi_i\right)}{\partial X}\sum_{j=1}^{m}\phi_j\,d\Omega\Bigg)$$
$$-\sum_{i=1}^{l}P_i\psi_i\int_{\Omega^n}\frac{\partial\tilde{V}}{\partial Y}\,d\Omega - \frac{1}{R_e}\Bigg[-\int_{\Omega^{n+1}}\frac{\partial\left(\sum_{i=1}^{m}V_i\phi_i\right)}{\partial X}\frac{\partial\left(\sum_{j=1}^{m}\phi_j\right)}{\partial X}\,d\Omega + \int_{\Gamma}\sum_{j=1}^{m}\phi_j\,n_x$$
$$\frac{\partial\left(\sum_{i=1}^{m}V_i\phi_i\right)}{\partial X}\,d\Gamma - \int_{\Omega^{n+1}}\frac{\partial\left(\sum_{i=1}^{m}V_i\phi_i\right)}{\partial Y}\frac{\partial\left(\sum_{j=1}^{m}\phi_j\right)}{\partial Y}\,d\Omega + \int_{\Gamma}\left(\sum_{j=1}^{m}\phi_j\right)n_y$$
$$\frac{\partial\left(\sum_{i=1}^{m}V_i\phi_i\right)}{\partial Y}\,d\Gamma\Bigg] = 0$$

$$\frac{1}{\delta t}\int_{\Omega^{n+1}}\left(\sum_{i=1}^{m}V_i\phi_i\right)^{n+1}\left(\sum_{j=1}^{m}\phi_j\right)\,d\Omega \;-\; \frac{1}{\delta t}\int_{\Omega^{n+1}}\left(\left(\sum_{i=1}^{m}V_i\phi_i\right)^{n}\circ Y^n\right)\left(\sum_{j=1}^{m}\phi_j\right)$$
$$d\Omega + \frac{1}{2}\frac{W_i}{R_e}\Bigg(\int_{\Omega^{n+1}}\sum_{i=1}^{m}\frac{\partial^2\phi_i}{\partial X\partial Y}V_i\sum_{i=1}^{m}\frac{\partial\phi_i}{\partial Y}U_i\sum_{j=1}^{m}\phi_j\,d\Omega + \int_{\Omega^{n+1}}\sum_{i=1}^{m}\frac{\partial\phi_i}{\partial X}V_i\sum_{i=1}^{m}\frac{\partial\phi_i}{\partial Y}U_i$$
$$\sum_{j=1}^{m}\frac{\partial\phi_j}{\partial Y}\,d\Omega - \int_{\Omega^{n+1}}\sum_{i=1}^{m}V_i\phi_i\sum_{i=1}^{m}\frac{\partial^2\phi_i}{\partial Y^2}U_i\sum_{j=1}^{m}\frac{\partial\phi_j}{\partial X}\,d\Omega + \int_{\Omega^{n+1}}\sum_{i=1}^{m}\frac{\partial^2\phi_i}{\partial X\partial Y}V_i\sum_{i=1}^{m}\frac{\partial\phi_i}{\partial X}V_i$$
$$\sum_{j=1}^{m}\phi_j\,d\Omega + \int_{\Omega^{n+1}}\sum_{i=1}^{m}\frac{\partial\phi_i}{\partial Y}V_i\sum_{i=1}^{m}\frac{\partial\phi_i}{\partial X}V_i\sum_{j=1}^{m}\frac{\partial\phi_j}{\partial X}\,d\Omega - \int_{\Omega^{n+1}}\sum_{i=1}^{m}V_i\phi_i\sum_{i=1}^{m}\frac{\partial^2\phi_i}{\partial X^2}V_i\sum_{j=1}^{m}\frac{\partial\phi_j}{\partial Y}$$
$$d\Omega + \int_{\Omega^{n+1}}\sum_{i=1}^{m}\frac{\partial\phi_i}{\partial Y}V_i\sum_{i=1}^{m}\frac{\partial\phi_i}{\partial Y}V_i\sum_{j=1}^{m}\frac{\partial\phi_j}{\partial Y}\,d\Omega - 2\int_{\Omega^{n+1}}\sum_{i=1}^{m}V_i\phi_i\sum_{i=1}^{m}\frac{\partial^2\phi_i}{\partial Y^2}V_i\sum_{j=1}^{m}\frac{\partial\phi_j}{\partial Y}\,d\Omega$$
$$-3\int_{\Omega^{n+1}}\sum_{i=1}^{m}\frac{\partial\phi_i}{\partial Y}V_i\sum_{i=1}^{m}\frac{\partial\phi_i}{\partial Y}V_i\sum_{j=1}^{m}\frac{\partial\phi_j}{\partial Y}\,d\Omega - \int_{\Omega^{n+1}}\sum_{i=1}^{m}\frac{\partial^2\phi_i}{\partial Y^2}V_i\sum_{i=1}^{m}\frac{\partial\phi_i}{\partial X}U_i\sum_{j=1}^{m}\phi_j\,d\Omega$$
$$-\int_{\Omega^{n+1}}\sum_{i=1}^{m}\frac{\partial\phi_i}{\partial Y}V_i\sum_{i=1}^{m}\frac{\partial\phi_i}{\partial X}U_i\sum_{j=1}^{m}\frac{\partial\phi_j}{\partial Y}\,d\Omega - \int_{\Omega^{n+1}}\sum_{i=1}^{m}\frac{\partial^2\phi_i}{\partial X\partial Y}U_i\sum_{i=1}^{m}\frac{\partial\phi_i}{\partial X}V_i\sum_{j=1}^{m}\phi_j\,d\Omega$$
$$-2\int_{\Omega^{n+1}}\sum_{i=1}^{m}\frac{\partial^2\phi_i}{\partial Y^2}U_i\sum_{i=1}^{m}\frac{\partial\phi_i}{\partial X}V_i\sum_{j=1}^{m}\phi_j\,d\Omega - 2\int_{\Omega^{n+1}}\sum_{i=1}^{m}\frac{\partial\phi_i}{\partial Y}U_i\sum_{i=1}^{m}\frac{\partial\phi_i}{\partial X}V_i\sum_{j=1}^{m}\frac{\partial\phi_j}{\partial Y}\,d\Omega$$

$$-2\int_{\Omega^{n+1}}\sum_{i=1}^{m}\frac{\partial^2\phi_i}{\partial X\partial Y}V_i\sum_{i=1}^{m}\frac{\partial\phi_i}{\partial Y}U_i\sum_{j=1}^{m}\phi_j\,d\Omega-2\int_{\Omega^{n+1}}\sum_{i=1}^{m}\frac{\partial\phi_i}{\partial X}V_i\sum_{i=1}^{m}\frac{\partial\phi_i}{\partial Y}U_i\sum_{j=1}^{m}\frac{\partial\phi_j}{\partial Y}\,d\Omega$$
$$-2\int_{\Omega^{n+1}}\sum_{i=1}^{m}\frac{\partial^2\phi_i}{\partial X^2}V_i\sum_{i=1}^{m}\frac{\partial\phi_i}{\partial Y}V_i\sum_{j=1}^{m}\phi_j\,d\Omega-2\int_{\Omega^{n+1}}\sum_{i=1}^{m}\frac{\partial\phi_i}{\partial X}V_i\sum_{i=1}^{m}\frac{\partial\phi_i}{\partial Y}V_i\sum_{j=1}^{m}\frac{\partial\phi_j}{\partial X}\,d\Omega$$
$$-\int_{\Omega^{n+1}}\sum_{i=1}^{m}\frac{\partial\phi_i}{\partial Y}U_i\sum_{i=1}^{m}\frac{\partial\phi_i}{\partial Y}U_i\sum_{j=1}^{m}\frac{\partial\phi_j}{\partial Y}\,d\Omega\Bigg)-\left(\sum_{i=1}^{l}P_i\psi_i\right)\int_{\Omega^n}\sum_{j=1}^{m}\frac{\partial\phi_j}{\partial Y}\,d\Omega$$
$$-\frac{1}{R_e}\Bigg[-\int_{\Omega^{n+1}}\sum_{i=1}^{m}\frac{\partial\phi_i}{\partial X}V_i\sum_{j=1}^{m}\frac{\partial\phi_j}{\partial X}\,d\Omega+\int_{\Gamma}\sum_{j=1}^{m}\phi_j n_x\sum_{i=1}^{m}\frac{\partial\phi_i}{\partial X}V_i\,d\Gamma$$
$$-\int_{\Omega^{n+1}}\sum_{i=1}^{m}\frac{\partial\phi_i}{\partial Y}V_i\sum_{j=1}^{m}\frac{\partial\phi_j}{\partial Y}\,d\Omega+\int_{\Gamma}\sum_{j=1}^{m}\phi_j n_y\sum_{i=1}^{m}\frac{\partial\phi_i}{\partial Y}V_i\,d\Gamma\Bigg]=0$$

$$\frac{1}{\delta t}\int_{\Omega^{n+1}}\left(V_i\,\phi_i\right)^{n+1}\phi_j\,d\Omega-\frac{1}{\delta t}\int_{\Omega^{n+1}}\left(\left(V_i\,\phi_i\right)^{n}\circ Y^n\right)\phi_j\,d\Omega+\frac{1}{2}\frac{W_i}{R_e}\Bigg(\int_{\Omega^{n+1}}\frac{\partial^2\phi_i}{\partial X\partial Y}\frac{\partial\phi_i}{\partial Y}$$
$$\phi_j\,d\Omega+\int_{\Omega^{n+1}}\frac{\partial\phi_i}{\partial X}\frac{\partial\phi_i}{\partial Y}\frac{\partial\phi_j}{\partial Y}\,d\Omega-\int_{\Omega^{n+1}}V_i\phi_i\frac{\partial^2\phi_i}{\partial Y^2}\frac{\partial\phi_j}{\partial X}\,d\Omega+\int_{\Omega^{n+1}}\frac{\partial^2\phi_i}{\partial X\partial Y}\frac{\partial\phi_i}{\partial X}\phi_j\,d\Omega$$
$$+\int_{\Omega^{n+1}}\frac{\partial\phi_i}{\partial Y}\frac{\partial\phi_i}{\partial X}\frac{\partial\phi_j}{\partial X}\,d\Omega-\int_{\Omega^{n+1}}V_i\phi_i\frac{\partial^2\phi_i}{\partial X^2}\frac{\partial\phi_j}{\partial Y}\,d\Omega+\int_{\Omega^{n+1}}\frac{\partial\phi_i}{\partial Y}\frac{\partial\phi_i}{\partial Y}\frac{\partial\phi_j}{\partial Y}\,d\Omega$$
$$-2\int_{\Omega^{n+1}}V_i\phi_i\frac{\partial^2\phi_i}{\partial Y^2}\frac{\partial\phi_j}{\partial Y}\,d\Omega-3\int_{\Omega^{n+1}}\frac{\partial\phi_i}{\partial Y}\frac{\partial\phi_i}{\partial Y}\frac{\partial\phi_j}{\partial Y}\,d\Omega-\int_{\Omega^{n+1}}\frac{\partial^2\phi_i}{\partial Y^2}\frac{\partial\phi_i}{\partial X}\phi_j\,d\Omega$$
$$-\int_{\Omega^{n+1}}\frac{\partial\phi_i}{\partial Y}\frac{\partial\phi_i}{\partial X}\frac{\partial\phi_j}{\partial Y}\,d\Omega-\int_{\Omega^{n+1}}\frac{\partial^2\phi_i}{\partial X\partial Y}\frac{\partial\phi_i}{\partial X}\phi_j\,d\Omega-\int_{\Omega^{n+1}}\frac{\partial\phi_i}{\partial Y}\frac{\partial\phi_i}{\partial X}\frac{\partial\phi_j}{\partial X}\,d\Omega$$
$$-2\int_{\Omega^{n+1}}\frac{\partial^2\phi_i}{\partial Y^2}\frac{\partial\phi_i}{\partial X}\phi_j\,d\Omega-2\int_{\Omega^{n+1}}\frac{\partial\phi_i}{\partial Y}\frac{\partial\phi_i}{\partial X}\frac{\partial\phi_j}{\partial Y}\,d\Omega-2\int_{\Omega^{n+1}}\frac{\partial^2\phi_i}{\partial X\partial Y}\frac{\partial\phi_i}{\partial Y}\phi_j\,d\Omega$$
$$-2\int_{\Omega^{n+1}}\frac{\partial\phi_i}{\partial X}\frac{\partial\phi_i}{\partial Y}\frac{\partial\phi_j}{\partial Y}\,d\Omega-2\int_{\Omega^{n+1}}\frac{\partial^2\phi_i}{\partial X^2}\frac{\partial\phi_i}{\partial Y}\phi_j\,d\Omega-2\int_{\Omega^{n+1}}\frac{\partial\phi_i}{\partial X}\frac{\partial\phi_i}{\partial Y}\frac{\partial\phi_j}{\partial X}\,d\Omega$$
$$-\int_{\Omega^{n+1}}\frac{\partial\phi_i}{\partial Y}\frac{\partial\phi_i}{\partial Y}\frac{\partial\phi_j}{\partial Y}\,d\Omega\Bigg)-\psi_i\int_{\Omega^n}\frac{\partial\phi_j}{\partial Y}\,d\Omega-\frac{1}{R_e}\Bigg[-\int_{\Omega^{n+1}}\frac{\partial\phi_i}{\partial X}\frac{\partial\phi_j}{\partial X}\,d\Omega-\int_{\Omega^{n+1}}\frac{\partial\phi_i}{\partial Y}$$
$$\frac{\partial\phi_j}{\partial Y}d\Omega\Bigg]=\int_{\Gamma}\phi_j n_x\frac{\partial\phi_i}{\partial X}\,d\Gamma+\int_{\Gamma}\phi_j n_y\frac{\partial\phi_i}{\partial Y}\,d\Gamma$$

$$\frac{1}{\delta t}\int_{\Omega^{n+1}}V_i^{n+1}\phi_i^{n+1}\phi_j^{n+1}d\Omega-\frac{1}{\delta t}\int_{\Omega^{n+1}}\left(V_i^n\phi_i^n\circ Y^n\right)\phi_j^{n+1}d\Omega+\frac{1}{2}\frac{W_i}{R_e}\Bigg(\int_{\Omega^{n+1}}\frac{\partial^2\phi_i^n}{\partial X\partial Y}$$
$$\frac{\partial\phi_i^{n+1}}{\partial Y}\phi_j d\Omega+\int_{\Omega^{n+1}}\frac{\partial\phi_i^{n+1}}{\partial X}\frac{\partial\phi_i^n}{\partial Y}\frac{\partial\phi_j^{n+1}}{\partial Y}\,d\Omega-\int_{\Omega^{n+1}}V_i^{n+1}\phi_i^{n+1}\frac{\partial^2\phi_i^n}{\partial Y^2}\frac{\partial\phi_j^{n+1}}{\partial X}\,d\Omega$$

$$+\int_{\Omega^{n+1}}\frac{\partial^2\phi_i^n}{\partial X\partial Y}\frac{\partial\phi_i^{n+1}}{\partial X}\phi_j^{n+1}d\Omega+\int_{\Omega^{n+1}}\frac{\partial\phi_i^n}{\partial Y}\frac{\partial\phi_i^{n+1}}{\partial X}\frac{\partial\phi_j^{n+1}}{\partial X}\,d\Omega-\int_{\Omega^{n+1}}V_i^{n+1}\phi_i^{n+1}\frac{\partial^2\phi_i^n}{\partial X^2}$$
$$\frac{\partial\phi_j^{n+1}}{\partial Y}\,d\Omega+\int_{\Omega^{n+1}}\frac{\partial\phi_i^{n+1}}{\partial Y}\frac{\partial\phi_i^n}{\partial Y}\frac{\partial\phi_j^{n+1}}{\partial Y}\,d\Omega-2\int_{\Omega^{n+1}}V_i^n\phi_i^n\frac{\partial^2\phi_i^{n+1}}{\partial Y^2}]\frac{\partial\phi_j^{n+1}}{\partial Y}\,d\Omega-3\int_{\Omega^{n+1}}\frac{\partial\phi_i^n}{\partial Y}$$
$$\frac{\partial\phi_i^{n+1}}{\partial Y}\frac{\partial\phi_j^{n+1}}{\partial Y}\,d\Omega-\int_{\Omega^{n+1}}\frac{\partial^2\phi_i^{n+1}}{\partial Y^2}\frac{\partial\phi_i^n}{\partial X}\phi_j^{n+1}d\Omega-\int_{\Omega^{n+1}}\frac{\partial\phi_i^{n+1}}{\partial Y}\frac{\partial\phi_i^n}{\partial X}\frac{\partial\phi_j^{n+1}}{\partial Y}\,d\Omega$$
$$-\int_{\Omega^{n+1}}\frac{\partial^2\phi_i^n}{\partial X\partial Y}\frac{\partial\phi_i^{n+1}}{\partial X}\phi_j^{n+1}d\Omega-\int_{\Omega^{n+1}}\frac{\partial\phi_i^n}{\partial Y}\frac{\partial\phi_i^{n+1}}{\partial X}\frac{\partial\phi_j^{n+1}}{\partial X}\,d\Omega-2\int_{\Omega^{n+1}}\frac{\partial^2\phi_i^{n+1}}{\partial Y^2}\frac{\partial\phi_i^n}{\partial X}\phi_j^{n+1}$$
$$d\Omega-2\int_{\Omega^{n+1}}\frac{\partial\phi_i^{n+1}}{\partial Y}\frac{\partial\phi_i^n}{\partial X}\frac{\partial\phi_j^{n+1}}{\partial Y}\,d\Omega-2\int_{\Omega^{n+1}}\frac{\partial^2\phi_i^n}{\partial X\partial Y}\frac{\partial\phi_i^{n+1}}{\partial Y}\phi_j^{n+1}d\Omega$$
$$-2\int_{\Omega^{n+1}}\frac{\partial\phi_i^n}{\partial X}\frac{\partial\phi_i^{n+1}}{\partial Y}\frac{\partial\phi_j^{n+1}}{\partial Y}\,d\Omega-2\int_{\Omega^{n+1}}\frac{\partial^2\phi_i^{n+1}}{\partial X^2}\frac{\partial\phi_i^n}{\partial Y}\phi_j^{n+1}d\Omega$$
$$-2\int_{\Omega^{n+1}}\frac{\partial\phi_i^{n+1}}{\partial X}\frac{\partial\phi_i^n}{\partial Y}\frac{\partial\phi_j^{n+1}}{\partial X}\,d\Omega-\int_{\Omega^{n+1}}\frac{\partial\phi_i^n}{\partial Y}\frac{\partial\phi_i^{n+1}}{\partial Y}\frac{\partial\phi_j^{n+1}}{\partial Y}\,d\Omega\Bigg)-\psi_i^{n+1}\int_{\Omega^n}\frac{\partial\phi_j^{n+1}}{\partial Y}\,d\Omega$$
$$-\frac{1}{R_e}\left[-\int_{\Omega^{n+1}}\frac{\partial\phi_i^{n+1}}{\partial X}\frac{\partial\phi_j^{n+1}}{\partial X}\,d\Omega-\int_{\Omega^{n+1}}\frac{\partial\phi_i^{n+1}}{\partial Y}\frac{\partial\phi_j^{n+1}}{\partial Y}\,d\Omega\right]=\int_\Gamma\phi_j^{n+1}n_x\frac{\partial\phi_i^{n+1}}{\partial X}d\Gamma$$
$$+\int_\Gamma\phi_j^{n+1}n_y\frac{\partial\phi_i^{n+1}}{\partial Y}d\Gamma \quad (4.27)$$

From Eqs. (4.26) to (4.27), we obtain the discretized system of nonlinear algebraic equations in the compact form:

$$[K(U,V)]\{X\}=\{Q\},$$

where $K(U,V)$ is the global stiffness matrix, X is the solution vector, and Q represents the global load (or boundary) vector.

The matrix representation of K, X, and Q is given by:

$$\underbrace{\begin{bmatrix}K_{11}&K_{12}&B_1\\K_{21}&K_{22}&B_2\\B_1^T&B_2^T&K_{33}\end{bmatrix}}_{K}\underbrace{\begin{bmatrix}U_h\\V_h\\P_h\end{bmatrix}}_{X}=\underbrace{\begin{bmatrix}Q_1\\Q_2\\Q_3\end{bmatrix}}_{Q} \quad (4.28)$$

Here, K is the block stiffness matrix, X is the block solution vector, and Q is the block boundary vector.

The local elemental contributions of the block stiffness matrix, for example K_{11}^{ij}, are computed as

$$
\begin{aligned}
K_{11}^{ij} &= \frac{1}{\delta t}\int_{\Omega^{n+1}} \phi_i^{n+1}\phi_j^{n+1}\,d\Omega - \frac{1}{\delta t}\int_{\Omega^{n+1}} \left(U_i^n\,\phi_i^n \circ X^n\right)\phi_j^{n+1}\,d\Omega \\
&+ \frac{1}{2}\frac{W_i}{R_e}\Bigg(\int_{\Omega^{n+1}} \frac{\partial^2\phi_i}{\partial X\partial Y}\frac{\partial\phi_i}{\partial X}\phi_j\,d\Omega + \int_{\Omega^{n+1}} \frac{\partial\phi_i}{\partial Y}\frac{\partial\phi_i}{\partial X}\frac{\partial\phi_j}{\partial X}\,d\Omega - \int_{\Omega^{n+1}} U_i\phi_i\frac{\partial^2\phi_i}{\partial X^2}\frac{\partial\phi_j}{\partial Y}\,d\Omega \\
&\quad + \int_{\Omega^{n+1}} \frac{\partial^2\phi_i}{\partial X\partial Y}\frac{\partial\phi_i}{\partial Y}\phi_j\,d\Omega + \int_{\Omega^{n+1}} \frac{\partial\phi_i}{\partial X}\frac{\partial\phi_i}{\partial Y}\frac{\partial\phi_j}{\partial Y}\,d\Omega - \int_{\Omega^{n+1}} U_i\phi_i\frac{\partial^2\phi_i}{\partial Y^2}\frac{\partial\phi_j}{\partial X}\,d\Omega \\
&\quad + \int_{\Omega^{n+1}} \left(\frac{\partial\phi_i}{\partial X}\right)^2\frac{\partial\phi_j}{\partial X}\,d\Omega - 2\int_{\Omega^{n+1}} U_i\phi_i\frac{\partial^2\phi_i}{\partial X^2}\frac{\partial\phi_j}{\partial X}\,d\Omega - 3\int_{\Omega^{n+1}} \left(\frac{\partial\phi_i}{\partial X}\right)^2\frac{\partial\phi_j}{\partial X}\,d\Omega \\
&\quad - \int_{\Omega^{n+1}} \frac{\partial^2\phi_i}{\partial X^2}\frac{\partial\phi_i}{\partial Y}\phi_j\,d\Omega - \int_{\Omega^{n+1}} \frac{\partial\phi_i}{\partial X}\frac{\partial\phi_i}{\partial Y}\frac{\partial\phi_j}{\partial X}\,d\Omega - \int_{\Omega^{n+1}} \frac{\partial^2\phi_i}{\partial X\partial Y}\frac{\partial\phi_i}{\partial Y}\phi_j\,d\Omega \\
&\quad - \int_{\Omega^{n+1}} \frac{\partial\phi_i}{\partial X}\frac{\partial\phi_i}{\partial Y}\frac{\partial\phi_j}{\partial Y}\,d\Omega - 2\int_{\Omega^{n+1}} \frac{\partial^2\phi_i}{\partial X^2}\frac{\partial\phi_i}{\partial Y}\phi_j\,d\Omega - 2\int_{\Omega^{n+1}} \frac{\partial\phi_i}{\partial X}\frac{\partial\phi_i}{\partial Y}\frac{\partial\phi_j}{\partial X}\,d\Omega \\
&\quad - 2\int_{\Omega^{n+1}} \frac{\partial^2\phi_i}{\partial X\partial Y}\frac{\partial\phi_i}{\partial X}\phi_j\,d\Omega - 2\int_{\Omega^{n+1}} \frac{\partial\phi_i}{\partial Y}\frac{\partial\phi_i}{\partial X}\frac{\partial\phi_j}{\partial X}\,d\Omega - 2\int_{\Omega^{n+1}} \frac{\partial^2\phi_i}{\partial Y^2}\frac{\partial\phi_i}{\partial X}\phi_j\,d\Omega \\
&\quad - 2\int_{\Omega^{n+1}} \frac{\partial\phi_i}{\partial Y}\frac{\partial\phi_i}{\partial X}\frac{\partial\phi_j}{\partial Y}\,d\Omega - \int_{\Omega^{n+1}} \left(\frac{\partial\phi_i}{\partial X}\right)^2\frac{\partial\phi_j}{\partial X}\,d\Omega\Bigg) - \frac{1}{R_e}\Bigg(\int_{\Omega^{n+1}} \frac{\partial\phi_i}{\partial X}\frac{\partial\phi_j}{\partial X}\,d\Omega \\
&\qquad\qquad + \int_{\Omega^{n+1}} \frac{\partial\phi_i}{\partial Y}\frac{\partial\phi_j}{\partial Y}\,d\Omega\Bigg).
\end{aligned}
$$

Furthermore, the off-diagonal components are

$$K_{12}^{ij} = 0, \qquad K_{21}^{ij} = 0.$$

$$
\begin{aligned}
K_{22}^{ij} &= \frac{1}{\delta t}\int_{\Omega^{n+1}} \phi_i^{n+1}\phi_j^{n+1}\,d\Omega - \frac{1}{\delta t}\int_{\Omega^{n+1}} \left(V_i^n\,\phi_i^n \circ Y^n\right)\phi_j^{n+1}\,d\Omega \\
&+ \frac{1}{2}\frac{W_i}{R_e}\Bigg(\int_{\Omega^{n+1}} \frac{\partial^2\phi_i}{\partial X\partial Y}\frac{\partial\phi_i}{\partial Y}\phi_j\,d\Omega + \int_{\Omega^{n+1}} \frac{\partial\phi_i}{\partial X}\frac{\partial\phi_i}{\partial Y}\frac{\partial\phi_j}{\partial Y}\,d\Omega - \int_{\Omega^{n+1}} V_i\phi_i\frac{\partial^2\phi_i}{\partial Y^2}\frac{\partial\phi_j}{\partial X}\,d\Omega \\
&\quad + \int_{\Omega^{n+1}} \frac{\partial^2\phi_i}{\partial X\partial Y}\frac{\partial\phi_i}{\partial X}\phi_j\,d\Omega + \int_{\Omega^{n+1}} \frac{\partial\phi_i}{\partial Y}\frac{\partial\phi_i}{\partial X}\frac{\partial\phi_j}{\partial X}\,d\Omega - \int_{\Omega^{n+1}} V_i\phi_i\frac{\partial^2\phi_i}{\partial X^2}\frac{\partial\phi_j}{\partial Y}\,d\Omega \\
&\quad + \int_{\Omega^{n+1}} \left(\frac{\partial\phi_i}{\partial Y}\right)^2\frac{\partial\phi_j}{\partial Y}\,d\Omega - 2\int_{\Omega^{n+1}} V_i\phi_i\frac{\partial^2\phi_i}{\partial Y^2}\frac{\partial\phi_j}{\partial Y}\,d\Omega - 3\int_{\Omega^{n+1}} \left(\frac{\partial\phi_i}{\partial Y}\right)^2\frac{\partial\phi_j}{\partial Y}\,d\Omega \\
&\quad - \int_{\Omega^{n+1}} \frac{\partial^2\phi_i}{\partial Y^2}\frac{\partial\phi_i}{\partial X}\phi_j\,d\Omega - \int_{\Omega^{n+1}} \frac{\partial\phi_i}{\partial Y}\frac{\partial\phi_i}{\partial X}\frac{\partial\phi_j}{\partial Y}\,d\Omega - \int_{\Omega^{n+1}} \frac{\partial^2\phi_i}{\partial X\partial Y}\frac{\partial\phi_i}{\partial X}\phi_j\,d\Omega \\
&\quad - \int_{\Omega^{n+1}} \frac{\partial\phi_i}{\partial Y}\frac{\partial\phi_i}{\partial X}\frac{\partial\phi_j}{\partial X}\,d\Omega - 2\int_{\Omega^{n+1}} \frac{\partial^2\phi_i}{\partial Y^2}\frac{\partial\phi_i}{\partial X}\phi_j\,d\Omega - 2\int_{\Omega^{n+1}} \frac{\partial\phi_i}{\partial Y}\frac{\partial\phi_i}{\partial X}\frac{\partial\phi_j}{\partial Y}\,d\Omega
\end{aligned}
$$

$$- 2\int_{\Omega^{n+1}} \frac{\partial^2\phi_i}{\partial X\partial Y}\frac{\partial\phi_i}{\partial Y}\phi_j\, d\Omega - 2\int_{\Omega^{n+1}} \frac{\partial\phi_i}{\partial X}\frac{\partial\phi_i}{\partial Y}\frac{\partial\phi_j}{\partial Y}\, d\Omega - 2\int_{\Omega^{n+1}} \frac{\partial^2\phi_i}{\partial X^2}\frac{\partial\phi_i}{\partial Y}\phi_j\, d\Omega$$
$$- 2\int_{\Omega^{n+1}} \frac{\partial\phi_i}{\partial X}\frac{\partial\phi_i}{\partial Y}\frac{\partial\phi_j}{\partial X}\, d\Omega - \int_{\Omega^{n+1}} \left(\frac{\partial\phi_i}{\partial Y}\right)^2\frac{\partial\phi_j}{\partial Y}\, d\Omega\Bigg) - \frac{1}{R_e}\Bigg(\int_{\Omega^{n+1}} \frac{\partial\phi_i}{\partial X}\frac{\partial\phi_j}{\partial X}\, d\Omega$$
$$+ \int_{\Omega^{n+1}} \frac{\partial\phi_i}{\partial Y}\frac{\partial\phi_j}{\partial Y}\, d\Omega\Bigg),$$

$$K_{33}^{ij} = 0,$$

The entries K_{13}, K_{23} and K_{31}, K_{32} are the pressure matrices with their respective transposes, given by

$$B_1^{ij} = \psi_i^{n+1}\int_{\Omega^n} \frac{\partial\phi_j^{n+1}}{\partial X}\, d\Omega,$$

$$B_2^{ij} = \psi_i^{n+1}\int_{\Omega^n} \frac{\partial\phi_j^{n+1}}{\partial Y}\, d\Omega,$$

$$\left(B_1^{ij}\right)^t = \phi_j^{n+1}\int_{\Omega^n} \frac{\partial\psi_i^{n+1}}{\partial X}\, d\Omega,$$

$$\left(B_2^{ij}\right)^t = \phi_j^{n+1}\int_{\Omega^n} \frac{\partial\psi_i^{n+1}}{\partial Y}\, d\Omega,$$

$$Q_1 = \int_\Gamma \phi_j^{n+1}\, n_x\, \frac{\partial\phi_i^{n+1}}{\partial X}\, d\Gamma + \int_\Gamma \phi_j^{n+1}\, n_y\, \frac{\partial\phi_i^{n+1}}{\partial Y}\, d\Gamma,$$

$$Q_2 = \int_\Gamma \phi_j^{n+1}\, n_x\, \frac{\partial\phi_i^{n+1}}{\partial X}\, d\Gamma + \int_\Gamma \phi_j^{n+1}\, n_y\, \frac{\partial\phi_i^{n+1}}{\partial Y}\, d\Gamma,$$

$$Q_3 = 0.$$

The discrete system of non-linear algebraic equations in matrix form can be expressed as

$$\begin{bmatrix} K_{11} & 0 & B_1 \\ 0 & K_{22} & B_2 \\ B_1^T & B_2^T & 0 \end{bmatrix}\begin{bmatrix} U \\ V \\ P \end{bmatrix} = \begin{bmatrix} Q_1 \\ Q_2 \\ 0 \end{bmatrix} \tag{4.29}$$

We consider a triangular element for discretizing the computational domain, as shown in the figure below For each triangular element, let us define the shape functions at the three nodes:

$$\text{Node } 1 : (u_1, v_1), \quad \text{Node } 2 : (u_2, v_2), \quad \text{Node } 3 : (u_3, v_3)$$

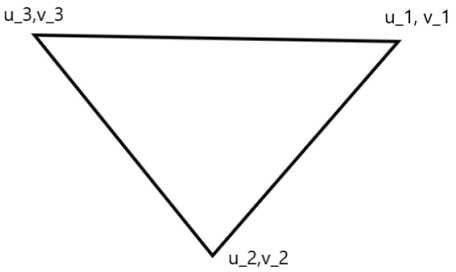

FIGURE 4.2: Linear Triangular Element

Each shape function $N_i(u, v)$ is assumed to be linear and expressed as:

$$U_i(u, v) = a + bu + cv$$

which can also be written in matrix form as

$$U = \begin{bmatrix} 1 & u & v \end{bmatrix} \begin{bmatrix} a \\ b \\ c \end{bmatrix} \tag{4.30}$$

To determine the coefficients a, b, c, we substitute the nodal coordinates into the above expression, leading to

$$\begin{bmatrix} U_1 \\ U_2 \\ U_3 \end{bmatrix} = \begin{bmatrix} 1 & u_1 & v_1 \\ 1 & u_2 & v_2 \\ 1 & u_3 & v_3 \end{bmatrix} \begin{bmatrix} a \\ b \\ c \end{bmatrix}$$

Therefore,

$$\begin{bmatrix} a \\ b \\ c \end{bmatrix} = \begin{bmatrix} 1 & u_1 & v_1 \\ 1 & u_2 & v_2 \\ 1 & u_3 & v_3 \end{bmatrix}^{-1} \begin{bmatrix} U_1 \\ U_2 \\ U_3 \end{bmatrix}$$

The area A of the triangular element with vertices $(u_1, v_1), (u_2, v_2), (u_3, v_3)$ is given by:

$$A = \frac{1}{2} \Big| u_1(v_2 - v_3) + u_2(v_3 - v_1) + u_3(v_1 - v_2) \Big|$$

The determinant of the coordinate matrix is

$$\Delta = \begin{vmatrix} 1 & u_1 & v_1 \\ 1 & u_2 & v_2 \\ 1 & u_3 & v_3 \end{vmatrix} = u_1(v_2 - v_3) + u_2(v_3 - v_1) + u_3(v_1 - v_2) = 2A$$

Thus, the coefficients a, b, c can be obtained explicitly as:

$$\begin{bmatrix} a \\ b \\ c \end{bmatrix} = \frac{1}{2A} \begin{bmatrix} u_2v_3 - u_3v_2 & u_3v_1 - u_1v_3 & u_1v_2 - u_2v_1 \\ v_2 - v_3 & v_3 - v_1 & v_1 - v_2 \\ u_3 - u_2 & u_1 - u_3 & u_2 - u_1 \end{bmatrix} \begin{bmatrix} U_1 \\ U_2 \\ U_3 \end{bmatrix} \tag{4.31}$$

Substituting Eq. (4.31) into Eq. (4.30), we obtain:

$$U = \begin{bmatrix} 1 & u & v \end{bmatrix} \frac{1}{2A} \begin{bmatrix} u_2v_3 - u_3v_2 & u_3v_1 - u_1v_3 & u_1v_2 - u_2v_1 \\ v_2 - v_3 & v_3 - v_1 & v_1 - v_2 \\ u_3 - u_2 & u_1 - u_3 & u_2 - u_1 \end{bmatrix} \begin{bmatrix} U_1 \\ U_2 \\ U_3 \end{bmatrix}$$

Defining the local shape functions ϕ_i as

$$\phi_i = \frac{1}{2A}\big(a_i + b_i u + c_i v\big),$$

the approximate solution within the triangular element can finally be expressed as

$$U(u, v) = \sum_{i=1}^{3} \phi_i(u, v)\, U_i \tag{4.32}$$

For a linear triangular element, the approximate solutions for velocity components U, V, and pressure P are expressed in terms of the shape functions ϕ_i and ψ_i as

$$U = \sum_{i=1}^{3} U_i\, \phi_i, \quad V = \sum_{i=1}^{3} V_i\, \phi_i, \quad P = \sum_{i=1}^{3} P_i\, \psi_i.$$

Substituting these approximations into Eq. (4.24), we obtain

$$\frac{1}{\delta t} \int_{\Omega^{n+1}} \left(\sum_{i=1}^{3} U_i \phi_i \right)^{n+1} \sum_{j=1}^{3} \phi_j \tilde{U}_j \, d\Omega - \frac{1}{\delta t} \int_{\Omega^{n+1}} \left(\left(\sum_{i=1}^{3} U_i \phi_i \right)^{n} \circ X^n \right) \sum_{j=1}^{3} \phi_j \tilde{U}_j \, d\Omega$$

$$+\frac{1}{2}\frac{W_i}{R_e}\Bigg(\int_{\Omega^{n+1}}\sum_{i=1}^{3}\frac{\partial^2\phi_i}{\partial X\partial Y}U_i\sum_{i=1}^{3}\frac{\partial\phi_i}{\partial X}V_i\sum_{j=1}^{3}\phi_j\tilde{U}_j\,d\Omega+\int_{\Omega^{n+1}}\sum_{i=1}^{3}\frac{\partial\phi_i}{\partial Y}U_i\sum_{i=1}^{3}\frac{\partial\phi_i}{\partial X}V_i$$
$$\sum_{j=1}^{3}\frac{\partial\phi_j}{\partial X}\tilde{U}_j\,d\Omega-\int_{\Omega^{n+1}}\sum_{i=1}^{3}U_i\phi_i\sum_{i=1}^{3}\frac{\partial^2\phi_i}{\partial X^2}V_i\sum_{j=1}^{3}\frac{\partial\phi_j}{\partial Y}\tilde{U}_j\,d\Omega+\int_{\Omega^{n+1}}\sum_{i=1}^{3}\frac{\partial^2\phi_i}{\partial X\partial Y}U_i$$
$$\sum_{i=1}^{3}\frac{\partial\phi_i}{\partial Y}U_i\sum_{j=1}^{3}\phi_j\tilde{U}_j\,d\Omega+\int_{\Omega^{n+1}}\sum_{i=1}^{3}\frac{\partial\phi_i}{\partial X}U_i\sum_{i=1}^{3}\frac{\partial\phi_i}{\partial Y}U_i\sum_{j=1}^{3}\frac{\partial\phi_j}{\partial Y}\tilde{U}_j\,d\Omega-\int_{\Omega^{n+1}}\sum_{i=1}^{3}U_i\phi_i$$
$$\sum_{i=1}^{3}\frac{\partial^2\phi_i}{\partial Y^2}U_i\sum_{j=1}^{3}\frac{\partial\phi_j}{\partial X}\tilde{U}_j\,d\Omega+\int_{\Omega^{n+1}}\sum_{i=1}^{3}\frac{\partial\phi_i}{\partial X}U_i\sum_{i=1}^{3}\frac{\partial\phi_i}{\partial X}U_i\sum_{j=1}^{3}\frac{\partial\phi_j}{\partial X}\tilde{U}_j\,d\Omega-2\int_{\Omega^{n+1}}$$
$$\sum_{i=1}^{3}U_i\phi_i\sum_{i=1}^{3}\frac{\partial^2\phi_i}{\partial X^2}U_i\sum_{j=1}^{3}\frac{\partial\phi_j}{\partial X}\tilde{U}_j\,d\Omega-3\int_{\Omega^{n+1}}\sum_{i=1}^{3}\frac{\partial\phi_i}{\partial X}U_i\sum_{i=1}^{3}\frac{\partial\phi_i}{\partial X}U_i\sum_{j=1}^{3}\frac{\partial\phi_j}{\partial X}\tilde{U}_j\,d\Omega$$
$$-\int_{\Omega^{n+1}}\sum_{i=1}^{3}\frac{\partial^2\phi_i}{\partial X^2}U_i\sum_{i=1}^{3}\frac{\partial\phi_i}{\partial Y}V_i\sum_{j=1}^{3}\phi_j\tilde{U}_j\,d\Omega-\int_{\Omega^{n+1}}\left(\sum_{i=1}^{3}\frac{\partial\phi_i}{\partial X}U_i\right)\left(\sum_{i=1}^{3}\frac{\partial\phi_i}{\partial Y}V_i\right)$$
$$\sum_{j=1}^{3}\frac{\partial\phi_j}{\partial X}\tilde{U}_j\,d\Omega-\int_{\Omega^{n+1}}\sum_{i=1}^{3}\frac{\partial^2\phi_i}{\partial X\partial Y}U_i\sum_{i=1}^{3}\frac{\partial\phi_i}{\partial Y}U_i\sum_{j=1}^{3}\phi_j\tilde{U}_j\,d\Omega-\int_{\Omega^{n+1}}\sum_{i=1}^{3}\frac{\partial\phi_i}{\partial X}U_i$$
$$\sum_{i=1}^{3}\frac{\partial\phi_i}{\partial Y}U_i\sum_{j=1}^{3}\frac{\partial\phi_j}{\partial Y}\tilde{U}_j\,d\Omega-2\int_{\Omega^{n+1}}\sum_{i=1}^{3}\frac{\partial^2\phi_i}{\partial X^2}V_i\sum_{i=1}^{3}\frac{\partial\phi_i}{\partial Y}U_i\sum_{j=1}^{3}\phi_j\tilde{U}_j\,d\Omega-2\int_{\Omega^{n+1}}$$
$$\sum_{i=1}^{3}\frac{\partial\phi_i}{\partial X}V_i\sum_{i=1}^{3}\frac{\partial\phi_i}{\partial Y}U_i\sum_{j=1}^{3}\frac{\partial\phi_j}{\partial X}\tilde{U}_j\,d\Omega-2\int_{\Omega^{n+1}}\sum_{i=1}^{3}\frac{\partial^2\phi_i}{\partial X\partial Y}U_i\sum_{i=1}^{3}\frac{\partial\phi_i}{\partial X}U_i\sum_{j=1}^{3}\phi_j\tilde{U}_j d\Omega$$
$$-2\int_{\Omega^{n+1}}\sum_{i=1}^{3}\frac{\partial\phi_i}{\partial Y}U_i\sum_{i=1}^{3}\frac{\partial\phi_i}{\partial X}V_i\sum_{j=1}^{3}\frac{\partial\phi_j}{\partial X}\tilde{U}_j\,d\Omega-2\int_{\Omega^{n+1}}\sum_{i=1}^{3}\frac{\partial^2\phi_i}{\partial Y^2}U_i\sum_{i=1}^{3}\frac{\partial\phi_i}{\partial X}U_i\sum_{j=1}^{3}\phi_j\tilde{U}_j$$
$$d\Omega-2\int_{\Omega^{n+1}}\sum_{i=1}^{3}\frac{\partial\phi_i}{\partial Y}U_i\sum_{i=1}^{3}\frac{\partial\phi_i}{\partial X}U_i\sum_{j=1}^{3}\frac{\partial\phi_j}{\partial Y}\tilde{U}_j\,d\Omega-\int_{\Omega^{n+1}}\sum_{i=1}^{3}\frac{\partial\phi_i}{\partial X}V_i\sum_{i=1}^{3}\frac{\partial\phi_i}{\partial X}V_i\sum_{j=1}^{3}\frac{\partial\phi_j}{\partial X}$$
$$\tilde{U}_j\,d\Omega\Bigg)-\sum_{i=1}^{3}P_i\,\psi_i\int_{\Omega^n}\sum_{j=1}^{3}\frac{\partial\phi_j}{\partial X}\tilde{U}_j\,d\Omega-\frac{1}{R_e}\Bigg[-\int_{\Omega^{n+1}}\sum_{i=1}^{3}\frac{\partial\phi_i)}{\partial X}U_i\sum_{j=1}^{3}\frac{\partial\phi_j}{\partial X}\tilde{U}_j\,d\Omega$$
$$+\int_\Gamma\left(\sum_{j=1}^{3}\phi_j\tilde{U}_j\right)n_x\sum_{i=1}^{3}\frac{\partial\phi_i}{\partial X}U_i d\Gamma-\int_{\Omega^{n+1}}\sum_{i=1}^{3}\frac{\partial\phi_i}{\partial Y}U_i\sum_{j=1}^{3}\frac{\partial\phi_j}{\partial Y}\tilde{U}_j\,d\Omega+\int_\Gamma\sum_{j=1}^{3}\phi_j\tilde{U}_j$$
$$n_y\sum_{i=1}^{3}\frac{\partial\phi_i}{\partial Y}U_i d\Gamma\Bigg]=0 \quad (4.33)$$

Similarly, substituting into Eq. (4.25), we obtain

$$\frac{1}{\delta t}\int_{\Omega^{n+1}}\left(\sum_{i=1}^{3}V_i\phi_i\right)^{n+1}\sum_{j=1}^{3}\phi_j\tilde{V}_j\,d\Omega-\frac{1}{\delta t}\int_{\Omega^{n+1}}\left(\left(\sum_{i=1}^{3}V_i\phi_i\right)^{n}\circ Y^n\right)\sum_{j=1}^{3}\phi_j\tilde{V}_j\,d\Omega$$

$$
\begin{aligned}
&+\frac{1}{2}\frac{W_i}{R_e}\Bigg(\int_{\Omega^{n+1}}\sum_{i=1}^{3}\frac{\partial^2\phi_i}{\partial X\partial Y}V_i\sum_{i=1}^{3}\frac{\partial\phi_i}{\partial Y}U_i\sum_{j=1}^{3}\phi_j\tilde{V}_j\,d\Omega+\int_{\Omega^{n+1}}\sum_{i=1}^{3}\frac{\partial\phi_i}{\partial X}V_i\sum_{i=1}^{3}\frac{\partial\phi_i}{\partial Y}U_i\\
&\sum_{j=1}^{3}\frac{\partial\phi_j}{\partial Y}\tilde{V}_j\,d\Omega-\int_{\Omega^{n+1}}\sum_{i=1}^{3}V_i\phi_i\sum_{i=1}^{3}\frac{\partial^2\phi_i}{\partial Y^2}U_i\sum_{j=1}^{3}\frac{\partial\phi_j}{\partial X}\tilde{V}_j\,d\Omega+\int_{\Omega^{n+1}}\sum_{i=1}^{3}\frac{\partial^2\phi_i}{\partial X\partial Y}V_i\\
&\sum_{i=1}^{3}\frac{\partial\phi_i}{\partial X}V_i\sum_{j=1}^{3}\phi_j\tilde{V}_j\,d\Omega+\int_{\Omega^{n+1}}\sum_{i=1}^{3}\frac{\partial\phi_i}{\partial Y}V_i\sum_{i=1}^{3}\frac{\partial\phi_i}{\partial X}V_i\sum_{j=1}^{3}\frac{\partial\phi_j}{\partial X}\tilde{V}_j\,d\Omega-\int_{\Omega^{n+1}}\sum_{i=1}^{3}V_i\phi_i\\
&\sum_{i=1}^{3}\frac{\partial^2\phi_i}{\partial X^2}V_i\sum_{j=1}^{3}\frac{\partial\phi_j}{\partial Y}\tilde{V}_j\,d\Omega+\int_{\Omega^{n+1}}\sum_{i=1}^{3}\frac{\partial\phi_i}{\partial Y}V_i\sum_{i=1}^{3}\frac{\partial\phi_i}{\partial Y}V_i\sum_{j=1}^{3}\frac{\partial\phi_j}{\partial Y}\tilde{V}_j\,d\Omega-2\int_{\Omega^{n+1}}\sum_{i=1}^{3}V_i\\
&\phi_i\sum_{i=1}^{3}\frac{\partial^2\phi_i}{\partial Y^2}V_i\sum_{j=1}^{3}\frac{\partial\phi_j}{\partial Y}\tilde{V}_j\,d\Omega-3\int_{\Omega^{n+1}}\left(\sum_{i=1}^{3}\frac{\partial\phi_i}{\partial Y}V_i\right)\left(\sum_{i=1}^{3}\frac{\partial\phi_i}{\partial Y}V_i\right)\left(\sum_{j=1}^{3}\frac{\partial\phi_j}{\partial Y}\tilde{V}_j\right)d\Omega\\
&-\int_{\Omega^{n+1}}\left(\sum_{i=1}^{3}\frac{\partial^2\phi_i}{\partial Y^2}V_i\right)\left(\sum_{i=1}^{3}\frac{\partial\phi_i}{\partial X}U_i\right)\left(\sum_{j=1}^{3}\phi_j\tilde{V}_j\right)d\Omega-\int_{\Omega^{n+1}}\sum_{i=1}^{3}\frac{\partial\phi_i}{\partial Y}V_i\sum_{i=1}^{3}\frac{\partial\phi_i}{\partial X}U_i\\
&\left(\sum_{j=1}^{3}\frac{\partial\phi_j}{\partial Y}\tilde{V}_j\right)d\Omega-\int_{\Omega^{n+1}}\sum_{i=1}^{3}\frac{\partial^2\phi_i}{\partial X\partial Y}U_i\sum_{i=1}^{3}\frac{\partial\phi_i}{\partial X}V_i\sum_{j=1}^{3}\phi_j\tilde{V}_jd\Omega\\
&-\int_{\Omega^{n+1}}\left(\sum_{i=1}^{3}\frac{\partial\phi_i}{\partial Y}V_i\right)\left(\sum_{i=1}^{3}\frac{\partial\phi_i}{\partial X}V_i\right)\left(\sum_{j=1}^{3}\frac{\partial\phi_j}{\partial X}\tilde{V}_j\right)d\Omega-2\int_{\Omega^{n+1}}\left(\sum_{i=1}^{3}\frac{\partial^2\phi_i}{\partial Y^2}U_i\right)\\
&\left(\sum_{i=1}^{3}\frac{\partial\phi_i}{\partial X}V_i\right)\left(\sum_{j=1}^{3}\phi_j\tilde{V}_j\right)d\Omega-2\int_{\Omega^{n+1}}\sum_{i=1}^{3}\frac{\partial\phi_i}{\partial Y}U_i\sum_{i=1}^{3}\frac{\partial\phi_i}{\partial X}V_i\sum_{j=1}^{3}\frac{\partial\phi_j}{\partial Y}\tilde{V}_jd\Omega\\
&-2\int_{\Omega^{n+1}}\left(\sum_{i=1}^{3}\frac{\partial^2\phi_i}{\partial X\partial Y}V_i\right)\left(\sum_{i=1}^{3}\frac{\partial\phi_i}{\partial Y}U_i\right)\left(\sum_{j=1}^{3}\phi_j\tilde{V}_j\right)d\Omega-2\int_{\Omega^{n+1}}\left(\sum_{i=1}^{3}\frac{\partial\phi_i}{\partial X}V_i\right)\\
&\left(\sum_{i=1}^{3}\frac{\partial\phi_i}{\partial Y}U_i\right)\left(\sum_{j=1}^{3}\frac{\partial\phi_j}{\partial Y}\tilde{V}_j\right)d\Omega-2\int_{\Omega^{n+1}}\sum_{i=1}^{3}\frac{\partial^2\phi_i}{\partial X^2}V_i\sum_{i=1}^{3}\frac{\partial\phi_i}{\partial Y}V_i\sum_{j=1}^{3}\phi_j\tilde{V}_jd\Omega\\
&-2\int_{\Omega^{n+1}}\left(\sum_{i=1}^{3}\frac{\partial\phi_i}{\partial X}V_i\right)\left(\sum_{i=1}^{3}\frac{\partial\phi_i}{\partial Y}V_i\right)\left(\sum_{j=1}^{3}\frac{\partial\phi_j}{\partial X}\tilde{V}_j\right)d\Omega-\int_{\Omega^{n+1}}\left(\sum_{i=1}^{3}\frac{\partial\phi_i}{\partial Y}U_i\right)\\
&\left(\sum_{i=1}^{3}\frac{\partial\phi_i}{\partial Y}U_i\right)\left(\sum_{j=1}^{3}\frac{\partial\phi_j}{\partial Y}\tilde{V}_j\right)d\Omega\Bigg)-\left(\sum_{i=1}^{3}P_i\psi_i\right)\int_{\Omega^n}\sum_{j=1}^{3}\frac{\partial\phi_j}{\partial Y}\tilde{V}_j\,d\Omega\\
&-\frac{1}{R_e}\Bigg[-\int_{\Omega^{n+1}}\left(\sum_{i=1}^{3}\frac{\partial\phi_i}{\partial X}V_i\right)\left(\sum_{j=1}^{3}\frac{\partial\phi_j}{\partial X}\tilde{V}_j\right)d\Omega+\int_{\Gamma}\sum_{j=1}^{3}\phi_j\tilde{V}_jn_x\sum_{i=1}^{3}\frac{\partial\phi_i}{\partial X}V_id\Gamma\\
&-\int_{\Omega^{n+1}}\left(\sum_{i=1}^{3}\frac{\partial\phi_i}{\partial Y}V_i\right)\left(\sum_{j=1}^{3}\frac{\partial\phi_j}{\partial Y}\tilde{V}_j\right)d\Omega+\int_{\Gamma}\left(\sum_{j=1}^{3}\phi_j\tilde{V}_j\right)n_y\left(\sum_{i=1}^{3}\frac{\partial\phi_i}{\partial Y}V_i\right)d\Gamma\Bigg]=0
\end{aligned}
\tag{4.34}
$$

Equations (4.33) and (4.34) are solved using the finite element method (FEM) in

`FreeFEM++`. These equations, along with the corresponding boundary conditions, are implemented within the computational domain. The developed code is utilized to compute numerical solutions for different parameter values.

Chapter 5

Numerical Results and Discussion

This chapter presents a detailed numerical investigation of viscoelastic fluid flow in a square lid-driven cavity using the Upper Convected Maxwell (UCM) model. The Finite Element Method (FEM) implemented in FreeFEM++ is used to examine the influence of the Weissenberg number (W_i) on the velocity distribution, flow structure, drag force and drag coefficient within the cavity.

5.1 Validation of Numerical Results

To show the accurate implementation of the model problem in FreeFEM++ and validate our computed results for the present problem, the following test model problem as discussed by Khan et al. [1] is implemented. The drag force on the upper lid of the cavity is calculated for comparison with the results of Khan et al. [1] as shown in Table 5.1.

It can be seen that the drag force computed for different Wissenberg numbers and at different Reynolds numbers is in good agreement with the results of Khan et al. [1].

This shows the accurate implementation of the model in the FreeFEM++ and validates our computed results for accuracy.

R_e	Wi	F_d - Khan et al. [1]	F_d - Present
200	0	0.0252350	0.0252413
	2	0.0229625	0.0229389
	4	0.0204830	0.0204821
1000	0	0.165313	0.165375
	4	0.168016	0.168102
	6	0.167988	0.167993
	8	0.161894	0.161907

TABLE 5.1: Comparison of drag force at the lid of the cavity.

5.2 Horizontal Velocity Distribution (U-velocity)

The horizontal velocity (U) profiles along the vertical centerline of the cavity are examined for different Reynolds numbers while varying the Weissenberg number (W_i). The comparison highlights the influence of elasticity on the flow dynamics, particularly on the maximum and minimum velocity magnitudes.

For $R_e = 1$, as shown in Figure 5.1, the U-velocity exhibits a smooth and symmetric profile when $W_i = 10^{-4}$, indicating dominance of viscous effects. As W_i increases to 10^{-3}, the peak velocity slightly rises due to elastic contributions. At $W_i = 10^{-2}$, a significant enhancement in the maximum velocity is observed, demonstrating that viscoelasticity strongly affects the momentum transfer even at low Reynolds numbers.

At $R_e = 1$, inertia is negligible, and the flow is mainly governed by viscous and elastic stresses. The stretched polymer molecules create strong elastic stresses that are larger along the flow direction than across it, causing anisotropy in the stress field. The shear stress also increases due to elastic resistance to deformation, making the flow direction-dependent and dominated by elastic effects rather than inertia.

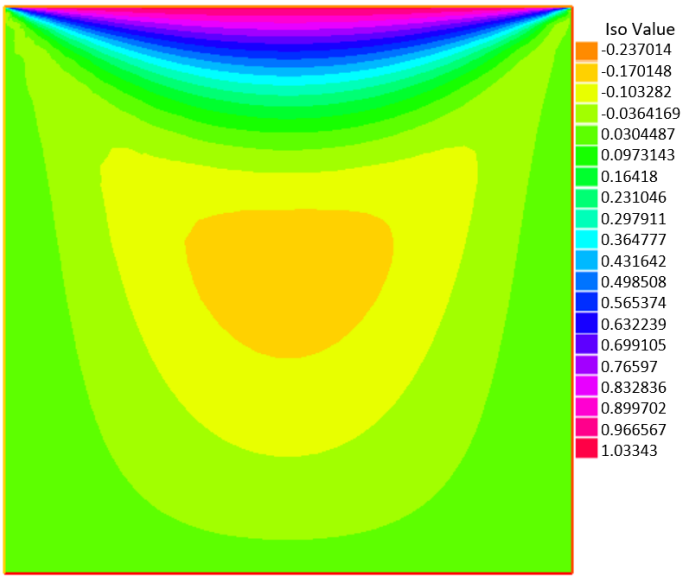

(a) $R_e = 1$, $W_i = 0.005$

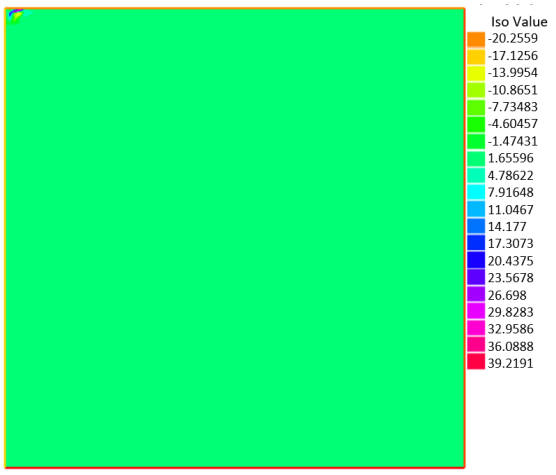

(b) $R_e = 1$, $W_i = 0.008$

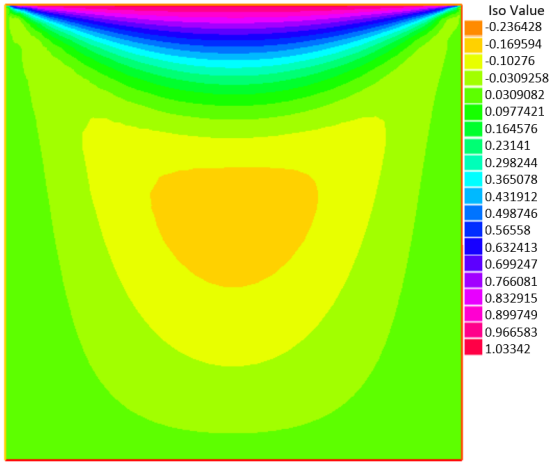

(c) $R_e = 1$, $W_i = 0.009$

FIGURE 5.1: Horizontal velocity (U) profiles at the vertical centerline for $R_e = 1$ and varying W_i.

At $R_e = 51$ (Figure 5.2), the U-velocity profile initially resembles that of a Newtonian fluid at low W_i. However, as W_i increases, the peak velocity noticeably rises, and the velocity profile becomes more deformed.

When $W_i \geq 0.01$, elastic stresses significantly accelerate the core flow region, and the minimum velocity near the cavity bottom becomes less negative, implying a reduction in recirculation strength.

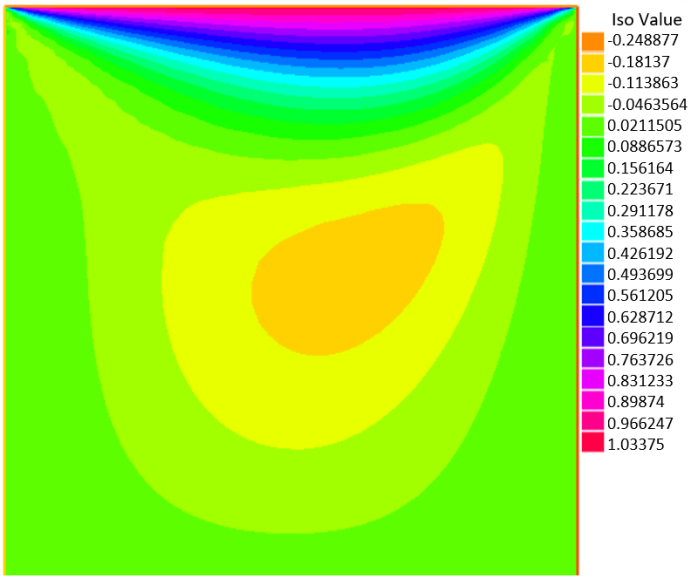

(a) $R_e = 51$, $W_i = 0.005$

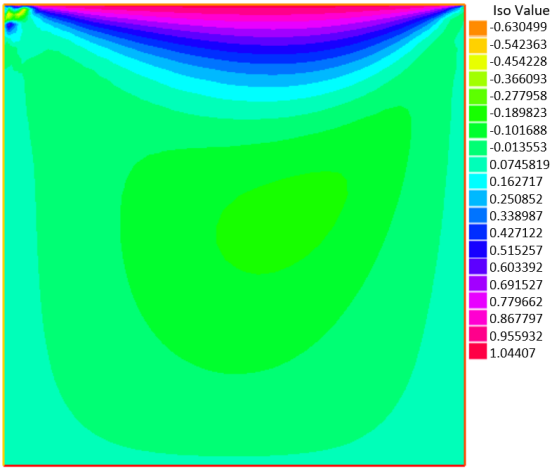

(b) $R_e = 51$, $W_i = 0.008$

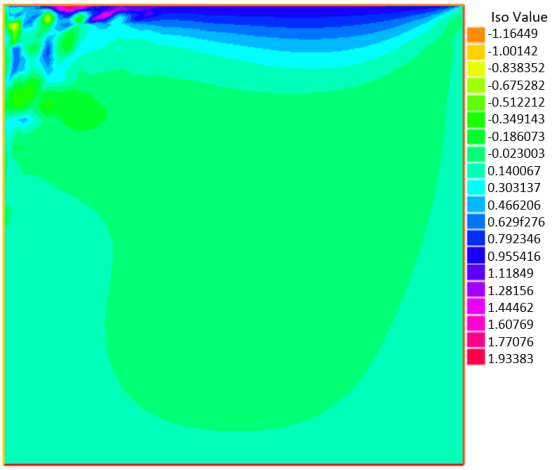

(c) $R_e = 51$, $W_i = 0.009$

FIGURE 5.2: Horizontal velocity (U) profiles at the vertical centerline for $R_e = 51$ and varying W_i.

For $R_e = 101$, as illustrated in Figure 5.3, the effects of elasticity become more pronounced. At very low W_i, the flow behaves similarly to a Newtonian fluid, but as W_i increases, the peak velocity rises sharply. When $W_i = 0.008$, a strong velocity overshoot is observed, resulting in a highly asymmetric profile. This indicates that viscoelastic stresses dominate the inertial forces, causing faster fluid transport near the moving lid.

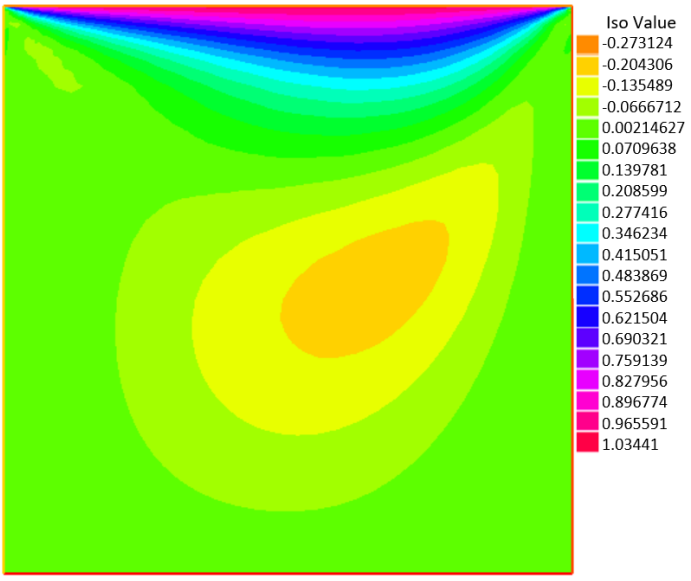

(a) $R_e = 101$, $W_i = 0.005$

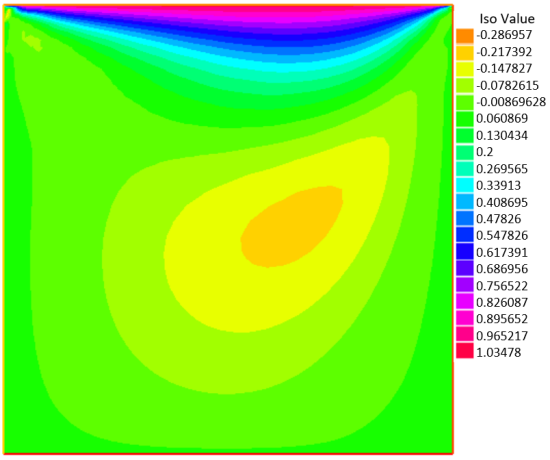

(b) $R_e = 101$, $W_i = 0.008$

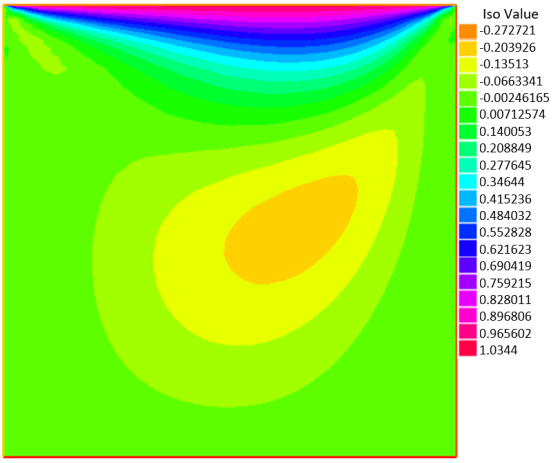

(c) $R_e = 101$, $W_i = 0.009$

FIGURE 5.3: Horizontal velocity (U) profiles at the vertical centerline for $R_e = 101$ and varying W_i.

At $R_e = 151$ (Figure 5.4), the velocity profile remains smooth at lower W_i, but when W_i exceeds 10^{-3}, a noticeable increase in the maximum U-velocity is observed. The velocity gradients near the moving lid become steeper, indicating enhanced acceleration of fluid particles close to the top wall.Meanwhile, the vortex strength in the lower cavity weakens slightly due to increased elasticity.

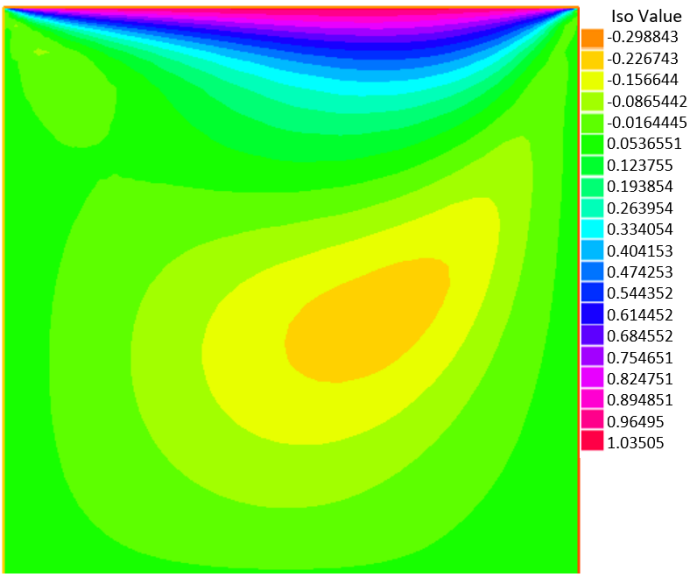

(a) $R_e = 151$, $W_i = 0.005$

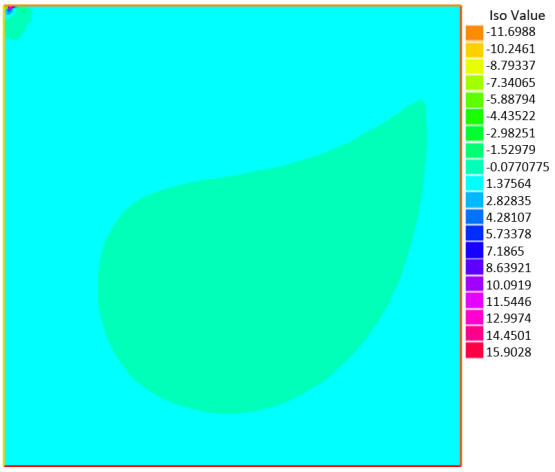

(b) $R_e = 151$, $W_i = 0.008$

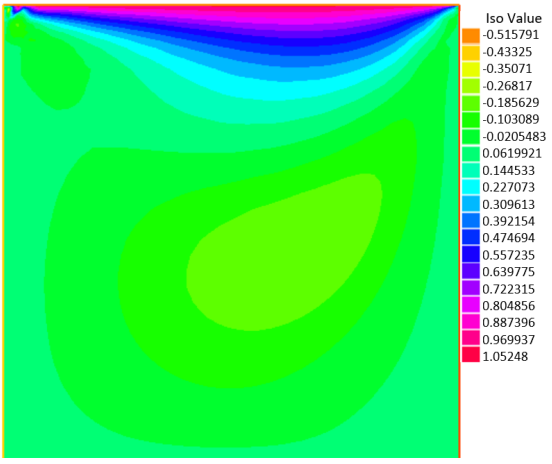

(c) $R_e = 151$, $W_i = 0.009$

FIGURE 5.4: Horizontal velocity (U) profiles at the vertical centerline for $R_e = 151$ and varying W_i.

Finally, for $R_e = 201$ (Figure 5.5), the U-velocity profile at low W_i shows Newtonian-like behavior, but as W_i increases, a sharp rise in peak velocity occurs.

When $W_i \geq 0.01$, viscoelastic effects dominate the flow dynamics, leading to highly skewed velocity profiles. This results in enhanced transport along the moving lid and significant modifications in flow separation near the cavity bottom.

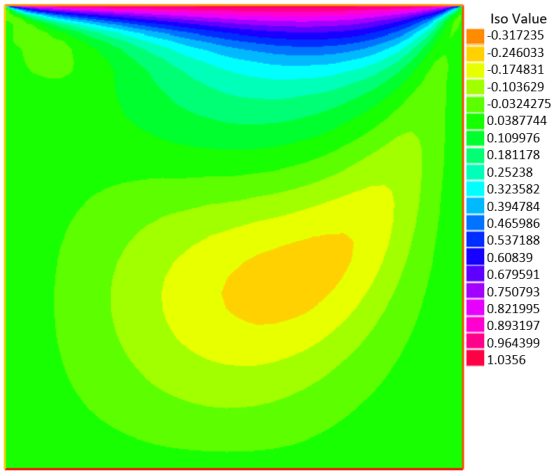

(a) $R_e = 201$ $W_i = 0.005$

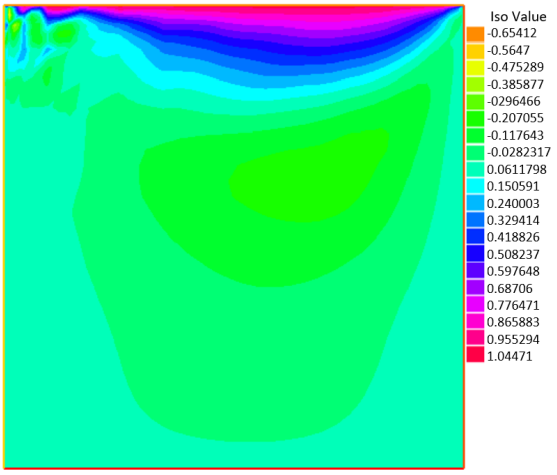

(b) $R_e = 201$ $W_i = 0.008$

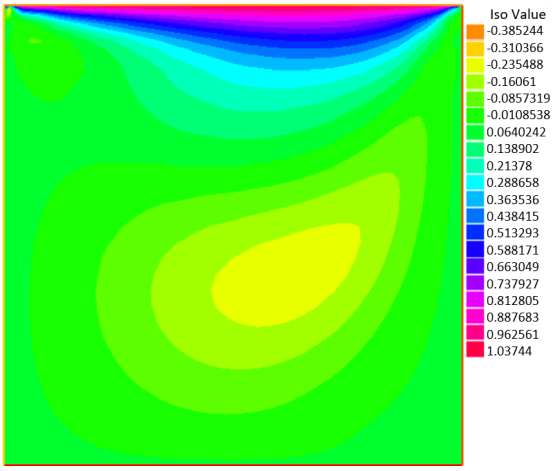

(c) $R_e = 201$ $W_i = 0.009$

FIGURE 5.5: Horizontal velocity (U) profiles at the vertical centerline for $R_e = 201$ and varying W_i.

5.3 Vertical Velocity Distribution (V-velocity)

The vertical velocity (V) profiles along the horizontal centerline of the cavity are analyzed for different Reynolds numbers (R_e) and Weissenberg numbers (W_i). These profiles provide insights into the influence of viscoelastic effects on upward and downward fluid motion within the cavity.

For $R_e = 1$, as shown in Figure 5.6, the V-velocity remains nearly symmetric about the cavity center when $W_i = 10^{-4}$, reflecting a dominance of viscous effects. As W_i increases to 10^{-3}, a slight upward shift in the peak V-velocity is observed, whereas

at $W_i = 10^{-2}$, viscoelasticity becomes significant, causing a noticeable increase in upward velocities near the cavity center.

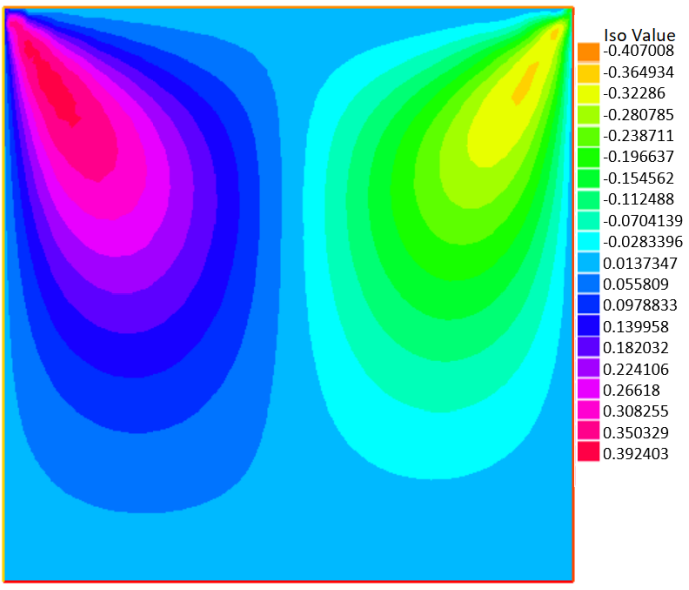

(a) $R_e = 1$, $W_i = 0.005$

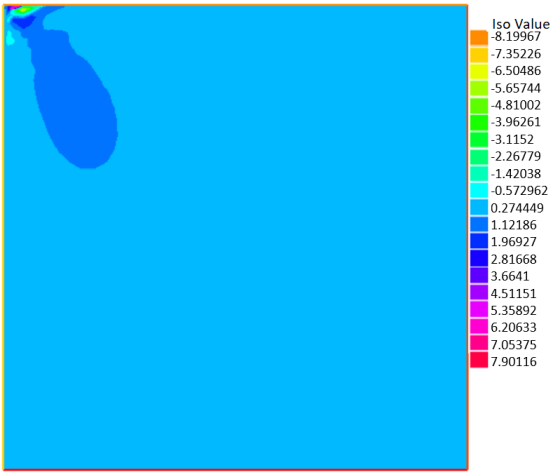

(b) $R_e = 1$, $W_i = 0.008$

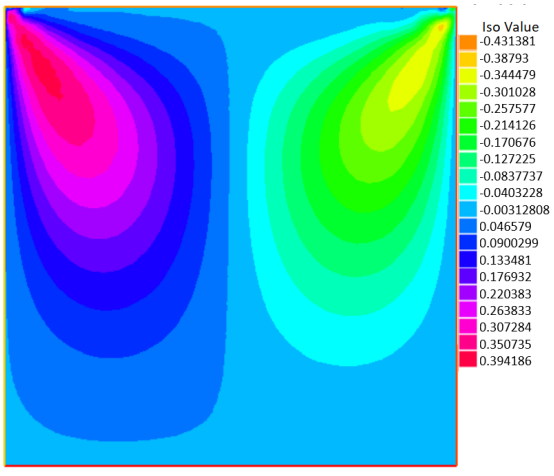

(c) $R_e = 1$, $W_i = 0.009$

FIGURE 5.6: Vertical velocity (V) profiles along the horizontal centerline for $R_e = 1$ and varying W_i.

At $R_e = 51$ (Figure 5.7), the V-velocity distribution shows a similar trend. For small W_i, the velocity peaks remain close to their Newtonian positions, but as W_i increases, the upward velocities near the cavity center become stronger. Elasticity enhances vertical motion in the core, whereas the downward velocity near the walls weakens slightly, leading to a more flattened profile at higher W_i.

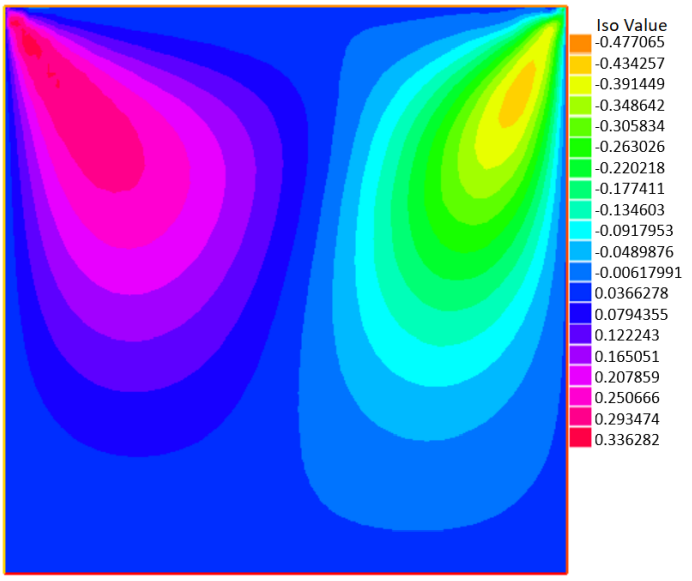

(a) $R_e = 51$, $W_i = 0.005$

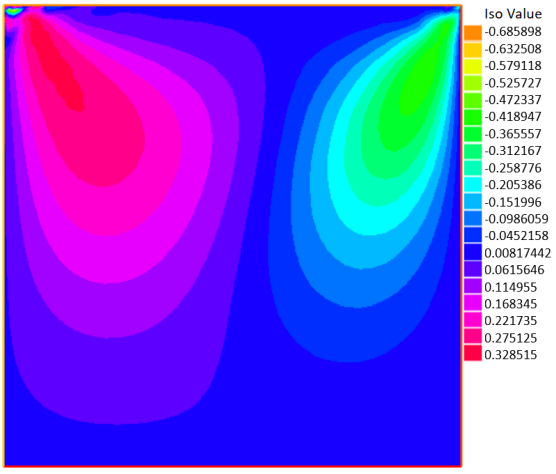

(b) $R_e = 51$, $W_i = 0.008$

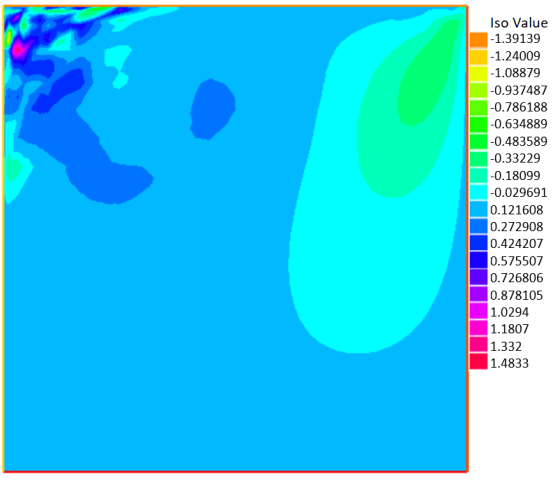

(c) $R_e = 51$, $W_i = 0.009$

FIGURE 5.7: Vertical velocity (V) profiles along the horizontal centerline for $R_e = 51$ and varying W_i.

For $R_e = 101$ (Figure 5.8), the effect of viscoelasticity becomes much stronger. At very low W_i, the flow closely resembles Newtonian behavior, but for $W_i \geq 10^{-3}$, the peak upward velocities increase significantly, accompanied by a pronounced distortion in the profile.

At $W_i = 0.01$, the enhanced elasticity causes a considerable shift in the velocity peak location, suggesting that elastic stresses dominate over inertial effects in the central region.

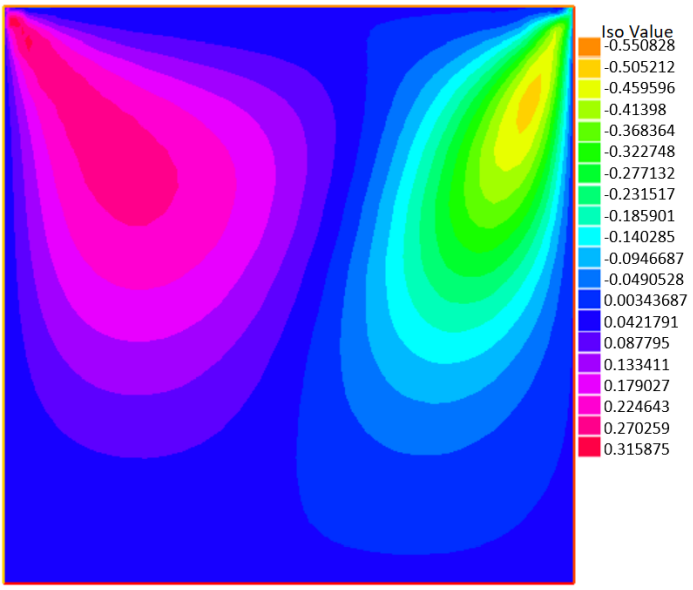

(a) $R_e = 101$, $W_i = 0.005$

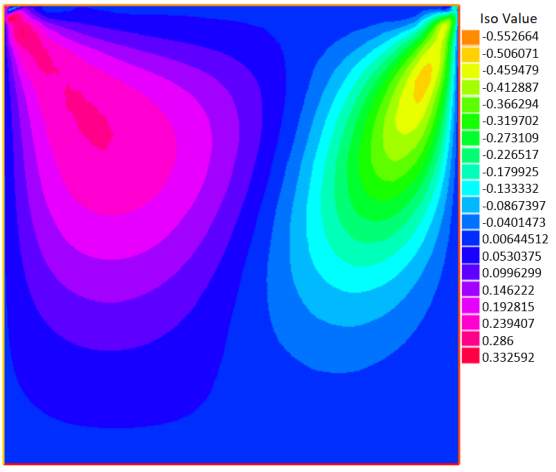

(b) $R_e = 101$, $W_i = 0.008$

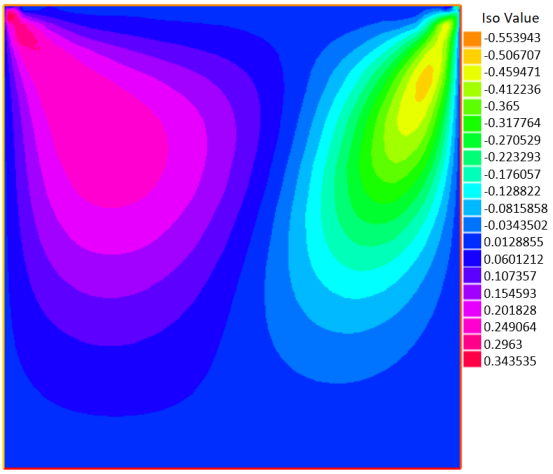

(c) $R_e = 101$, $W_i = 0.009$

FIGURE 5.8: Vertical velocity (V) profiles along the horizontal centerline for $R_e = 101$ and varying W_i.

For $R_e = 151$ (Figure 5.9), at low W_i, the V-velocity profile remains nearly symmetric and Newtonian-like, but as W_i increases beyond 10^{-3}, the vertical velocity magnitude rises sharply in the cavity center.

Additionally, the negative velocity peaks near the sidewalls become weaker, indicating that elasticity suppresses the strength of downward recirculations, leading to a more accelerated upward core flow.

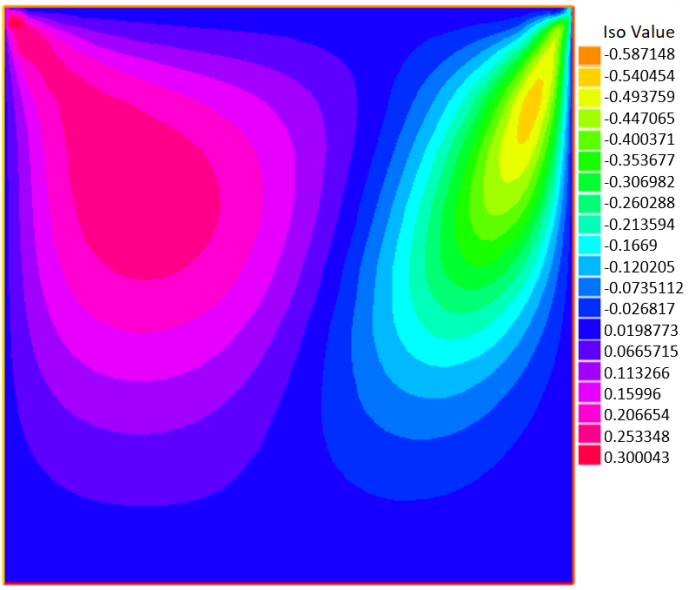

(a) $R_e = 151$, $W_i = 0.005$

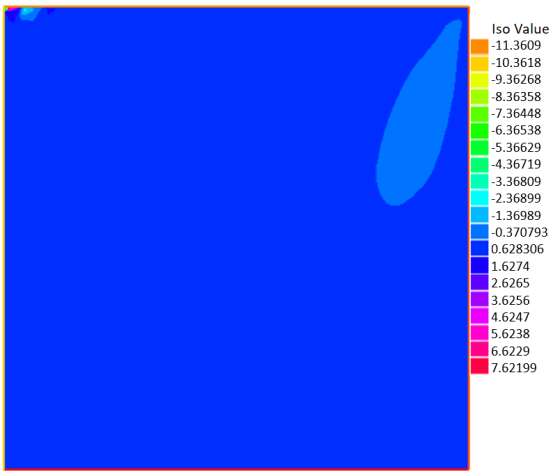

(b) $R_e = 151$, $W_i = 0.008$

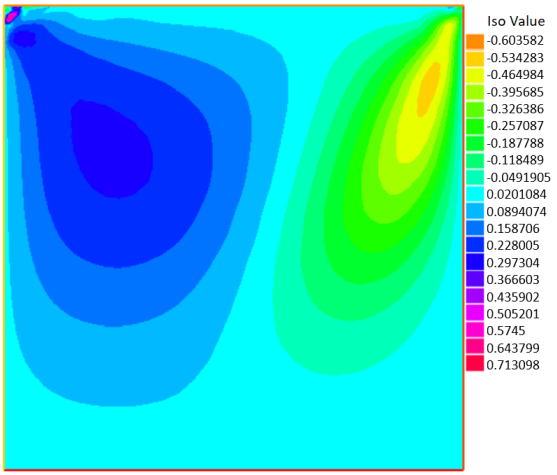

(c) $R_e = 151$, $W_i = 0.009$

FIGURE 5.9: Vertical velocity (V) profiles along the horizontal centerline for $R_e = 151$ and varying W_i.

Finally, for $R_e = 201$ (Figure 5.10), the vertical velocity shows a significant transformation as W_i increases. At $W_i = 10^{-4}$, the profile is Newtonian-like with symmetric peaks, but at $W_i = 10^{-3}$, the upward velocity intensifies while the negative peaks near the walls diminish.

At $W_i = 0.01$, a strong asymmetry develops, with a dominant upward flow near the cavity center and weaker downward recirculations along the sidewalls, demonstrating that elastic stresses completely reshape the vertical velocity distribution at higher Reynolds numbers.

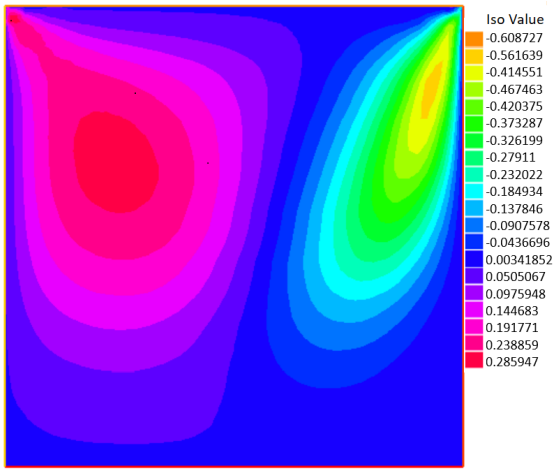

(a) $R_e = 201$ $W_i = 0.005$

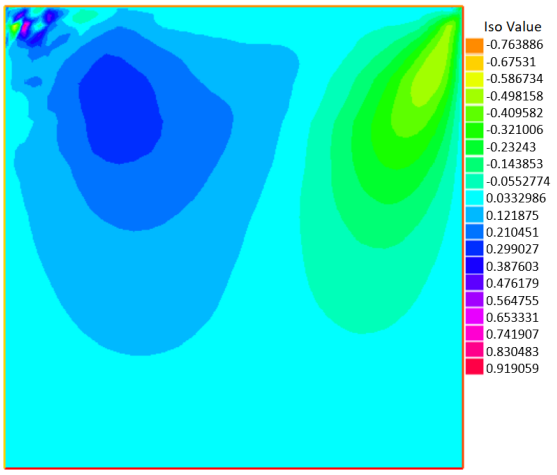

(b) $R_e = 201$ $W_i = 0.008$

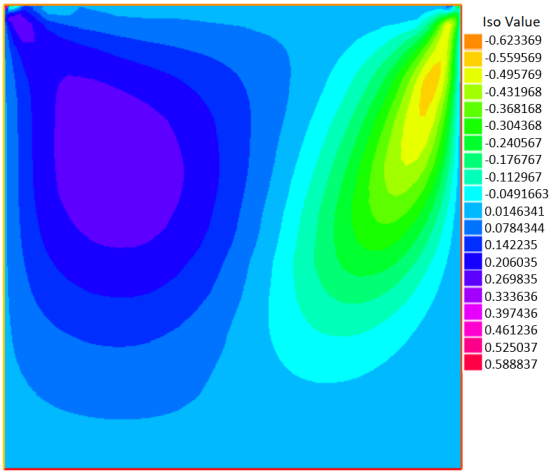

(c) $R_e = 201$ $W_i = 0.009$

FIGURE 5.10: Vertical velocity (V) profiles along the horizontal centerline for $R_e = 201$ and varying W_i.

R_e	$\lvert U_{\max}\rvert$	$\lvert V_{\max}\rvert$	$\lvert U_{\min}\rvert$	$\lvert V_{\min}\rvert$
1	1.0334	0.392	0.237	0.407
51	1.0338	0.336	0.2489	0.477
101	1.0344	0.3158	0.2731	0.551
151	1.0351	0.300	0.2968	0.587
201	1.0356	0.2859	0.317	0.608

TABLE 5.2: Velocity extrema at $W_i = 0.005$.

The data from Table 5.2 are plotted in Figure **??** to visualize the variation of velocity extrema with Reynolds number for a fixed Weissenberg number $W_i = 0.005$.

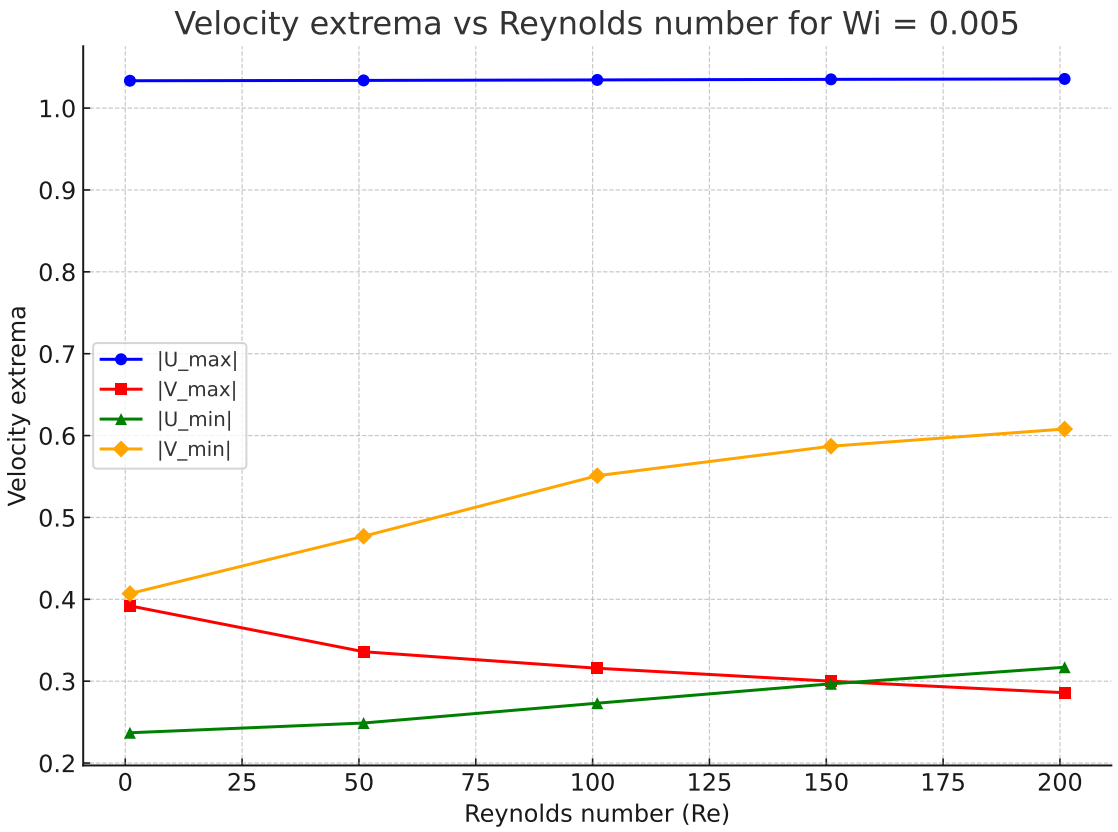

FIGURE 5.11: Velocity extrema ($|U_{\max}|$, $|V_{\max}|$, $|U_{\min}|$, $|V_{\min}|$) as functions of Reynolds number at $W_i = 0.005$.

At this low W_i, the flow remains largely Newtonian with minimal elastic effects. The maximum horizontal velocity $|U_{\max}|$ stays nearly constant, starting at approximately 1.0334 for $R_e = 1$ and reaching only 1.0356 at $R_e = 201$. This stability indicates that inertial effects have little influence on $|U_{\max}|$ when elasticity is weak.

In contrast, the vertical velocity extrema vary more noticeably. As R_e increases, $|V_{\max}|$ decreases gradually from 0.392 to 0.2859, while $|V_{\min}|$ rises from 0.407 to 0.608. Similarly, the minimum horizontal velocity $|U_{\min}|$ shows a modest increase from 0.237 to 0.317. These slow, consistent changes suggest that the flow is dominated by Newtonian characteristics, with only minor elastic contributions affecting vertical velocities and secondary vortex formations.

R_e	$\lvert U_{\max}\rvert$	$\lvert V_{\max}\rvert$	$\lvert U_{\min}\rvert$	$\lvert V_{\min}\rvert$
1	39.219	7.900	20.256	8.199
51	1.044	0.328	0.630	0.685
101	1.034	0.332	0.2869	0.5526
151	15.900	7.622	11.698	11.360
201	1.0447	0.919	0.654	0.764

TABLE 5.3: Velocity extrema at $W_i = 0.008$.

Figure 5.12 visualizes the velocity extrema variation for $W_i = 0.008$.

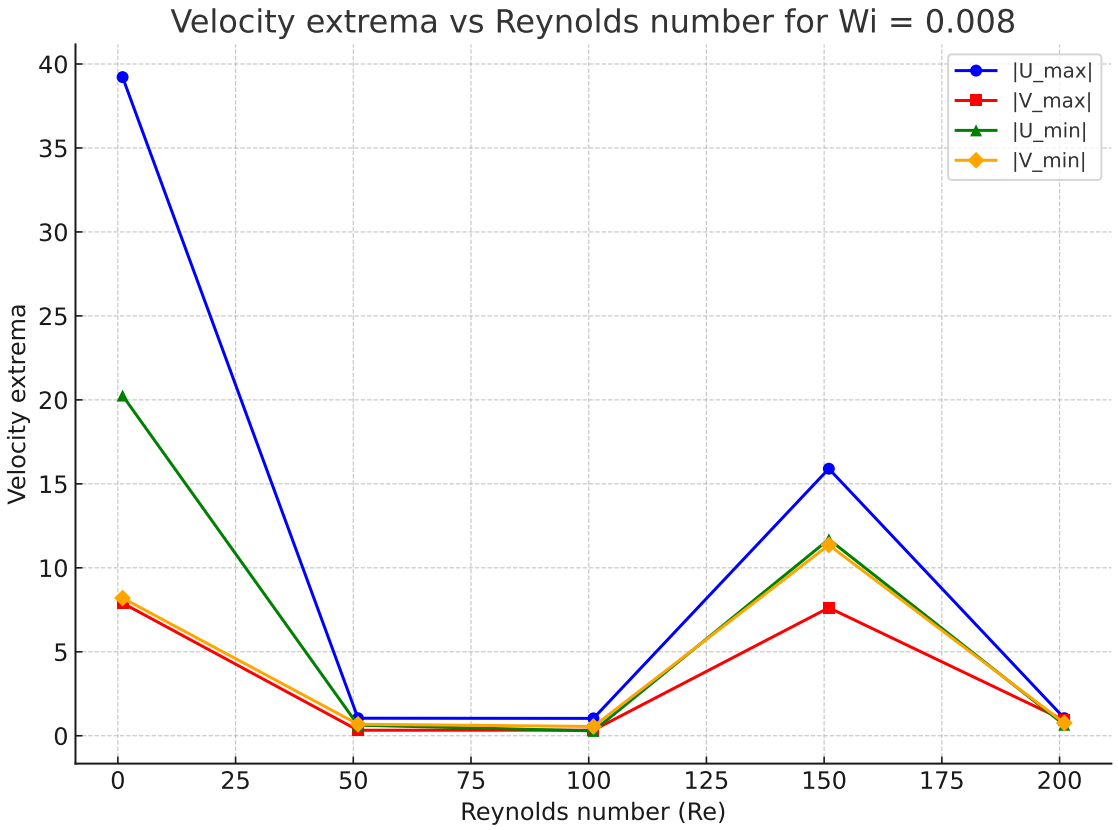

FIGURE 5.12: Velocity extrema ($|U_{\max}|$, $|V_{\max}|$, $|U_{\min}|$, $|V_{\min}|$) versus Reynolds number at $W_i = 0.008$.

At $R_e = 1$, $|U_{\max}|$ reaches an unusually high value of 39.219, while $|U_{\min}|$ is 20.256. The vertical extrema are smaller but still significant, with $|V_{\max}| \approx 7.900$ and $|V_{\min}| \approx 8.199$. These abnormally high initial velocities suggest strong elastic stresses dominating the flow at extremely low Reynolds numbers.

As R_e increases to 51 and 101, all extrema drop sharply, indicating a shift toward a more stable flow regime. Interestingly, at $R_e = 151$, both $|U_{\max}|$ and $|V_{\max}|$ surge to 15.900 and 7.622, respectively, suggesting strong recirculatory vortices or intensified secondary flows caused by inertial–elastic interactions.

However, this peak is transient: at $R_e = 201$, the extrema decrease again, confirming a non-monotonic response of the system at this W_i.

This trend highlights the competing influence of elasticity and inertia, producing transitional flow regimes where velocity peaks emerge rather than increasing or decreasing steadily.

R_e	$\lvert U_{\max}\rvert$	$\lvert V_{\max}\rvert$	$\lvert U_{\min}\rvert$	$\lvert V_{\min}\rvert$
1	1.0334	0.394	0.2364	0.431
51	1.934	1.483	1.1644	1.390
101	1.0344	0.344	0.2727	0.554
151	1.0525	0.713	0.516	0.603
201	1.0374	0.588	0.385	0.6234

TABLE 5.4: Velocity extrema at $W_i = 0.009$.

Figure 5.13 illustrates the corresponding variation of velocity extrema at $W_i = 0.009$.

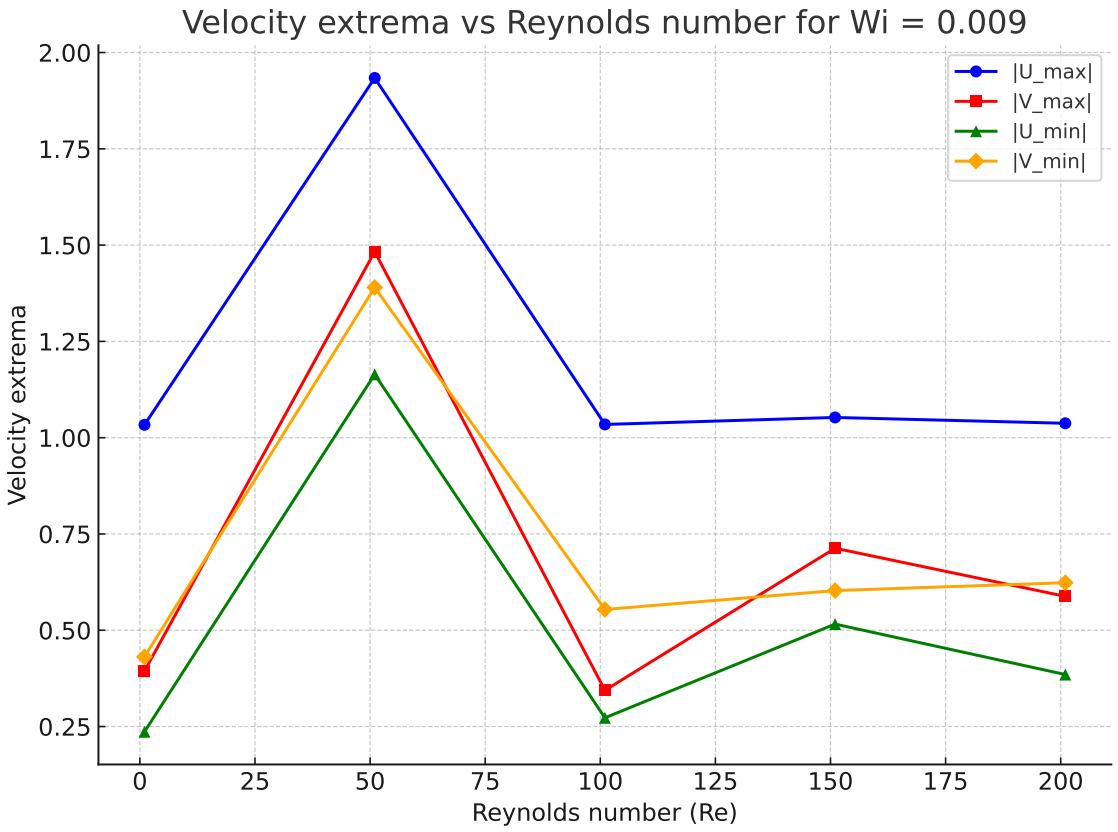

FIGURE 5.13: Velocity extrema ($|U_{\max}|$, $|V_{\max}|$, $|U_{\min}|$, $|V_{\min}|$) versus Reynolds number at $W_i = 0.009$.

At $R_e = 1$, the extrema remain close to those observed for $W_i = 0.005$, indicating weak elastic effects: $|U_{\max}| = 1.0334$, $|U_{\min}| = 0.2364$, $|V_{\max}| = 0.394$, and $|V_{\min}| = 0.431$.

However, at $R_e = 51$, there is a significant rise across all extrema, with $|U_{\max}| = 1.934$ and $|V_{\max}| = 1.483$, highlighting strong inertial–elastic coupling that amplifies secondary flows and vortex formations.

Beyond $R_e = 51$, the extrema exhibit a non-monotonic trend. Both $|U_{\max}|$ and $|U_{\min}|$ decrease gradually but remain slightly above their baseline values, while $|V_{\max}|$ and $|V_{\min}|$ stabilize in the range 0.3–0.7.

Compared to the smoother variations at $W_i = 0.005$, these results indicate a transitional flow regime where elasticity enhances inertial effects, leading to stronger fluctuations in the velocity field and more complex vortex dynamics.

5.4 Calculation of Drag Force at the Lid

In a lid-driven cavity, the motion of the top boundary induces shear within the fluid domain, giving rise to both viscous and elastic stresses. These stresses collectively generate a drag force on the moving lid (upper boundary γ_1). The drag force quantifies the net horizontal force exerted by the fluid on the top wall per unit depth, assuming two-dimensional flow, and is expressed as:

$$F_D = \int_{\gamma_1} \tau_{xy}\, dx, \tag{5.1}$$

where τ_{xy} represents the tangential (shear) stress component along the lid.

For a Newtonian fluid, the shear stress is defined as:

$$\tau_{xy} = \mu \left(\frac{\partial u}{\partial y} + \frac{\partial v}{\partial x} \right), \tag{5.2}$$

where μ is the dynamic viscosity, and u and v denote the velocity components along the x- and y-directions, respectively.

However, for a viscoelastic fluid governed by the Upper Convected Maxwell (UCM) model, the total shear stress consists of two components: a solvent (Newtonian) contribution and a polymeric (elastic) contribution.

Thus, the total stress tensor is expressed as:

$$\tau_{xy} = \tau_{xy}^{(s)} + \tau_{xy}^{(p)} = \mu_s \left(\frac{\partial u}{\partial y} + \frac{\partial v}{\partial x} \right) + \tau_{xy}^{(p)}, \tag{5.3}$$

where μ_s denotes the solvent viscosity and $\tau_{xy}^{(p)}$ represents the polymeric shear stress, which is obtained directly from the constitutive equation of the UCM model.

5.4.1 Discussion of Drag Force and Drag Coefficient

In this sub-section, we discuss the effect of the Reynolds number (Re) and the Weissenberg number (W_i) on the drag force (F_d) and drag coefficient (C_d) for the lid-driven cavity flow problem. Tables 5.5 and 5.6 present the computed results for two different density ratios, $\rho = 1000$ and $\rho = 1$, respectively. The drag force F_d is calculated on the top moving lid, whereas C_d represents the corresponding non-dimensional drag coefficient.

Table 5.5 illustrates the variation of F_d and C_d with different values of W_i and Re for a high-density case ($\rho = 1000$). A clear trend is observed where, for a fixed Reynolds number, increasing W_i leads to a gradual reduction in the drag force. For instance, at $Re = 1$, the drag force decreases from $F_d = 21028$ for $W_i = 0.005$ to $F_d = 20837$ for $W_i = 0.009$. This reduction indicates that viscoelastic effects induced by higher W_i mitigate the resistive forces acting on the top lid. A similar decreasing trend is observed in the drag coefficient C_d, although the variations are comparatively less pronounced.

The effect of Re is also significant. At a fixed W_i, increasing the Reynolds number results in a substantial decrease in F_d. For example, at $W_i = 0.005$, F_d drops sharply from 21028 at $Re = 1$ to 121.67 at $Re = 201$. This behavior reflects the transition from a highly viscous regime at low Re to an inertia-dominated regime at higher Re. Although the drag coefficient C_d also decreases with increasing Re, its relative reduction is smoother compared to the drag force. Table 5.5 shows that for a dense fluid ($\rho = 1000$), both F_d and C_d decrease with increasing W_i and Re. The effect of W_i becomes more noticeable at higher Re, where elasticity significantly reduces the drag on the moving lid.

Table 5.6 presents the computed F_d and C_d for the low-density case ($\rho = 1$). The overall variation patterns with W_i and Re remain consistent with Table 5.5—increasing W_i reduces both F_d and C_d, while increasing Re leads to a significant reduction in F_d. However, the absolute values of F_d are considerably smaller compared to the $\rho = 1000$ case. For example, at $Re = 1$ and $W_i = 0.005$, the drag force is $F_d = 21.028$ here, whereas it was $F_d = 21028$ in Table 5.5. This difference arises from the direct

R_e	W_i	F_d	C_d
1	0.005	21028	42.056
	0.0065	23634	47.268
	0.008	10071	20.142
	0.009	20837	41.675
51	0.005	420.589	0.8412
	0.0065	5421.808	100.844
	0.008	495.116	0.9902
	0.009	182.624	0.3652
101	0.005	221.279	0.4424
	0.0065	5221.928	100.444
	0.008	223.208	0.4464
	0.009	223.064	0.4461
151	0.005	154.79	0.3094
	0.0065	155.263	0.31
	0.008	157.457	0.3149
	0.009	156.643	0.3133
201	0.005	121.29	0.2426
	0.0065	121.67	0.2432
	0.008	145.455	0.2909
	0.009	127.375	0.2548

TABLE 5.5: Variation of F_d and C_d with R_e and W_i for $\rho = 1000$.

R_e	W_i	F_d	C_d
1	0.005	21.028	42.056
	0.0065	23.634	47.268
	0.008	10.071	20.142
	0.009	20.837	41.675
51	0.005	0.4206	0.8412
	0.0065	50.422	100.844
	0.008	0.495	0.9902
	0.009	0.182	0.3652
101	0.005	0.2212	0.4424
	0.0065	5.222	100.444
	0.008	0.2332	0.4464
	0.009	0.233	0.4461
151	0.005	0.1547	0.3094
	0.0065	0.155	0.31
	0.008	0.157	0.3149
	0.009	0.156	0.3133
201	0.005	0.1213	0.2426
	0.0065	0.1216	0.2432
	0.008	0.145	0.2909
	0.009	0.127	0.2548

TABLE 5.6: Variation of F_d and C_d with R_e and W_i for $\rho = 1$.

proportionality of F_d to the fluid density, confirming that $F_d \propto \rho U^2$. An important observation is that the drag coefficient C_d remains unaffected by the variation in density. For corresponding Re and W_i values, C_d is identical in both tables, which demonstrates its non-dimensional nature and independence from ρ. This makes C_d a more universal parameter for characterizing the lid-driven cavity flow behavior across fluids of varying densities.

Table 5.6 shows that for a low-density fluid ($\rho = 1$), the absolute drag force is significantly lower, but the overall trends with respect to W_i and Re are similar to those observed for the high-density case.

From the the Tables 5.5 and 5.6, it is observed that increasing the Weissenberg number W_i consistently reduces both F_d and C_d, especially at higher Reynolds numbers. Increasing the Reynolds number Re causes a sharp reduction in F_d due to the dominance of inertial effects, while C_d decreases more gradually. The drag force F_d scales directly with the fluid density ρ, whereas the drag coefficient C_d remains unaffected, highlighting its universality. Viscoelastic effects become more significant in reducing the drag when both Re and W_i are large.

Chapter 6

Conclusion

The present study has comprehensively investigated the behavior of viscoelastic fluid flow inside a square cavity, modeled using the Upper Convected Maxwell (UCM) constitutive framework. The governing constitutive equations were first derived in their complete component form and subsequently transformed into a non-dimensional formulation incorporating two key dimensionless parameters: the Reynolds number (R_e) and the Weissenberg number (W_i). To simulate the flow numerically, the weak formulation of the coupled momentum and constitutive equations was developed and implemented using the finite element method within the FreeFem++ platform.

The main goal of this work was to examine the influence of elastic effects, represented by the Weissenberg number, on the cavity flow for different fixed Reynolds numbers. Simulations were conducted for $R_e = 1, 51, 101, 151$, and 201, with W_i varying over a range of small values. The results demonstrate that increasing elasticity induces significant modifications in the flow structure. At low Reynolds numbers (e.g., $R_e = 1$), elastic stresses dominate the flow dynamics, accumulating along streamlines and producing strong anisotropy in both the stress and velocity fields. These effects lead to pronounced deviations from Newtonian behavior, including the generation of subsidiary flows and distortion of vortex structures as W_i increases.

At higher Reynolds numbers, inertial effects become more influential; however, elasticity continues to play a significant role, particularly near boundary layers and regions of high strain rates. The interaction between inertia and elasticity at intermediate and large R_e results in sharp velocity and stress gradients as well as the emergence

of complex flow structures. These trends are clearly reflected in the computed contour plots and velocity profiles, which exhibit increasingly nonlinear characteristics with growing W_i.

To further investigate the flow features, the extreme values of the horizontal and vertical velocity components ($U_{\max}, V_{\max}, U_{\min}, V_{\min}$) were documented for different Reynolds numbers at fixed W_i. The results reveal nonlinear and, in some cases, non-monotonic variations, indicating that the flow field is highly sensitive to the combined effects of inertia and elasticity. Generally, peak velocity magnitudes increase with R_e, but their spatial locations shift depending on W_i, highlighting the redistribution of momentum induced by viscoelastic effects.

Additionally, the drag forces acting on the top cavity lid were computed, and the corresponding drag coefficients were determined for various (R_e, W_i) combinations. The findings indicate that W_i strongly influences both the drag force (F_d) and the drag coefficient (C_d). At low Reynolds numbers, the drag force is particularly sensitive to elasticity, and instances of negative drag values were observed, primarily attributed to strong elastic recoil or localized stress overshoots that temporarily reverse the flow direction. At higher Reynolds numbers, the drag force becomes more stable and generally increases in magnitude, although its dependence on W_i remains nonlinear.

It is further observed that increasing the Weissenberg number W_i consistently reduces both F_d and C_d, with this effect becoming more pronounced at larger Reynolds numbers. Likewise, increasing R_e leads to a significant decrease in F_d due to the growing dominance of inertial forces, while C_d decreases at a comparatively slower rate. Importantly, the drag force F_d scales directly with the fluid density ρ, whereas the drag coefficient C_d remains independent of ρ, confirming its universality. Overall, viscoelastic effects become increasingly significant in reducing drag when both R_e and W_i attain relatively large values. While the present work has contributed to a better understanding of viscoelastic fluid behavior in lid-driven cavity flows, several avenues remain open for further exploration. Future studies may focus on extending the analysis to advanced constitutive models, exploring higher Weissenberg number regimes, and considering three-dimensional geometries. Incorporating thermal effects, validating results with experiments, and investigating drag reduction strategies can also

provide deeper insights and broaden the applicability of the findings to real-world engineering and industrial problems.

Bibliography

[1] M. Khan, M. Memon, and E. Bonyah, "Investigation of relaxation time on viscoelastic two-dimensional flow characteristics using freefem++," *Journal of Mathematics*, vol. 2022, pp. 1–15, 2022.

[2] R. Bird, R. Armstrong, and O. Hassager, *Dynamics of Polymeric Liquids, Volume 1: Fluid Mechanics*. Wiley-Interscience, 2nd ed., 1987.

[3] J. Oldroyd, "On the formulation of rheological equations of state," *Proceedings of the Royal Society of London. Series A*, vol. 200, no. 1063, p. 523–541, 1950.

[4] R. Fattal and R. Kupferman, "Constitutive laws for the matrix-logarithm of the conformation tensor," *Journal of Non-Newtonian Fluid Mechanics*, vol. 123, p. 281–285, 2005.

[5] M. Hulsen, R. Fattal, and R. Kupferman, "Flow of viscoelastic fluids past a cylinder: comparison of numerical methods," *Journal of Non-Newtonian Fluid Mechanics*, vol. 127, p. 27–39, 2005.

[6] L. Zhu, E. Lauga, and L. Brandt, "Self-propulsion in viscoelastic fluids: pushers vs. pullers," *Physics of Fluids*, vol. 24, no. 5, p. 051902, 2012.

[7] B. Sebastian and P. Dittrich, "Microfluidics to mimic blood flow in health and disease," *Annual Review of Fluid Mechanics*, vol. 50, pp. 483–504, 2018.

[8] M. A. Alves, P. J. Oliveira, and F. T. Pinho, "Numerical methods for viscoelastic fluid flows," *Annual Review of Fluid Mechanics*, vol. 53, pp. 509–541, 2021.

[9] J. Lopez and M. Avila, "The lid-driven square microcavity flow: Recirculations and bifurcations," *Physics of Fluids*, vol. 32, no. 1, p. 013605, 2020.

[10] M. Renardy, "Numerical study of the flow of viscoelastic fluids past a cylinder," *Journal of Non-Newtonian Fluid Mechanics*, vol. 20, p. 23–36, 1986.

[11] P. Pakdel and G. McKinley, "Elastic instabilities in extensional viscoelastic flows," *Physical Review Letters*, vol. 77, no. 12, p. 2459, 1996.

[12] R. Sureshkumar and A. Beris, "The effect of elastic stress on the stability of planar shear flow," *Journal of Non-Newtonian Fluid Mechanics*, vol. 60, pp. 53–72, 1995.

[13] A. Souvaliotis and A. Beris, "Numerical simulation of viscoelastic lid-driven cavity flows," *Journal of Non-Newtonian Fluid Mechanics*, vol. 45, p. 1–41, 1992.

[14] D. Gezae, "Numerical analysis of viscoelastic lid-driven cavity flows at various weissenberg numbers," *Alexandria Engineering Journal*, 2022.

[15] M. Aboubacar and M. Webster, "Simulation of viscoelastic flows in a lid-driven cavity using a combination of finite-volume and finite-element methods," *Journal of Non-Newtonian Fluid Mechanics*, vol. 102, p. 65–103, 2001.

[16] L. Xue, J. Zhang, and Y. Liu, "Three-dimensional simulations of viscoelastic fluid flow in a lid-driven cubic cavity," *Journal of Non-Newtonian Fluid Mechanics*, vol. 222, pp. 164–177, 2015.

[17] A. Grillet and E. Shaqfeh, "Experimental study of viscoelastic flow instabilities in lid-driven cavity flows," *Journal of Rheology*, 2002.

[18] R. Poole and M. Escudier, "Viscoelastic flow instabilities in planar contractions," *Journal of Non-Newtonian Fluid Mechanics*, vol. 144, p. 65–78, 2007.

[19] X. Li and J. Fang, "Numerical study of thermal effects on viscoelastic lid-driven cavity flows," *Computers Fluids*, vol. 95, p. 107–119, 2014.

[20] I. e. a. Cheddadi, "A new matrix-free finite element method for viscoelastic flows," *Journal of Non-Newtonian Fluid Mechanics*, vol. 166, p. 546–553, 2011.

[21] P. Oliveira and F. Pinho, "Numerical simulation of non-linear elastic flows in a 2d cavity using finite-volume methods," *Journal of Non-Newtonian Fluid Mechanics*, vol. 95, p. 325–348, 1999.

[22] Y. Fan and X. Luo, "Comparison of different viscoelastic models in cavity flows," *Computational Mechanics*, 2020.

[23] N. Phan-Thien and R. Tanner, *Engineering Rheology*. World Scientific, 2017.

[24] P. Arratia, C. Thomas, J. Diorio, and J. Gollub, "Elastic instabilities of polymer solutions in cross-slot flow," *Physical Review Letters*, vol. 96, p. 144502, 2006.

[25] A. Zydney and C. Colton, "Flow of viscoelastic fluids through porous media," *AIChE Journal*, vol. 32, p. 214–223, 1986.

[26] H. Anton, I. Bivens, and S. Davis, *Calculus early transcendentals*. Chichester, 2013.

[27] G. Holzapfel, *Nonlinear Solid Mechanics: A Continuum Approach for Engineering*. John Wiley & Sons, Ltd, 2000.

[28] R. W. Fox, A. T. McDonald, and P. J. Pritchard, *Introduction to Fluid Mechanics*. John Wiley & Sons, Inc., 7th ed., 2006.

[29] R. K. Bansal, *A textbook of fluid mechanics*. Firewall Media, 2005.

[30] F. White, *Fluid Mechanics*. New York: McGraw-Hill Education, 7th ed., 2011.

[31] Y. Cengel and J. Cimbala, *Fluid Mechanics: Fundamentals and Applications*. McGraw-Hill Education, 3rd ed., 2014.